酸偵測離子孔道在海馬迴內中間神經元的細胞特異性表現

Cell Type-Specific Expression of Acid-Sensing Ion Channels in Hippocampal Interneurons

學生：翁儒韻 (Ju-Yun Weng)

指導教授：連正章 (Cheng-Chang Lien, Ph.D.)

國立陽明大學

神經科學研究所

博士論文

Doctoral Dissertation

Institute of Neuroscience

National Yang-Ming University

中華民國九十九年六月

June, 2010

致謝

博士學位和論文的完成，代表著許多的事情，而為了這些事，我必須感謝很多人。對於父親和母親（翁明圓、梁婉真）長年來養育之恩和不求回報的支持，我的感謝難以言表。在完成論文的此時，正要和未婚妻盧幸岑步入禮堂，這麼多年來，只有她常常為我加油，我是一個不會抱怨和傾訴壓力的人，但也只有她多少能體會我的感受，希望在有生之年，不要辜負她花在我身上的這些青春。還有我的狗 Husky，雖然他的無理取鬧老是讓我不知所措，但回到家看著他可愛的樣子，總能紓解不少壓力。姊姊翁世芬和哥哥翁億齡對於家裡老么的關心我也由衷感謝，在知道我口試通過時電話那頭興奮的心情，讓我很能體會他們跟我一樣等這刻很久了。

在神研所這麼多年，所上的每個老師都是見證我成長的人，他們每個人或多或少都給了我在博士學習生涯中寶貴的建議。大學的啟蒙老師林崇智老師領著我進入實驗室裡，現任生科院院長的高閬仙教授，則是給了我認識神經科學契機的人，當畢業典禮中見到她時，奇妙的回憶令我百感交集。神研所裡的第一個指導教授孫興祥老師真是世界上最慈祥的人，她總是放手讓我去做我所有想做的事，然後給予我她能夠給予的支持，在孫老師實驗室裡的那些年，我比其他人更幸運地認識了神經膠細胞，讓我在看待神經科學方面有著更寬廣的角度。進入神研所不久後，我意識到我對神經電生理學的興趣，我總是覺得當一個神經科學家，即使不做電生理也不能不懂電生理，在即將完成第一篇文章時，劉福清老師實驗室裡的姚皓傑學長介紹我認識將要從國外回神研所任教的連正章老師，他熱心地幫我找尋了到連老師實驗室學習電生理的機會，也是他

在我念完碩一的時候，積極地鼓勵我直升博士班，他在所上的時候，我就已經老是纏著他問東問西了，而我在所上的兩個重要決定，也都有了他幫的大忙，很遺憾由於父親的過世，不能出席他的婚禮，對於這個神研所學長的一切，我畢生難忘，當然他也給了我做出人生中最重要決定的機會，轉移到連正章老師的電生理實驗室。在了解到如此一來不知何時才能畢業之後，我的母親非常的反對，我能諒解她的擔憂，延遲了幾年的畢業，希望能讓她了解一切是值得的。

到了連老師實驗室後，當時已博三的我一切從頭來過，陌生的環境、陌生的領域，處在空蕩蕩的實驗室裡，心裡卻交錯著壓力與期待。感謝連老師的辛勤，他很快的把一切都建構起來，並以身作則的教導一切一個神經生理學家該有的條件。他是我看過教學最認真的老師了，論文和博士學位的完成，要論功勞的話，他可能做的比我還多。放著醫生不做跑來日以繼夜的待在實驗室裡，他對神經科學的熱情一直督促著這個實驗室，他給予我的，遠遠超過一個身為指導教授該做的，如果要說恩師是什麼，大概就是這個樣子了。

在一個地方待久了，如果不是過很爽的話，一定會有著同甘共苦的人，那就是我的學弟妹們，身為連老師的第一個學生與第一個博士班學生，當然有著一大堆的學弟妹們。廖健瑋、朱國彰和葉韋均，他們三個和我同時進入了連老師實驗室也一起度過了草創時期，特別有革命情感，尤其葉韋均，沒來得及跟你炫耀我的畢業，希望你不要太介意了。林晏竹、詹筑方、江柏翰、許璨廷、劉于超、吳樸射、高永恬、陳韋均、李政達、謝育鳴、郭翊慧、王思懿等人，謝謝你們曾經協助與忍受過我，尤其林晏竹，分到同一個計畫大概是運氣不太好，不過很感謝她一起參與過這個計畫的完成。

也要感謝百忙之中出席口試的口試委員們：台大生理所的郭鐘金老師、台大藥理所的符文美老師、中研院生醫所的陳志成老師、台大動物所的閔明源老師。在台灣從事電生理學的實驗常常由於從事相關實驗方法的人不多，而疏於與他人溝通討論，這次的口試讓我有機會與多位國內頂尖的電生理學家與酸離子孔道專家面對面的討論，也因為諸位老師們在口試時的提問，給了我從不同角度審視自己研究的機會，也讓我意識到論文寫作與期刊寫作的差異性，更讓我了解到，從事科學研究，單打獨鬥絕不是一個好選擇，做研究並不是創作，而是一個追求真理的方法，多和其他學者溝通、討論和分享才能更客觀的看待自己的研究成果。對於論文的完成，諸位口試委員們讓我有莫大的啟示。

最後要把這份論文獻給我的家人，包括我的未婚妻和狗兒子，尤其是我老爸，雖然他沒來得及看到我畢業，但我想對他說：爸，你兒子博士班畢業了，也要結婚了，不用再為我操心了。我也要對我老媽說：妳已經急了一輩子，不要再急了，妳能夠做的就是這樣，未來我的人生妳只要有顆心，就能讓我走得下去。我也想勉勵自己和所有看到這篇論文的人，一如蘋果創辦人 Steve Jobs 所言：Stay foolish, stay hungry，身為一個科學人，對於知識應當保持謙遜與飢渴，熱情才是我們的動力。

翁儒韻

中華民國九十九年七月二十六日

Abstract

Acid-sensing ion channels (ASICs) belong to degenerin/epithelial Na^+ channel family and are widely distributed in brains. They are voltage-independent Na^+ channels, which can be activated by extracellular H^+. ASIC currents in hippocampal GABAergic inhibitory interneurons are larger than pyramidal neurons (PNs) and preferentially conducted to terminate seizures. However, exact characteristics and compositions of native ASICs in interneurons of numerous types remain unclear. Nucleated patch recordings and single-cell RT-PCR were combined to study ASICs in interneurons of rat hippocampal acute brain slices. We uncovered cell type-specific ASIC expression in dendritic and perisomatic inhibitory interneurons. Our results show that O-LM cells (O-LMs) of dendritic inhibition exhibited about 6-fold ASIC current density higher than PNs in CA1 subfield. Surprisingly, perisomatic inhibitory basket cells (BCs) in dentate gyrus expressed comparable ASIC currents to PNs. By non-stationary fluctuation analysis, we found more ASICs in O-LMs account for the larger ASIC current density. Furthermore, different gating and mRNA expression suggested that the subunit compositions of ASICs are ASIC1a/2a in O-LMs and ASIC1a in BCs. Besides, sensitivity to the specific antagonist of ASIC1a homomers, psalmotoxin 1, indicated that ASICs in BCs are ASIC1a homomers. Functional ASIC currents were also expressed on dendrites of these three neuronal types. Here, we demonstrate channel number, gating and subunit compositions of ASICs are heterogeneously expressed among PNs, dendritic and perisomatic inhibitory interneurons. By providing comparisons of ASICs in interneurons, our findings are potentially important to distinct roles of interneurons in physiology and pathology.

中文摘要

酸偵測離子孔道是廣泛分布於腦中，能被細胞外的氫離子活化並對膜電位不敏感的鈉離子孔道。前人已報導過，由於表現較錐狀神經元更多的酸偵測離子孔道，伽馬丁氨基酪酸性抑制性中間神經元在癲癇發作時，更容易被胞外氫離子給去極化，進而反過來抑制癲癇症狀。然而在腦內種類繁多的中間神經元上，酸偵測離子孔道的精確的特性與組成尚未被釐清。結合胞核內含細胞膜的電生理箝制技術與單細胞反轉錄技術，我們針對來自即性海馬迴腦切片的中間神經元上的酸偵測離子孔道進行研究。我們發現，酸偵測離子孔道會以細胞特異性的方式表現在樹突抑制性與細胞周圍抑制性的中間神經元上。結果顯示，樹突抑制性的始層－分子層細胞上的酸偵測離子孔道，其電流密度約是錐狀神經元的六倍大。出乎意料地，齒狀迴中細胞周圍抑制性的籃狀細胞上的酸偵測子孔道，只表現約等於錐狀細胞上的電流密度。這三種細胞上電流密度上的差異，可能是始層－分子層細胞膜上離子孔道數目較多的緣故。此外，電流調節與行為上的差異則暗示著，這三種細胞上酸偵測離子孔道的次分子組成不同。在始層－分子層細胞與錐狀神經元上都有表現酸偵測離子孔道第一 a 亞型與第二亞型次分子的信息核醣核酸，但絕大多數在籃狀細胞上能被我們偵測到的都只是第一 a 亞型。Psalmotoxin1是對酸偵測離子孔道第一 a 型具高度專一性的抑制劑，它能顯著抑制籃狀細胞上的酸偵測離子孔道電流，卻對始層－分子層細胞毫無影響。最後，我們也發現了功能性的酸偵測離子孔道也表現在這三種細胞的樹突上。我們的研究闡明：酸離子孔道的孔道數目、特性與次分子組成，是差異化地表現在錐狀細胞、樹突抑制性與細胞周圍抑制性的中間神經元上。藉由清楚仔細地研究在中間神經元上酸偵測離子孔道，我們的研究對於中間神經元在生理與病理上的不同角色之認識非常的重要。

Table of Content

Abbreviations

1. AC: accommodating
2. ASIC: acid-sensing ion channel
3. AP: action potential
4. BC: basket cell
5. CA: Cornu Ammon
6. CCK: cholecystokinin
7. CN: calcineurin
8. DG: dentate gyrus
9. FS: fast-spiking
10. GAD65: glutamate decarboxylase 65
11. NF3: neurofilament 3
12. NSFA: non-stationary fluctuation analysis
13. O-LM: oriens lacunosum-moleculare cell
14. PcTX1: psalmotoxin 1
15. PN: pyramidal neuron
16. PV: parvalbumin
17. scRT-PCR: single-cell RT-PCR
18. SOM: somatostatin
19. STUT: stuttering

Introduction

Structures and Characteristics of Acid-Sensing Ion Channels

Acid-sensing ion channels (ASICs) are one of degenerin/epithelial Na^+ superfamily. They are activated by extracellular H^+ and insensitive to voltage changes. 4 ASIC genes have been cloned and 7 different subunits, ASIC1a, ASIC1b, ASIC1b2, ASIC2a, ASIC2b, ASIC3 and ASIC4, which are produced by alternative splicing, have been identified. Each subunit shares a similar structure with a large cysteine-rich extracellular domain, two transmembrane domains, and intracellular carboxyl and amino termini (Wemmie et al., 2006; Jasti et al., 2007). The crystal structure of the chicken ASIC1 deletion mutant implies that a functional ASIC is composed of homo- or heterotrimer (Jasti et al., 2007; Carnally et al., 2008) Extracellular pH value drop can induce an inward current and prolonged acidic environment causes obvious desensitization (Waldmann et al., 1997). Previous studies indicated that recombinant ASICs composed of homo- or heterotrimeric channels differ in gating kinetics and pH sensitivity. ASICs preferentially conduct Na^+ but still show small permeability to other cations (e.g. H^+, K^+, Li^+ and Ca^{2+}) (Wemmie et al., 2006). Several studies indicate that only ASIC1a homotrimeric complexes are permeable to Ca^{2+} (Xiong et al., 2004; Yermolaieva et al., 2004; Wang et al., 2006; Xu and Duan, 2009), but some other reports conclude the Ca^{2+} permeability of ASIC1a homotrimers is very low and Ca^{2+} elevation during activation of ASIC1a homotrimers could be caused by indirect mechanisms (Zhang and Canessa, 2002; Samways et al., 2009). All ASICs can be blocked by amiloride, which is a non-selective antagonist of degenerin/epithelial Na^+ family, but only ASIC1a homotrimeric composition can be inhibited by

psalmotoxin 1 (PcTX1), which is a kind of peptide extracted from South America tarantula Psalmopoeus cambridgei (Baron et al., 2002; Chen et al., 2005; Xiong et al., 2008; Samways et al., 2009; Ziemann et al., 2009). Collectively, the hallmarks of ASICs are transient currents with apparent desensitization, deep pH dependency, Na^+ selectivity and sensitivity to amiloride.

Gating of ASIC Currents

ASIC1a is the principal subunit for a functional ASIC, and ASIC2 subunit plays a major modulatory role. Typical ASIC currents cannot be induced in ASIC1a knockout mice (Wemmie et al., 2002; Askwith et al., 2004; Ziemann et al., 2008). Studies of heterologous expression systems indicate that ASIC2 subunits affect kinetics, pH dependency, and responses to modulatory agents. For example, ASIC1a/2a heterotrimers have higher half-maximal activation ($pH_{0.5}$) than ASIC1a homotrimers (Askwith et al., 2004). Lack of ASIC2a subunits speeds up desensitization and slows down recovery from desensitization (Askwith et al., 2004). FRRFamide, FMRFamide and related neuropeptides are known to prolong the ASIC1a-mediated current. In the presence of ASIC2a, this prolongation is further extended (Askwith et al., 2000). Some extracellular cations also influence the gating of ASICs. High concentration of extracellular Ca^{2+} competes with H^+ for the binding sites to attenuate the amplitudes of ASICs (Immke and McCleskey, 2003). In contrast, Zn^{2+} can potentiate ASIC2-containing ASIC currents (Baron et al., 2001; Gao et al., 2004; Zhang et al., 2008). ASIC2b and ASIC4 homotrimeric complexes cannot generate currents. ASIC3 homotrimers have fastest desensitization rate and most high sensitivity to acid in rat ($pH_{0.5}$ = 6.7)(Sutherland et al., 2001). Nevertheless, pH sensitivity

could be species-specific because ASIC1a homomers are most sensitive to H^+ in mouse ($pH_{0.5}$ = 6.8)(Benson et al., 2002). Characteristics of ASIC1a/2b compositions have not been clearly identified. Briefly, functional ASICs in brains, which are composed of ASIC1a homotrimers or ASIC1a coupled to other subunits, can probably provide high pH-sensing diversity in various neural cells.

Distribution of ASICs in the Nervous System

All ASIC subunits are distributed in nervous systems. Only transcripts of ASIC1a, ASIC2a and ASIC2b are enriched in brains (Price et al., 1996; Waldmann et al., 1996; García-Añoveros et al., 1997; Waldmann et al., 1997; Biagini et al., 2001). All ASICs are also found in retina (Ettaiche et al., 2004; Lilley and Robbins, 2005; Molliver et al., 2005; Vessey et al., 2005). Immunostaining and western blotting results indicate that ASIC1a is highly expressed in olfactory bulb, whisker barrel cortex, cingulate cortex, striatum, nucleus accumbens, amygdala, cerebellar cortex and hippocampus (Wemmie et al., 2002; Wemmie et al., 2003). From cellular point of view, ASIC1a subunits are located in somata and dendrites of pyramidal neurons (PNs) of cortical and hippocampal cultures (Alvarez de la Rosa et al., 2003; Wemmie et al., 2003; Zha et al., 2006; Zha et al., 2009). A recent research further indicates that the direct association between ASIC2a and PSD-95 can interact with ASIC1a to enrich functional ASICs at dendritic spines (Zha et al., 2009). These interactions influence postsynaptic spine number and sensitivity to extracellular pH. However, some immunostaining results suggest that ASIC1a is expressed homogeneously throughout neuronal membranes, but not just

preferentially enriched in spines (Alvarez de la Rosa et al., 2003). Nevertheless, subcellular distribution of ASIC1a in somata and dendrites implies that H^+ co-released with neurotransmitters from presynaptic vesicles can potentially activate ASICs (Wemmie et al., 2006). In addition to dorsal root ganglion neurons and spinal cord (Alvarez de la Rosa et al., 2002; Ichikawa and Sugimoto, 2002; Ugawa et al., 2005), ASIC3 is also discovered in hypothalamus by immunostaining and RT-PCR recently (Meng et al., 2009). ASIC4 is widely distributed in the nervous system as well, and it may need to associate with ASIC1a for functions (Donier et al., 2008). Details about ASIC4 have not been clearly documented. Taken together, ASICs are widely expressed in CNS and PNS. The various compositions and heterogeneous distribution in different regions of the nervous system suggest that ASICs may play different functional roles.

Physiological Functions of ASICs in Brains

Most of physiological functions of ASICs in the brain have been accumulated by ASIC1a knockout mice and related behavioral experiments (Wemmie et al., 2002; Ziemann et al., 2009). Extracellular recordings and behavioral experiments of ASIC1a knockout mice suggest that ASICs participate in learning and memory. Researchers have found that NMDA-dependent long-term potentiation (LTP) at CA3-CA1 synapses is impaired in ASIC1a null mice (Wemmie et al., 2002). ASICs are proposed to unblock Mg^{2+} on NMDA receptors to facilitate LTP. Results of Morris water maze suggest that ASIC1a null mice exhibit mild and reversible defects in spatial learning and memory (Wemmie et al., 2002). In addition, ASICs are enriched in other brain regions

beside hippocampus, especially in amygdala and cerebellum (Wemmie et al., 2002; Wemmie et al., 2003). ASIC1a null mice show defects in cue and context fear conditioning (Wemmie et al., 2003). Besides, ASICs can also make amygdalae sense acidosis and trigger CO_2-induced fear behaviors (Ziemann et al., 2009). Mice without functional ASICs are also abnormal in cerebellum-dependent eye blink conditioning, which is an index for associative learning and memory (Wemmie et al., 2002). Moreover, many ASIC-associated proteins have been identified (Wemmie et al., 2006; Zha et al., 2009). Functions of ASICs at cellular level may be further revealed in the near future. In fact, activation of protein kinase C pathway is proposed to increase current amplitudes of ASIC2b/3 heteromers in DRG neurons (Deval et al., 2004). Beside mechanosensation and nociception, ASICs in CNS, nowadays, have been proven to involve in many physiological functions, such as spatial learning, fear conditioning and eye blink conditioning.

ASICs in Pathological Conditions

In many pathological conditions, such as tissue inflammation, neurotrauma, epileptic seizures and ischemia stroke, accumulation of lactic acid due to enhanced anaerobic glucose metabolism and H^+ from ATP hydrolysis decrease brain pH (Xiong et al., 2008). This acidosis in pathological conditions can possibly activate ASICs. Increasing evidence suggests that activation of ASICs in these pathological conditions further causes neuronal injury. For instance, cells lacking ASIC1a are more resistant to ischemia in a model of oxygen-glucose deprivation (Xiong et al., 2004). Enhanced ASIC responses by dynorphin opioid peptides could induce more severe neuronal death (Sherwood

and Askwith, 2009). PcTX1, which is a potent selective antagonist for ASIC1a homotrimers, can work oppositely to protect neurons against ASIC-mediated neuronal death (Pignataro et al., 2007). ASICs also contribute to axonal degeneration in experimental autoimmune encephalomyelitis, which is a mouse model of multiple sclerosis (Friese et al., 2007). Amiloride, a nonselective ASICs blocker, prevents this neuronal injury. The following neuronal deaths could be explained by ASIC-mediated Ca^{2+} influx to cause glutamate-independent excitotoxicity (Xiong et al., 2004; Xiong et al., 2008). Blockade of ASICs may avoid membrane being depolarized by acidosis in pathological conditions. However in epilepsy, extracellular H^+ is reported to depolarize interneurons preferentially via activation of ASICs to inhibit population principal cells and terminate seizures (Ziemann et al., 2008). In addition, the retina needs ASIC2 to function normally and prevent light-induced retinal degeneration (Ettaiche et al., 2004). In brief, ASICs in the nervous system can be activated in pathological conditions and in turn induce neuronal death. On the other hand, activation of ASICs in interneurons is helpful to seizure termination.

Hippocampus

The hippocampus is a bi-lateral limbic structure and locates beneath the neocortex. The name, hippocampus, comes from the appearance similar to a “seahorse” (from Greek: ἵππος, "horse" and Greek: κάμπος, "sea monster"). Anatomically, the hippocampal formation contains the hippocampus, the subiculum and the entorhinal cortex. The dentate gyrus (DG) and hippocampal proper, which can be subdivided into Cornu Amonnis subfields from 1 to 3

(CA1-CA3), form the hippocampus. A transverse slice of hippocampus reveals a trisynaptic circuit, which includes three connected pathways. Basically, information will be transmitted from neocortex layer II to DG by perforant pathway. The DG passes the information to the CA3 region through mossy fibers, then the CA3 region further send Schaffer Collaterals to the CA1 region. Last, CA1 region transmits the information back to entorhinal cortex through subiculum.

The hippocampal subfields can also be subdivided. For example, there are 5 layers in the CA1 region. Where the somata of glutamatergic pyramidal cells locate is called stratum pyramidale. Axons of pyramidal cells will penetrate stratum oriens and form axonal bundles in stratum alveus where is the major output of the hippocampus. The proximal dendrites of pyramidal cells are located in the stratum radiatum where Schaffer Collaterals form synapses. The distal part of dendrites of pyramidal cells is called stratum lacunosum/moleculare where they receive inputs from entorhinal cortex layer III.

Since the famous H.M. case has been discovered, this well laminated structure has been considered as a center of learning and memory for decades. The H.M. patient, who lost two-thirds of his hippocampal formation and amygdale in both hemispheres to cure his intractable epilepsy, showed heavy anterograde and moderate retrograde amnesia. He could not transform declarative short-term memory into long-term memory. Nevertheless, his working memory and procedural memory remained intact. This regrettable case drastically manifests the relation between memory and hippocampus. Countless studies, which aim at finding where and how memory is stored in the brain, have focused on hippocampus thereafter.

Furthermore, the hippocampus is vulnerable to some neurological disorders, such as Alzheimer's disease and temporal lobe epilepsy. The hippocampus is the first brain region that is affected by Alzheimer's disease (West et al., 1994). The profound death of neurons in hippocampus leads to defects in spatial memory and episodic memory. Though the underlying molecular and cellular mechanisms of why the hippocampus is suffered from Alzheimer's disease are complicated and still in debate, many previous studies have suggested this strong link for years. The hippocampus is also noted because of its high susceptibility to temporal lobe epilepsy. After repetitive status epilepticus, there will be neuronal cell deaths in hippocampus, and hippocampal circuits will be rewired. For instance, the dendritic inhibition onto CA1 pyramidal cells is selectively lost and the perisomatic inhibition is preserved (Cossart et al., 2001). Besides, mossy fibers of granule cells in DG are drastically sprouted and GABA responses of granule cells are increased (Davenport et al., 1990; Gibbs et al., 1997; Nusser et al., 1998). There are plenty of changes in hippocampus in pathological conditions and this tight relation indicates an important role of hippocampus for normal brain functions.

Although the connections within the hippocampus are actually much more complicated than what are mentioned here, its crucial roles to mammalian brains and clear anatomically identified structure make the hippocampus a good choice for exploring the molecular and cellular mechanisms underlying how the brain works.

Oriens Lacunosum-Moleculare Cells (O-LMs) and Basket Cells (BCs)

Interneurons are highly diverse in the brain (McBain and Fisahn, 2001; Jonas et al., 2004; Markram et al., 2004; Klausberger and Somogyi, 2008). O-LMs and BCs are typical distal dendritic and perisomatic inhibitory interneurons, respectively. These two types of interneurons differ in morphology and function. O-LMs' fusiform somata with bipolar dendrites are located within stratum oriens and their axons penetrate stratum pyramidale, stratum radiatum and reach lacunosum-moleculare layer to inhibit distal dendrites of PNs in CA1 region (Miles et al., 1996; Martina et al., 2000; Lalo et al., 2007; Klausberger and Somogyi, 2008). BCs' somata locate in granule cell layer and border of granule cell layer and hilus in DG. BCs spread their basket-like axons around perisomatic regions of granule cells (Cobb et al., 1995; Miles et al., 1996; Kraushaar and Jonas, 2000; Aponte et al., 2008). Both O-LMs and BCs can roughly identified by somata locations, dendrites and electrophysiological properties, but confirmation should be made by morphological reconstruction. Poullie and Scanziani's work indicates that dendritic inhibitory O-LMs and perisomatic inhibitory BCs serve as signal integrators and coincidence detectors in the CA1 region, respectively. BCs detect onset of a series of action potential (AP) transmitted into the CA1 subfiled and then O-LMs reflect the rate and frequency. By this two operation modes, recurrent inhibitions can shift from perisomatic region to distal dendrites of PNs. Therefore, information coded by a series of APs may be routed by O-LMs and BCs (Pouille and Scanziani, 2004). During theta activity in rodent brains, BCs fire at the descending phase of theta activity and O-LMs fire at the through of the field potential (Klausberger et al., 2003). Miles' work also indicates that perisomatic inhibitory interneurons can

suppress repetitive discharge of Na^+-dependent APs and dendritic inhibitory interneurons can suppress Ca^{2+}-dependent APs (Miles et al., 1996). Hence, these two morphological distinct interneuron types differ in many functional aspects. It is important to analyze ASICs in O-LMs and BCs to reveal specific functional roles of ASICs on interneurons of functional differences.

ASICs on GABAergic Inhibitory Interneurons of Hippocampus

Functions of ASICs in GABAergic interneurons are noticed recently (Ziemann et al., 2008), however, the details about ASICs in interneurons remain unclear. Dissociated and cultured inhibitory neurons from hippocampal CA1 region exhibit larger current density than excitatory PNs (Cho and Askwith, 2008; Ziemann et al., 2008). ASIC1a knockout mice show a delayed seizure termination in kainate or pentylenetetrazole-induced seizure models (Ziemann et al., 2008). Although evidence provided by previous studies seems indirect to correlate seizure termination and ASICs on interneurons, results based on ASIC1a knockout mice still suggest that ASICs on interneurons play an anti-epileptic role in brains. Moreover, there is highly diverse, at least 21 subtypes, in interneurons in hippocampal CA1 region, which can be distinguished by their firing patterns, axonal arborization, morphology and cell markers (Klausberger and Somogyi, 2008). Dissociated and culture interneurons are less informative about interneurons subtypes. We chose two morphologically typical interneurons of hippocampus, O-LMs and BCs, from acute brain slices as targets to examine whether ASICs expression among interneuron subtypes is homogeneous or heterogeneous. We made comparisons between O-LMs, PNs and BCs in hippocampus. The experimental results will probably lead us to

further understand the physiological functions of ASICs in brains and reveal differential effects of ASICs in GABAergic interneurons of hippocampus.

Aims of This Study

The brain is a highly diverse and complicated network. Plenty types of neural cells form connections to functionally couple together for brain functions. For normal brain functions, this complicated network has to be well regulated. Local GABAergic microcircuitry of interneurons in hippocampus is one of the most important regulations in the brain. For example, the shunting inhibition between interneurons in mature hippocampal DG is proven to be crucial for strong gamma oscillations (Bartos et al., 2002; Vida et al., 2006), which may serve as reference signals for temporal encoding of information in neuronal ensembles (Singer, 1999; Buzsáki and Draguhn, 2004). Besides, loss of control of inhibition from interneurons could be one of the causes of epilepsy. ASICs also play some roles in epilepsy and ischemia (Xiong et al., 2004; Xiong et al., 2006; Ziemann et al., 2008). Since native ASICs in acute brain slices have not been clearly characterized, we only realize two things about ASICs in interneurons: higher current density and seizure termination (Cho and Askwith, 2008; Ziemann et al., 2008). However, diversity in types of interneurons may lead to various responses to pH fluctuations among interneurons. Therefore, we studied ASICs in two typical types of interneurons: O-LMs and BCs of rat hippocampal acute slices to verify this possibility. Electrophysiology and gene expression-profile of ASICs were correlated by nucleated patch recording and scRT-PCR. Understanding ASICs in GABAergic interneurons can possibly shed the light on functions of ASICs on hippocampal microcircuits. Our work is the first study about native ASICs in GABAergic inhibitory interneurons in hippocampus. The results should lay a good foundation for future studies about functions of ASICs in GABAergic inhibitory interneurons in hippocampus.

Materials and Methods

Patch Clamp Techniques in Hippocampal Slices

Transverse hippocampal slices of 300 μm thickness were cut from the brains of 15- to 23-d-old male Sprague-Dawley rats using a vibrotome (DSK-1000, Dosaka, Kyoto, Japan) as described previously (Lien et al., 2002; Liao and Lien, 2009). Animals were sacrificed by decapitation in agreement with national and institutional guidelines and all procedures were approved by the Animal Care and Use Committee of National Yang-Ming University. Brain slices were sectioned in the ice-cold cutting saline containing (in mM): 87 NaCl, 25 $NaHCO_3$, 1.25 NaH_2PO_4, 2.5 KCl, 10 glucose, 75 sucrose, 0.5 $CaCl_2$ and 7 $MgCl_2$. Following sectioning, slices were incubated in the cutting saline (oxygenated with 95% O_2/5% CO_2) in a holding chamber at 34 ˚C for 30-60 min, and then at room temperature until used. For electrophysiological recordings, an individual slice was transferred to a submersion recording chamber and was continuously superfused with oxygenated artificial cerebrospinal fluid containing (in mM): 125 NaCl, 25 $NaHCO_3$, 1.25 NaH_2PO_4, 2.5 KCl, 25 glucose, 2 $CaCl_2$ and 1 $MgCl_2$. Experiments were performed under visual control using infrared differential interference contrast (IR-DIC) videomicroscopy (Stuart et al., 1993). O-LMs in the CA1 subfield were selected based on the following criteria (Lien et al., 2002; Liao and Lien, 2009): (1) location of a fusiform soma in the stratum oriens with bipolar dendrites; (2) a pronounced sag response upon 1-s hyperpolarizing current pulse (-300 pA) injection; (3) fast-spiking patterns (50-60 Hz) and pronounced fast afterhyperpolarization during 1-s depolarization. For CA1 PN recording, cells of large somata in the stratum pyramidale with accommodating firing patterns were chosen. BCs in DG were selected in accordance with

previous reports (Koh et al., 1995; Martina et al., 1998; Aponte et al., 2008): (1) a relatively large size of cell body near the border between granule cell layer and hilus; (2) high-frequency (≥ 70 Hz) AP phenotype; (3) relatively low input resistance (< 170 MΩ); (4) little sag response upon membrane hyperpolarization. The recording temperature was 22-24 ˚C.

Nucleated Patch and Whole-Cell Recordings

Whole-cell recordings were made by an Axopatch 200B amplifier (Molecular Devices, Palo Alto, CA). Pipette capacitance was compensated. Signals were low-pass filtered at 5 kHz (four-pole Bessel), and sampled at 10 kHz using a digitizer Digidata 1322A (Molecular Devices). Pulse sequences were generated by Digidata 1322A via pClamp 9.2 (Molecular Devices). Nucleated patch recordings were performed as previously described (Gentet et al., 2000; Lien et al., 2002). Nucleated patches were excised within 2 minutes as soon as firing patterns of neurons of interest were checked. Minor and major axes of nucleated patches were measured. It was assumed that nucleated patches were approximately ellipsoidal (Gentet et al., 2000) and the membrane surface area was calculated using the following formula:

$$Surface\ area = (major\ axis + minor\ axis)^2(\pi/4)$$

Fast Application of H^+

Fast application of H^+ on nucleated patches was performed as described previously (Koh et al., 1995). Double-barreled application pipettes were fabricated from theta glass capillaries (2 mm outer diameter, 0.3 mm wall thickness, 0.12 mm septum, Hilgenberg, Malsfeld, Germany), and mounted on a

piezoelectric-based solution switching system (Burleigh LSS-3000, EXFO, Ontario, Canada). The time necessary for complete exchange of solution was measured with an open patch pipette by switching between Na^+-rich and 20% Na^+-rich solutions. The 20-80% rise time of junction potential change was 227 ± 50 μs (n = 3). ASIC currents evoked by 2-s pulses of H^+ were applied every 15-30 s except in some pharmacological experiments; short pulses (50 ms) were used.

Focal H^+ Puffing to Dendrites

To visualize dendrites, we filled neurons with red fluorescent dye sulforhodamine 101 (10 μM) via somatic whole-cell recording. The dendrites were traced under epi-fluorescence microscope. To evoke ASIC currents along the dendrites, the puffing pipette was placed close to the dendrites. Voltage changes or ASIC currents were evoked by focal puffs of H^+ (~6 psi) using PicoSpritzer III (Parker Instrumentation, Pine Brook, NJ) in whole-cell current or voltage-clamp recording in the presence of 1-2 mM kynurenic acid and 1 μM SR95531. Acidic pH solution was injected via a patch pipette with an open tip (2 μm). The PicoSpritzer was triggered by an external TTL pulse generated by Digidata 1322A.

Morphological Analysis

A separate subset of CA1 pyramidal cells, O-LM cells and BCs were filled with biocytin (0.2 %) during recordings. After ~30 min recording, slices were fixed overnight with 4% paraformaldehyde in phosphate-buffered solution (PB; 0.1 M, pH 7.3). Following wash with PB, slices were incubated with fluorescein

isothiocyanate (FITC)-conjugated avidin-D (2 μl/ml; Invitrogen, Eugene, Oregon) in PB and 0.3% triton X-100 overnight at 4 ˚C. After wash, slices were embedded in mounting medium Vectashield® (Vector Laboratories, Burlingame, CA). Labeled cells were examined by a two-photon microscope using a pulsed titanium:sapphire laser (Chameleon-Ultra II tuned to 800 nm; Coherent, Portland, OR) attached to a Leica DM6000 CFS (Leica, Wetzlar, Germany) that was equipped with a 20X/0.50 numerical aperture water immersion objective (HCX APO L; Leica, Wetzlar, Germany). The two dimensional morphologies of the cells were reconstructed from a stack of 38-455 images (voxel size, 0.378-1.514 μm in the *x*-*y* plane; 0.4-0.99 μm along the *z*-axis) using ImageJ (v. 1.42q).

Solutions and Drugs

The Hepes-buffered Na^+-rich external solution used for fast application in the control barrel contained (mM): 135 NaCl, 5.4 KCl, 1.8 $CaCl_2$, 1 $MgCl_2$, 5 Hepes; pH adjusted to 7.4 with *N*-methyl-*D*-glucamine (NMDG). To evoke ASIC currents with various pH values, MES-buffered Na^+-rich external solution in the test barrel contained (mM): 135 NaCl, 5.4 KCl, 1.8 $CaCl_2$, 1 $MgCl_2$, 10 MES, adjusted to the desired values with NMDG. The intracellular solution contained (mM): 135 Kgluconate, 20 KCl, 0.1 EGTA, 2 $MgCl_2$, 4 Na_2ATP, 10 Hepes; pH adjusted to 7.3 with KOH. For low Na^+ experiments, Na^+ in the buffered Na^+-rich external solution was substituted by NMDG. For low Na^+/high Ca^{2+} experiments, concentrations of NaCl and $CaCl_2$ were varied as indicated. Bovine serum albumin (0.1 %) was added in external solutions containing the spider toxin PcTX1 (Peptide International, Louisville, KY) to prevent its absorption to

tubing and containers. Amiloride from Tocris Bioscience (Park Ellisville, MO) was dissolved in water to give 10 mM stock solution and stored at -20 ˚C. All other chemicals were from Sigma (St. Louis, MO) except where noted.

Data Analysis and Statistics

Data were analyzed and fitted with Clampfit 10.0 (Molecular Devices) and Mathematica 5.2 (Wolfram Research, Champaign, IL). Apparent input resistance was defined by the ratio of peak voltage change/1-s hyperpolarizing current (-100 pA). Desensitization and deactivation time constants of ASIC currents were obtained by fitting currents with the function:

$$I(t) = Ae^{-t/\tau_{decay}} + C$$

where A denotes the peak amplitude of current, τ_{decay} represents the desensitization or deactivation time constant and C denotes the amplitude of steady-state current. Concentration-response curves were fitted with the function:

$$f(c) = \frac{A}{1 + (\frac{EC_{50}}{C})^n}$$

, where A is the constant for the maximal effect, c denotes the concentration, EC_{50} represents the half-maximal effective concentration and n denotes the Hill coefficient. For measuring reversal potential, data points of I-V relations were fitted with 2nd order polynomials, from which the interpolated potentials were calculated. Theoretical reversal potential of sodium channels (E_{rev}) was plotted against external Na^+ concentration according to the Nernst equation:

$$E_{rev} = \frac{RT}{F} \ln \frac{[Na^+]_o}{[Na^+]_i}$$

, where $[Na^+]_o$, $[Na^+]_i$ are outer and inner Na^+ concentrations and F, R, T have standard thermodynamic meanings (Hille, 2001).

The single-channel conductance (γ) of ASIC was estimated by non-stationary fluctuation analysis (NSFA)(Hartveit and Veruki, 2007) of ASIC currents from 23 to 50 traces. To minimize errors due to rundown, the entire data set was divided into non-overlapping subsets of 7-10 traces (Engel and Jonas, 2005). Mean ensemble current and variances were determined for each subset and averaged. Mean variance (σ^2) *versus* mean current (I), for each sampling point, can then be obtained. To assign similar weights to all phases of the ensemble mean waveform, binning of I and corresponding σ^2 were used by dividing the mean current amplitude into a number of bins of equal amplitude (Hartveit and Veruki, 2007). The values of I and mean σ^2 of each bin were then further averaged. The averaged I was plotted against the averaged mean σ^2 and then fitted with the equation when they look like a parabola:

$$\sigma^2(I) = iI - \frac{I^2}{N} + {\sigma_b}^2$$

, developed from a binomial model, yielding values for apparent single-channel current i, total number of ion channel N available for activation. σ_b^2 is the variance of the background noise. In all BCs (n = 5) and some PNs (3 out of 7), the data can be adequately described with a straight line rather than a parabola. The slope of the variance-mean relation was plotted with the equation:

$$\sigma^2(I) = iI + {\sigma_b}^2$$

The single-channel chord conductance γ was calculated as:

$$\gamma = \frac{i}{V_m - E_{rev}}$$

The maximum open probability ($P_{o,\ max}$), corresponding to the fraction of available ion channels open at the time of the peak current (I_{peak}), can then be calculated from the following equation:

$$P_{O,\max} = \frac{I_{peak}}{iN}$$

Values indicate mean ± standard errors of the mean (SEM); error bars in figures also represent SEM. Statistical significance among groups was tested using the non-parametric Kruskal-Wallis test. When significant, pairwise comparisons by the Wilcoxon rank-sum test were then carried out for each pair of groups. All tests were performed at the significance level (p) indicated using Prism 5.0 (GraphPad, La Jolla, CA). Standard errors of reversal potentials were obtained by analyzing data of individual experiments separately. Standard errors of parameters of dose-response curves were calculated by a parametric bootstrap method (Efron and Tibshirani, 1998). 500 artificial data sets were generated in which the original values were replaced by normally distributed random numbers with means and SEM identical to those of the original data points, and were fitted as the original data set.

Single-Cell RT-PCR (scRT-PCR)

Single-cell gene expression profiles were analyzed using the scRT-PCR approach as previously described (Martina et al., 1998; Lien et al., 2002; Liss, 2002; Aponte et al., 2006). RNase-free patch-clamp buffer containing (mM): 140 KCl, $MgCl_2$, 5 Hepes, 5 EGTA (pH = 7.3) was autoclaved before used. Patch-clamp capillaries were baked overnight at 220 ˚C prior to use. The cytoplasm was harvested into the recording pipette, under visual control, without losing the gigaseal immediately after electrophysiological characterization. The

contents of the patch pipette (~2-5 μl) were expelled into a 0.2-ml PCR tube (Axygen Scientific, Union city, CA) containing 17 μl reverse transcription (RT) mix (SuperScript III platinum Two-Step qPCR Kit with SYBR green I, Invitrogen). The mix contained 5 μl diethylpyrocarbonate (DEPC)-treated water, 10 μl 2X RT reaction mix (oligo$(dT)_{20}$, random hexamers, $MgCl_2$ and dNTPs) and 2 μl RT enzyme mix (SuperScript III reverse transcriptase and recombinant ribonuclease inhibitor). Total volume was about 20 μl. After a series of incubation at different temperatures according to the manufacturer's instructions, the cDNA-containing tube was stored at –70 ˚C until used. The RNA strand in the RNA-DNA hybrid was then removed by adding 1 μl (2 U/μl) of E. coli RNase H and incubated at 37 ˚C for 20 minutes before PCR. Following cDNA synthesis, the cDNA solution of a single cell was split into 3 aliquots (5 μl) and each was used for gene amplification. A PCR approach with Rotor-Gene 3000 (Corbett Research, Sydney, Australia) or StepOnePlusTM Real-Time PCR system (Applied Biosystems, Foster, CA) was performed in a total volume of 25 μl with 1 μl of 10 μM primers (each), 5.5 μl DEPC-treated water and 12.5 μl Platinum SYBR Green qPCR SuperMix-UDG (Invitrogen) containing Platinum® *Taq* DNA polymerase, Mg^{2+}, uracil DNA glycosylase, proprietary stabilizers, and dNTPs with dUTP. Primers were designed with Perlprimer v1.1.14 and selected for maximal specificity and intron-overspanning amplicons (Table 1). For ASIC expression profiles, all analyzed neurons expressed NF3, indicating selective harvesting from neurons. To exclude the possibility of contaminations, no template control was performed in parallel to every PCR, and the reverse transcriptase was omitted in a subset of cells. Additional controls to exclude non-specific harvesting were performed by advancing pipettes into the slice and

taking them out without seal formation and suction (Martina et al., 1998; Lien et al., 2002).

Results

Identification of O-LMs, PNs and BCs of Hippocampus

We distinguished hippocampal neurons of interest based on locations, morphologies and firing patterns by whole-cell recording. Neurons were selected as described in Materials and Methods. Upon current injection for 1 second, firing patterns of PNs showed obvious accommodation and adaptation. With the same protocol, O-LMs could fire APs more than 50 Hz on average (Fig. 1A). Especially in BCs, average frequency of APs is 86.7 ± 2.9 Hz (n = 18). Accommodation and adaptation are most obvious in PNs, slight in O-LMs and rarely observed in BCs (Fig. 1A). Sag responses evoked by hyperpolarizing current (-300 pA) could be observed in both O-LMs and PNs but not BCs (Fig. 1A). The apparent input resistance of O-LMs, PNs and BCs are 335.6 ± 25 MΩ (n = 24), 176 ± 9.1 MΩ (n = 30) and 133.9 ± 5 MΩ (n = 18), respectively.

Different firing patterns of PNs and fast-spiking O-LMs and BCs are resulted from various sets of voltage-gated ion channels expressed on membranes. High proportion of A-type K^+ currents and R-type Ca^{2+} currents contribute to the burst and the decline in amplitudes of APs at the beginning of firing in PNs (Metz et al., 2005). Compared to PNs, fast-spiking interneurons, such as O-LMs and BCs, with optimized Na_V and K_V3 currents show much less obvious adaptation in APs evoked by trains of current injections (Martina and Jonas, 1997; Lien and Jonas, 2003).

Besides, nucleated patches from these three kinds of neurons showed different proportions of voltage-gated K^+ channels. With voltage steps from -100 mV to +70 mV, O-LMs and BCs exhibited larger proportion of sustained K^+ currents than PNs. In contrast, PNs showed highest A-type K^+ current

components among these three neuronal cell types (Du et al., 1996; Martina et al., 1998; Lien et al., 2002) (Fig. 2A). Since interneurons are highly divergent in hippocampus, morphological reconstructions of biocytin-loaded neurons were made to confirm the axonal arborizations of recorded O-LMs and BCs in a subset of experiments. *Post hoc* staining results revealed that axonal arborizations of O-LMs, which match the electrophysiological criteria, reached stratum lacunosum-moleculare of CA1 and innervated the distal dendrites of PNs (Fig. 1b). BCs, which match the electrophysiological criteria (see materials and methods), displayed patterns of perisomatic innervations within granule cells layer in DG (Fig. 1b, right). Furthermore, scRT-PCR analysis from electrophysiologically selected neurons indicated that PNs expressed transcripts of calcineurin (CN), which is specifically expressed in pyramidal neurons (Sík et al., 1998), but not glutamate decarboxylase 65 (GAD65) or parvalbumin (PV; Fig. 3A). Because both O-LMs and BCs are GABAergic interneurons, they should express mRNA of GAD65. Indeed, we could detect GAD65 in most O-LMs and BCs (Fig. 3A). O-LMs and BCs also showed mRNA expression of somatostatin (SOM; n = 6-8) and PV (n = 7-11; Fig. 3), respectively (Klausberger et al., 2003; Somogyi and Klausberger, 2005). Moreover, more than 90% of GAD65-positive BCs express PV (Fig. 3B). Analyses of scRT-PCR on interneurons confirmed most selected neurons, which fit the electrophysiological criteria, expressed specific cell markers for the given neuronal types (Fig. 3B). Therefore, by comparing the electrophysiological properties, such as firing patterns, sag responses, apparent input resistance and K_V currents; O-LMs, PNs and PV^+ BCs could be distinguished.

Higher ASIC Current Density in O-LMs

One of our goals is to verify and compare ASIC currents in hippocampal interneurons. To precisely measure the kinetics of fast responses induced by extracellular pH drops and avoid errors in voltage-clamp, nucleated patches were obtained from neurons of interest and extracellular pH values were switched from pH 7.4 to pH 5.0 within sub-millisecond level by a fast application system (Koh et al., 1995). By such configurations, we could detect transient inward currents with apparent desensitization at -60 mV on all these three neuronal types (Fig. 4A). Further analyses revealed that H^+-induced fast inward current on nucleated patches from O-LMs showed significant larger current amplitudes than PNs and BCs (Fig. 4B; O-LM, 237.9 ± 55.1 pA, n = 27; PN, 22.3 ± 1.9 pA, n = 27; BC, 22.4 ± 3.8 pA, n =19; $p < 0.001$, Wilcoxon rank-sum test). The corresponding current density of O-LMs is 6-fold larger (0.75 ± 0.08 pA/μm², n = 19) than PNs (0.11 ± 0.01 pA/μm², n = 27; $p < 0.001$ Wilcoxon rank-sum test). Surprisingly, another type of GABAergic inhibitory interneurons, BCs of perisomatic inhibition, expressed similar amplitude to PNs (0.12 ± 0.02 pA/μm², n = 19, p = 0.47, Wilcoxon rank-sum test). After obtaining stable nucleated patches, we applied voltage steps from -100 mV to +70 mV for 200 ms to record the K_V currents. Plotting ASIC current amplitudes versus ratio of peak currents between responses at 200 ms of K_V currents could clearly distinguish these three neuronal types (Fig. 2B). In sum, we found that not every type of interneuron has higher ASIC current density. Nucleated patches from perisomatic inhibitory BCs show significantly smaller H^+-activated current amplitudes than those from O-LMs.

We conducted some experiments to examine the possible ion channels, which cause the transient H^+-activated currents recorded from nucleated patches. Unlike the suppression in background outward currents of two-pore domain K^+ channels by extracellular H^+, which are responsible for maintaining resting membrane potentials (Taverna et al., 2005), most of these transient responses with desensitization could be reversibly blocked by 10 μM amiloride, which is a non-selective blocker of degenerin/epithelial channel family (Fig. 4A). We further confirmed the pH-dependence of these H^+-induced responses on nucleated patches from O-LMs by dose-response experiments. Extracellular H^+ concentration was decreased from pH 5.0 to 7.0 and the normalized peak responses were plotted. The Hill coefficient was 1.02 ± 0.0 and $pH_{0.5}$ (EC_{50}) was about 6.0 ± 0.0 (Fig. 5A). The reversal potential (E_{rev}) of the peak responses under normal condition ($[Na^+]_o/[Na^+]_i$ = 135 mM/8 mM) was about 62.3 ± 3.1 mV (n = 4), which was close to theoretical equilibrium potential of Na^+ (Fig. 5B). Besides, increase in $[Ca^{2+}]_o/[Na^+]_o$ ratio to 80 mM/50 mM and 100 mM/10 mM did not shifted the E_{rev} significantly (Fig. 5C). The changes in E_{rev} still followed the decrease in $[Na^+]_o$. Under such extremely high ratio of $[Ca^{2+}]_o/[Na^+]_o$, if these H^+-activated currents included larger portion of Ca^{2+} influx, the E_{rev} would be very positive. This result suggests that low Ca^{2+} permeability contribute to the H^+-activated currents. Extracellular Ca^{2+} is known to inhibit ASIC currents owing to the competition with extracellular H^+ to the binding sites (Immke and McCleskey, 2003), and we also observed 10 times of $[Ca^{2+}]_o$ (18 mM) could inhibit 60 ± 2.3 % of ASIC currents on nucleated patches from O-LMs (Fig. 6; n = 4, p < 0.05, Wilcoxon signed-rank test). Although we could not rule out the possibility that inactivation of potassium channels might contribute to these transient inward currents, by current

kinetics, pH-dependence, amiloride and Ca^{2+} blockade and Na^{+} selectivity, which are hallmarks of ASICs, we confirmed that majorities of these inward currents were mediated by ASICs and the amplitudes of ASIC currents in O-LMs are 6-fold larger than those in PNs and BCs.

More ASIC Channel Number on Nucleated Patches from O-LMs

Three possibilities could explain the higher current density of ASICs we observed from nucleated patches of O-LMs. The first possibility is higher open probability of ASICs in O-LMs than PNs and BCs. The second one is higher single-channel conductance of ASICs in O-LMs. The last is more functional ASIC number on the nucleated patches from the O-LM cell. We verified these possibilities by non-stationary fluctuation analysis (NSFA). External pH values were switched from 7.4 to 5.0 for 2-sec by a fast application system with a 20-second interval (Fig. 7A). Desensitization periods of at least 23 stable sweeps were analyzed. Variance-mean plots were fit by a parabolic function as described (see Materials and Methods) to retrieve information of single ASICs, such as single-channel conductance (γ), maximum open probability ($P_{o,\,max}$) and channel number (N) (Fig. 7B and 7C). Single-channel conductances of O-LMs, PNs and BCs are 5.05 ± 0.74, 6.57 ± 1.05 and 6.29 ± 1.75 pS, respectively (Fig. 7D). There is no significant difference in γ among these three neuron types (Fig. 7D; p = 0.72, Kruskal-Wallis test). $P_{o,\,max}$ was also similar between O-LMs and PNs (Fig. 7D; O-LM cells, 0.54 ± 0.06, n = 7 versus PNs, 0.48 ± 0.08, n = 4; p = 0.65, Wilcoxon rank-sum test). Notably, in all cases of BCs, we failed to retrieve $P_{o,\,max}$ and N possibly because of low open probability caused by fast desensitization and slow recovery under repetitive acid pulses. Last, we

discovered *N* of O-LMs was 427 ± 82 (n = 7), which was significantly larger than 69 ± 45 (Fig. 7D; n = 4; 3 of 7 cells were fitted with a linear function; $p < 0.05$ Wilcoxon rank-sum test) in PNs. Results revealed by NSFA suggest that more ASICs in nucleated patches from O-LMs account for higher ASIC current density than those of PNs and BCs.

ASIC Currents in Fast-Spiking and Non-fast Spiking Interneurons in DG

In addition to O-LMs in CA1 region and BCs in DG, we also examined ASIC currents in other interneuron types in DG. Non-fast spiking interneurons in DG were further subdivided into two groups, accommodating (AC) and stuttering (STUT) interneurons (Markram et al., 2004). In AC interneurons, amplitudes of APs were decreased upon 1-s depolarization in current-clamp mode (Fig. 8A). STUT interneurons, on the other hand, displayed discontinuous APs (Fig. 8A). By nucleated patch recording and fast application, we found interneurons with accommodating and stuttering firing patterns exhibited significantly larger H^+-activated current amplitudes than fast-spiking BCs (Fig. 8B). Compared to BCs, the amplitudes of ASIC currents in AC and STUT interneurons are 399 ± 36 (n = 15) and 406 ± 56 pA (Fig. 8B and 8C; n = 10), respectively. There is no significant difference in ASIC amplitudes between AC and STUT interneurons ($p > 0.05$, Wilcoxon rank-sum test). Besides, both AC and STUT had larger input resistance than BCs. Hence, we could plot H^+-activated currents against various input resistance to make discrimination between fast-spiking and non-fast spiking interneurons (Fig. 8D). These non-fast spiking interneurons still express larger transient H^+-activated currents with apparent desensitization than PV-positive soma-targeting BCs.

Functional ASICs on Dendrites of Hippocampal Neurons

Both ASIC1a and ASIC2 are distributed along dendrites of principal cells in CA1 region (Wemmie et al., 2003; Zha et al., 2006; Zha et al., 2009). Since nucleated patches were obtained from somata, we were also interested in whether functional ASICs are also expressed on dendrites of hippocampal neurons. Sulforhodamine 101 (SR101, 10 μM) was loaded into neurons of interest by recording pipette and focal acid was applied by an air puff system on red fluorescent dendrites of O-LMs, PNs and BCs in the presence of antagonists of ionotropic glutamate and $GABA_A$ receptors (Fig. 9B-D). First, we could detect amiloride-sensitive inward desensitized currents as we observed from nucleated patches (Fig. 9A). Later, by voltage-clamp configuration, O-LMs showed larger ASICs currents along dendrites (280 ± 65 pA, n = 8) than PNs (132 ± 28 pA, n = 9) and BCs (Fig. 9B-E; 52 ± 8 pA, n = 6). The decrease in total channel numbers could explain the observation that ASIC currents decrease with distance from soma. In addition, focal acid puff could induce series of APs in O-LMs but only subthreshold depolarization in PNs and BCs in current-clamp configuration (Fig. 9B-D and 9F). The spike number was also decreased with distance from soma. Here, we manifested the expression of functional ASICs on dendrites of hippocampal neurons. Consistent with results from nucleated patches, dendrites of O-LMs express more functional ASICs than PNs and BCs.

Differential Kinetics of ASIC Currents among Interneurons and PNs

ASICs with different absolute and relative abundance of ASIC1/2 display distinct kinetics (Askwith et al., 2004). To examine whether subunit compositions of functional ASICs among these three types of neurons are

different, we compared the ASIC kinetics first by nucleated patch recording and a fast application system. Deactivation of ASICs was fastest in O-LMs (Fig. 10A; 3.7 ± 0.3 ms, n = 10, p < 0.05, Kruskal-Wallis test) and shows no significant difference between PNs and BCs (Fig. 10A; PN, 9.3 ± 1.2 ms, n = 5; BC, 9.8 ± 1 ms, n = 6; p > 0.05, Wilcoxon rank-sum test). In addition, the time constant of desensitization of O-LMs was slower than those from PNs and BCs (Fig. 10B; 688 ± 97 ms, n = 26, p < 0.05, Kruskal-Wallis test). ASICs in BCs had comparable desensitization rate to PNs (Fig. 10B; PN, 470 ± 21 ms, n = 32; BC, 434 ± 34 ms, n =16; p > 0.05, Wilcoxon rank-sum test). Moreover, by paired-pulse protocol with different inter-pulse intervals, the difference in recovery from desensitization was revealed. ASICs in O-LMs could recovery completely within 10 seconds ($\tau_{recovery}$ = 0.96 ± 0.0 sec) but PNs and BCs took more than 6 minutes to recovery from desensitization (Fig. 11A; $\tau_{recovery}$ = 13.2 ± 0.1 and 42.8 ± 1.0 sec, respectively). For cumulative desensitization, the acid pulses were given every 20 seconds. Compared to the first peak responses, following ASIC currents induced by repetitive acid pulses in O-LMs remained stable (Fig. 11B). Nevertheless, the same stimulation protocol caused severe rundown in amplitudes of following ASIC currents in PNs and BCs. The rate and level of cumulative desensitization were most obvious in BCs and intermediate in PNs. By comparing current kinetics, we uncovered that ASIC gating is dependent on cell types.

Various ASIC Transcripts Detected by ScRT-PCR

Various ASIC subunit compositions may result in cell type-specific ASIC gating (Askwith et al., 2004; Wemmie et al., 2006). A study based on recombinant

ASICs overexpressed in CHO cells have suggested that absolute and relative amounts of ASIC1a and ASIC2 subunits are critical to the amplitudes and properties of functional ASICs (Askwith et al., 2004). Without ASIC2 subunits, ASIC1a homomultimers show much slower recovery rate and higher sensitivity to pH. They also proposed that ASIC1a/2a heteromultimer contribute to H^+-activated currents in hippocampal neurons. Based on differences in cumulative desensitization and recovery from desensitization, we hypothesized cell type-specific ASIC gating is caused by various subunit compositions. To examine this, we performed scRT-PCR. Neurofilament 3 (NF3) was considered as a neuronal marker and a positive control (Fig. 12). In all $NF3^+$ cells, the collective results of scRT-PCR showed both O-LMs and PNs expressed ASIC1a and ASIC2 transcripts, and most BCs had ASIC1a mRNA only (Fig. 12). This result implies that cell type-specific gating of ASICs in hippocampal neurons is caused by different ASIC subunit compositions.

Inhibition of ASIC Currents in BCs by PcTX1

To determine the existence of ASIC1a homomultimers in hippocampal neurons, we used PcTX1, which is a specific antagonist for ASIC1a homomers (Baron et al., 2002; Chen et al., 2005; Xiong et al., 2008; Samways et al., 2009). If functional ASICs on BCs are indeed composed of ASIC1a homomers, PcTX1 should suppress the ASIC current amplitudes in BCs. Extracellular solutions of pH 7.4 and 5.0 with or without PcTX-1 were applied for 50 ms every 15 sec to nucleated patches voltage-clamped at -100 mV. By this protocol, the amplitudes of ASICs remained stable all over the experimental periods. We found 30 nM PcTX1 suppressed 76% of ASIC amplitudes on nucleated patches obtained from

BCs (n = 6, p < 0.05, Wilcoxon signed-rank test) but had no effect to ASIC currents in O-LMs (n = 4, p > 0.05, Wilcoxon signed-rank test) or PNs (Fig. 13; n = 4, p > 0.05, Wilcoxon signed-rank test). This result is consistent with the expressions of ASIC1a/2 heteromultimers in O-LMs and PNs and ASIC1a homomultimers in BCs, which were revealed by scRT-PCR.

Heteromeric ASIC1a/2a in O-LMs and Homomeric ASIC1a in BCs

ASIC2a and ASIC2b are alternative splicing forms of ASIC2. What ASIC2a lacks is the exon 1 of ASIC2b. The rest of these two sequences show 98% similarity. We had tried several sets of primers to distinguish ASIC2a from ASIC2b, but we failed to detect any signal probably due to bad primer designs or inappropriate PCR conditions. To know the possible compositions of ASICs, we further compared our results of recovery from desensitization with previous recombinant ASICs overexpressed in CHO cell line (Askwith et al., 2004). The comparison revealed that the recovery of ASICs in O-LMs could qualitatively recapitulate the recovery of ASIC1a/2a heteromultimers (Fig. 14). On the other hand, recovery of ASICs in BCs could also partially recapitulate the recovery of ASIC1a homomultimers. Taken together, electrophysiological results, scRT-PCR analysis, PcTX1 sensitivity and comparison with recombinant ASICs suggested that the subunit compositions of functional ASICs in O-LMs and BCs are ASIC1a/2a and ASIC1a, respectively.

Discussions

Summary

This is the first study about ASICs in acute brain slices, to our knowledge, demonstrating that ASICs are heterogeneously expressed among hippocampal neurons, especially in interneurons. By combining electrophysiological techniques and scRT-PCR, we uncovered several findings in this study. First, ASIC currents are significantly larger in nucleated patches from O-LMs owing to higher channel number. Second, in all tested hippocampal neurons, including non-FS interneurons in DG, BCs particularly express less ASIC currents. Third, cell type-specific ASIC gating is due to different subunit compositions among O-LMs, PNs and BCs. Fourth, functional ASICs between O-LMs and BCs are composed of ASIC1a/2a and ASIC1a, respectively. Last, larger ASIC currents, which can induce APs, are also found in dendrites of O-LMs rather than PNs and BCs. Overall, our findings demonstrate that channel numbers, subunit compositions and gating of ASICs are cell type-specifically expressed between dendritic and perisomatic inhibitory GABAergic interneurons in hippocampus.

Comparisons between Native and Recombinant ASICs

Rare information about characteristics of native ASICs in cortex have been provided. Here we make some comparisons between native and recombinant ASICs. The single-channel conductance of recombinant ASICs obtained by single-channel recordings is 4.2 pS under 10 mM $[Ca^{2+}]_o$ and 11.2 pS under 1 mM $[Ca^{2+}]_o$ (Immke and McCleskey, 2003). The values are close to what we

obtained from NSFA (Fig. 7, 5.05, 6.57 and 6.29 pS for O-LMs, PNs and BCs, respectively). In addition, gating and kinetics of ASICs in this study quantitatively recapitulate the results from heterologous overexpression experiments (Askwith et al., 2004), whereas some differences still exist. Previous study shows recovery from desensitization of ASIC1a/2a heteromers is much faster than that of ASIC1a homomers and ASIC1a/2b heteromers, which is similar to what we observed (putative ASIC1a/2a heterotrimers in O-LMs vs putative ASIC1a homotrimers in BCs). However, the desensitization of the ASIC current is conflicting. Recombinant ASIC1a homomers display slower desensitization rate than that of ASIC1a/2a heteromers. ASIC currents on nucleated patches from O-LMs, in contrast, showed significantly slower desensitization than PNs and BCs. This conflict could be attributed to different post-translational modifications in recombinant and native ASICs. Different experimental methods and systems may also contribute to this contrast.

A study about ASIC subunit compositions has indicated that extracellular Zn^{2+} potentiates ASIC2a-containing ASIC currents (Baron et al., 2001). Therefore, Zn^{2+} modulation has been considered as an indicator for existence of ASIC2a subunit (Baron et al., 2002; Gao et al., 2004; Baron et al., 2008; Zhang et al., 2008). Another research about Zn^{2+} modulation, in contrast, indicates that Zn^{2+} works as a negative modulator of ASICs (Chu et al., 2004). Extracellular Zn^{2+} can persistently suppress ASIC current amplitudes mediated by not only ASIC1a/2a heteromers but also ASIC1a homomers in a high affinity way (Chu et al., 2004). The authors explained this conflict by proposing that the binding of Zn^{2+} to low-affinity sites(s) somehow interferes with the high-affinity binding site, thus reducing Zn^{2+} inhibition of the ASIC current. However in our case, ASIC currents in O-LMs, whose ASIC composition is ASIC1a/2a, showed no

differences with or without extracellular Zn^{2+} (Fig. 15). To test the hypothesis that binding of Zn^{2+} to low-affinity site(s) could affect the high Zn^{2+} modulation, we had tried low (1 μM) or high (300 μM) $[Zn^{2+}]_o$, but we observed no significant differences in ASIC currents (Fig. 15). In sum, low or high extracellular Zn^{2+}, exhibits no obvious modulation in our nucleated patches obtained from acute hippocampal slices and fast application system. Again, this difference could be resulted from the different experimental designs and systems.

Alternative Interpretations

In this study, we used multiple ways to manifest the expression of ASICs is cell type-specific in dendrite- and soma-targeting interneurons. Some experimental techniques and analyses, however, have drawbacks and limitations. These limitations may lead to various interpretations made based on our observations in this study.

The results of NSFA in this study suggest that nucleated patches from O-LMs have more channel number of ASIC. Nevertheless, the failure to fit the variance-mean plots of BCs by a polynomial function suggests a too low open probability and leads to the inability to estimate the channel number and open probability. Both smaller channel number and lower open probability can be used to explain the lower current density of ASICs in BCs. To obtain stable amplitudes of ASIC currents for NSFA, we had to repetitively apply acid pulses to a nucleated patch. The fast desensitized and slow recovery from desensitization of ASICs in BCs may lower the open probability in our experimental configurations. As a result, we could not rule out the possibility that lower ASIC current density in BCs is resulted from lower open probability.

Another potential problem of the NSFA of this study could be the initial slopes of the variance-mean plots of PNs. In some variance-mean plots of nucleated patches from PNs, the initial slopes are not as deeper as those of O-LMs implying that the single-channel current may not similar to those of O-LMs. If that was a case, both smaller channel number and single-channel conductance can explain the lower ASIC current density in PNs. Although the single-channel currents obtained by parabolic fitting suggest there is no significant difference among O-LMs, PNs and BCs, which is conflict to the difference in the initial slopes between O-LMs and PNs, the higher channel number in nucleated patches of O-LMs should be one of the reasons for higher ASIC current density.

In addition, to exchange extracellular solutions as fast as possible, we needed to put the nucleated patches close to the interface between neutral and acidic solutions released from theta tubes. If the interface was not clear enough, there could be a pH gradient on both sides of the interface. This invisible pH gradient could desensitize ASIC1a homomers in BCs more severely before the exchange to an acidic environment even we put the nucleated patches in a neutral solution. As a result, this pre-desensitization might partially contribute to smaller amplitudes of ASICs in PNs and BCs.

Although we detected larger dendritic ASIC currents in O-LMs by local acid puff, which is consistent with what we observed in nucleated patches, the imprecision of the air puff system cannot be ignored. Some experimental variations, such as the diameter of tips of the puff pipette and the distance between dendrites to the tip could not be controlled precisely in our experimental conditions. In addition, the fluorescent dendrites might grow into the deep parts of acute hippocampal slices; it was impossible to confirm how exact the pH values are the dendrites responded to. In other words, unlike to quantitative results done by nucleated patch recording and

the fast application system, we could not determine the exact dendritic ASIC current density in hippocampal neurons. Hence, direct dendritic outside-out patch recording may be necessary to compare dendritic ASIC currents in hippocampal neurons.

In figure 5, we performed dose-response experiments to demonstrate the pH dependence of H^+-activated currents on nucleated patches. However, the $pH_{0.5}$ obtained by Hill equation fitting could probably be underestimated. That is because acid solutions of pH 4.0 can actually induce larger currents in comparison with acid solutions of pH 5.0; the quick and severe rundown in amplitudes of following sweeps makes it difficult to obtain the average of peaks. Therefore, the reason why considering acid solutions of pH 5.0 as the plateau pH dose is because of the severe desensitization and slower recovery in amplitudes caused by the higher extracellular H^+ concentration.

These alternative interpretations resulted from experimental limitations or errors of estimations do not change the main story of this study. Though some of the details and conclusions may be affected, these potential problems should be verified and revised in the future.

Possible ASIC Compositions in PNs in Hippocampal CA1 Region

Possible ASIC compositions in PNs could be mixture of ASIC1a/2a and ASIC1a/2b. A recent research indicates that direct association between ASIC2a and PSD-95 can interact with ASIC1a to enrich functional ASICs in dendritic spines of PNs in mouse hippocampal CA1 region (Zha et al., 2009). Also, an earlier work suggests most of ASIC currents in PNs are through activation of ASIC1a/2a heteromers (Askwith et al., 2004). These reports suggest that functional ASIC compositions are ASIC1a/2a heteromers in PNs in mice. In

contrast to immunohistochemical results in mice, recovery from desensitization of ASIC currents of PNs in rats is much closer to compositions of ASIC1a/2b heteromers or ASIC1a homomers. By in situ hybridization, ASIC2b is expressed in PNs of hippocampus as well (Biagini et al., 2001). Owning to insensitivity to PcTX1, a selective antagonist of ASIC1a homomer, our results suggest that ASICs is not composed of ASIC1a homomers in PNs of rats. We did not concentrate on finding out the exact subunit compositions of ASICs in PNs. The cDNA sequences of ASIC2a and ASIC2b share 98% similarity and the specificity of antibodies for ASIC2 could also be a potential problem to tell ASIC2a from ASIC2b. Although our electrophysiological results support the existence of ASIC1a/2b heteromers in PNs of rats, we still cannot rule out the possibility that they could be mixture of ASIC1a/2a and ASIC1a/2b heteromers.

Functional Implications in Synaptic Transmission and Plasticity

Synaptic transmission is the most important way by how neuronal cells transmit signals. Functional ASICs are critical to LTP induction at CA3-CA1 synapses (Wemmie et al., 2002). ASIC1a is proposed to help activation of NMDA receptors for LTP induction by depolarizing the cell membrane and releasing Mg^{2+} blockade. Presynaptic release probability is increased in cortical neurons in ASIC1a null mice, suggesting that ASICs somehow influence synaptic efficacy (Cho and Askwith, 2008). By yeast two-hybrid assay, several important postsynaptic proteins, such as PSD-95, PICK and CaMKII, are reported to associate with ASICs (Wemmie et al., 2006). ASICs enriched at postsynaptic spines help spines become mature and responsive to acid (Zha et al., 2006; Zha et al., 2009). Moreover, H^+ is known to be loaded into synaptic

vesicles by vacuolar type H^+-ATPase and then co-released with neurotransmitters. Hence, ideal location and presynaptic H^+ release make ASICs a new candidate involved in synaptic transmission. However evoked synaptic ASIC currents, until now, have not been detected by whole-cell recording. In hippocampal primary culture, where nano ampere range of ASIC currents can be induced, blockade of AMPA receptors abolishes all excitatory synaptic transmission (Alvarez de la Rosa et al., 2003; Cho and Askwith, 2008). Amiloride, which can antagonize ASICs, has no effects to excitatory synaptic currents in cultured CA1 neurons. The lack of evidence about roles of ASIC in synaptic currents may be due to inappropriate experimental conditions (Wemmie et al., 2006). No any relevant results about evoked synaptic ASIC currents in acute brain slices have been published. Notably, interneurons in hilus have been proved to show significant ASIC expression (Wemmie et al., 2003) and recent studies, including ours, clarify interneurons have more functional ASIC currents (Cho and Askwith, 2008; Ziemann et al., 2008). Therefore, whether synaptic ASIC currents in interneurons in hilus can be detected by electrophysiology needs to be examined. Some other brain regions, such as the olfactory bulb, amygdala and cerebellum, express higher ASICs than hippocampus. It is still necessary to verify the roles of ASIC in synaptic transmission in these brain regions. On the other hand, FMRFamide and its related peptides could prolong ASIC gating and large extracellular loop of ASICs may also possibly response to other unidentified ligands (Askwith et al., 2000; Wemmie et al., 2006). Additionally, lactate, which is released by astrocytes for energy metabolism or accumulated by anaerobic respiration during ischemia, can enhance ASIC currents as well (Immke and McCleskey, 2001; Allen and Attwell, 2002). Therefore, many physiological components,

which are prominent for ASIC regulation, may be absent in ACSF. It is highly possible that synaptic ASIC currents can be recorded by *in vivo* whole-cell recording.

ASICs may also play some roles in synaptic transmission as presynaptic ion channels. ASIC2a is reported to locate not only in somata and dendrites but also in axons (Duggan et al., 2002; Zha et al., 2009). Presynaptic ASICs can make membrane potentials of axonal terminals more sensitive to extracellular pH fluctuations than those of somata because tiny axonal compartments with high input resistance require smaller excitatory inputs to fire APs. This possible regulatory role is similar to the depolarizing presynaptic $GABA_A$ receptors at hippocampal mossy fiber boutons, which can increase synaptic transmission and facilitate LTP induction (Ruiz et al., 2010). Therefore, if functional ASICs expressed at axonal terminals, small extracellular pH fluctuations are possible to depolarize presynaptic regions or even fire APs by activating presynaptic ASICs. Since roles of ASICs in synaptic transmission are unclear, both in pre- and postsynaptic regions, more effort is required to understand the roles of ASICs in synaptic transmission.

Possible Functions of Nonconducting States of ASICs

As mentioned previously, postsynaptic ASIC currents have not been recorded in the present studies. Although immunostaining results reveal that ASIC1a and ASIC2a are enriched in postsynaptic spines of PNs, both subunits are also expressed in somata and dendritic shafts. In a word, ASICs are distributed throughout the membrane of a neuron. There is another possibility that conducting Na^+ currents may not be the only destination of ASICs. The studies demonstrating that ASICs are required for

LTP at CA3-CA1 synapses and negligible evoked postsynaptic ASIC currents suggest that ASICs may exhibit their functions except current conduction. In other words, H^+ or other extracellular components could possibly activate ASICs without conducting currents. This kind of activation may still trigger some intracellular signaling for cellular functions. For instance, ASIC2 plays a negative modulator of rod phototransduction (Ettaiche et al., 2004). However, no direct evidence suggests synaptic ASIC currents can be recorded in the retina. Therefore, activation of ASICs probably help Mg^{2+} unblock on NMDA receptors through some ways other than conducting currents. Though extracellular H^+ activates ASIC currents to conduct Na^+ influx, we cannot rule out the possibility that ASICs may exert their functions without conducting currents.

Roles of ASIC3 and ASIC4 in the Brain

Although roles of ASIC3 and ASIC4 in brains have not been identified, their functions should be considered and elucidated in the near future. Cultured or dissociated hippocampal neurons without ASIC1a subunits exhibit no typical ASIC currents (Wemmie et al., 2002; Ziemann et al., 2008). Some left sustained currents could be resulted from inactivation of potassium channels (Taverna et al., 2005). However, by analyses of RT-PCR and immunohistochemical staining, a previous study indicates that beside dorsal root ganglia, ASIC3 subunits are also widely distributed in many brain regions of rats, such as hippocampus, amygdala, caudate putamen, prefrontal cortex and hypothalamus (Meng et al., 2009). Though there is no evidence in that study showing whether ASIC3 is also expressed in interneurons, it still implies that GABAergic interneurons have ASIC3 subunits. Whether functional ASIC3 is expressed in hippocampal neurons could be examined by

application of a selective inhibitor, APETx2 (Chagot et al., 2005). APETx2 can be used to potently and selectively suppress H^+-activated currents conducted by ASIC3-containing ASICs.

Besides, ASIC3 and 4 can possibly exert previous mentioned nonconducting functions. ASIC4 is the only one subunit that is not able to conduct currents, but it has a longer N-terminal domain compared to other ASIC subunits. That makes ASIC4 has more chances to associate with intracellular proteins. In fact, results of yeast two-hybrid assay reveal that ASICs have interactions with cytoskeletal proteins, enzymes, regulators of endocytosis and G protein-coupled pathways (Donier et al., 2008). These functionally distinct proteins, which can interact with ASICs, probably represent multiple intracellular functions of ASICs. In particular, the expression of ASIC4 downregulates both ASIC1a and ASIC3 in current amplitudes and protein levels (Donier et al., 2008). Whether distinct ASIC4 expression leads to various ASIC1a and ASIC3 expression in hippocampal neurons needs to be confirmed. In addition, ASIC2b/3 heteromers, but not ASIC3 homomers, can be positively regulated by protein kinase C pathway through the interaction between ASIC2b and PICK1 in DRG neurons (Deval et al., 2004). This interaction shifts the pH dependence of ASIC2b/3 toward a more physiological value. After confirming that both ASIC2b and 3 are expressed in the brain, such intracellular regulation may also happen in hippocampal neurons. Despite the fact that ASIC1a and ASIC2a subunits are heterogeneously expressed, ASIC3 and ASIC4 subunits may also play some roles in various pH sensitivity and intracellular signaling in hippocampal neurons. It is much more appropriate to consider ASIC3 and ASIC4 when thinking about functions of ASICs in the brain. Nevertheless, it will be difficult to isolate functions of ASIC4 due to lack of selective antagonists. Nowadays, only can PcTX1 and APETx2 be used to pharmacologically isolate ASIC1a homomers and ASIC3-containing ASICs,

respectively. If multiple sets of ASIC complexes are expressed in the same cells, the only way to differentiate is to use ASIC knockout mice. Mice lacking ASIC1a, ASIC2a and ASIC3 have been generated and studied for years. To reveal the roles of each kind of ASICs in neurophysiology, we need to generate or obtain different ASIC knockout mice. It is also necessary to conditionally eliminate ASICs in interneurons to elucidate why dendritic and perisomatic inhibitory interneurons exhibit distinct ASIC expressions and how GABAergic inhibition responses to extracellular pH fluctuations.

Differential Expressions of ASICs in Interneurons in Pathology Conditions

The blockade of functional ASICs, such as gene targeting or antagonists, can also prevent neuronal cell deaths caused by the acidosis accompanied with ischemia (Xiong et al., 2006; Pignataro et al., 2007; Xiong et al., 2008; Xu and Duan, 2009). Even after carrying out the procedures of focal ischemia mouse model (middle cerebral artery occlusion), intracerebroventricular administration of PcTX1, which is a specific blocker of ASIC1a homomers, can decrease the infract volume of the brain significantly. This post-ischematic protection can also be achieved by intranasal administration of PcTX1 through the nasal cavity, which is clinically useful (Pignataro et al., 2007). Therefore, the ASIC1a blockade has the potential to become an effective strategy to control post-ischemia neuronal damage. However, PcTX1 does not exhibit noticeable inhibition on ASIC currents in O-LMs and PNs (Fig. 13). Why does PcTX1 show neuroprotective effects in the ischemia mouse model? One possibility is that ASIC1a blockade prevents BCs being hyper-activated in the acidosis induced by ischemia; therefore the hyperpolarizing effect of perisomatic inhibitory BCs can further protect principal cells from glutamate-dependent excitotoxicity.

Each single BC can target 1500-2000 principal cells (Freund and Kali, 2008) and PcTX1 plus NMDA receptor antagonists exert better neuroprotective effects in the ischemia model (Xiong et al., 2004; Gao et al., 2005; Pignataro et al., 2007). In the neocortex, about 50% of all inhibitory interneurons are BCs (Markram et al., 2004). ASIC1a blockade protects BCs from excitotoxicity, and the widely distributed axons enable the survival BCs to prevent focal neuronal populations from glutamate-dependent excitotoxicity. The second possibility is that ASIC subunits are not homogeneously distributed on the cell membrane of a PN. Though the insensitivity to PcTX1 and detectable ASIC1a and 2 mRNAs suggest somatic ASICs of hippocampal PNs are not ASIC1a homomers, dendritic ASICs may still be composed of ASIC1a homomers. Because neurons are highly specialized cells, the density and subtype of ion channels may be distinct in axons, somata and dendrites (Hoffman et al., 1997). For example, unlike axons, which require Na_V for propagation of APs, dendrites of hippocampal BCs show no detectable Na_V currents (Hu et al., 2009). Since the dendritic membrane accounts for larger parts of total membrane area of a PN, blockade of dendritic ASIC1a homomers may be the reason why PcTX1 has effective post-ischematic neuroprotection.

Additionally, Our results, which clarify the differential expression of ASICs in interneurons, suggest that brain pH drops caused by acidosis have distinct impacts on hippocampal interneurons. Dendrite-targeting O-LMs have been reported to be more vulnerable than soma-targeting BCs in epilepsy (Morin et al., 1998; Cossart et al., 2001; Wittner et al., 2001; Wittner et al., 2005). What we uncovered in this study may explain the variant vulnerabilities of interneurons to epilepsy. AP could only be fired by acid puff on O-LMs with larger input resistance and ASIC density but not on PNs or BCs (Fig. 1, 4 and 9). In pathological conditions, depolarization induced by acidosis could allow more

Ca^{2+} influx through voltage-gated Ca^{2+} channel in O-LMs, whose Ca^{2+} buffer capacity is smaller than that of BCs (Liao and Lien, 2009). This Ca^{2+} influx could further induce glutamate-independent and Ca^{2+}-dependent excitotoxicity (Xiong et al., 2008). Besides, lactate, which is accumulated during epilepsy, may potentiate ASIC responses (Immke and McCleskey, 2001; Allen and Attwell, 2002). BCs, on the other hand, with less ASICs and larger Ca^{2+} buffer capacity are more resistant to acidosis-induced excitotoxicity (Aponte et al., 2008). As a result, based on previous studies and our results, the variant vulnerabilities of dendrite-targeting and soma-targeting interneurons can be explained by different ASIC current density and Ca^{2+} buffer capacity.

Although interneurons with higher ASIC current density, such as O-LMs, are more sensitive to epilepsy, they may play a network suppression role, at the beginning of epilepsy, because activation of ASICs can induce activity-dependent GABA release to inhibit neuronal hyperactivities. BCs, with lower ASIC current density, may be less helpful for the seizure termination during the onset of epilepsy but they should have a better chance to survive in the following neuronal injury. Collectively, our findings suggest that cell type-specific expression of ASICs and different Ca^{2+} buffer capacity of interneurons lead to different cellular vulnerability to epilepsy. Dendrite-targeting interneurons may play a more important role in spontaneous seizure termination than soma-targeting interneurons duo to higher ASIC current density.

Roles of Cell Type-Specific Expression of ASICs on Functional Dissimilarities of O-LMs and BCs

Many morphological, functional and intrinsic differences have been documented in O-LMs and BCs (Cobb et al., 1995; Miles et al., 1996; Kraushaar

and Jonas, 2000; Martina et al., 2000; Aponte et al., 2008; Klausberger and Somogyi, 2008; Liao and Lien, 2009). The gradual increases in EPSPs of O-LMs corresponding to the repetitive stimulation on Schaffer Collaterals makes dendrite-targeting O-LMs signal integrators, and soma-targeting BCs, on the other hand, with the gradual decreases in EPSPs serve as coincidence detectors (Pouille and Scanziani, 2004). Five various properties determine this functional dissimilarity: EPSC kinetics, membrane time constant, short-term plasticity, disynaptic inhibition of interneurons and dendritic properties (Martina et al., 2000; Pouille and Scanziani, 2004; Hu et al., 2009). This functional dissimilarity could be further magnified if ASICs involve in synaptic transmission onto these two types of interneurons. ASIC currents of fast recovery and slow desensitization in O-LMs maintain stable during repetitive stimulation. In contrast, slow recovered and fast desensitized ASIC currents in BCs will exhibit severe rundown in amplitudes corresponding to repetitive stimulation. This different ASIC gating possibly further influences the information processing in which O-LMs and BCs involve. Besides, heterogeneous expression of ASICs in interneurons implies that interneurons of dendritic inhibition or perisomatic inhibition could respond accordingly to brain pH changes in numerous situations. Therefore, differential ASIC expression between dendritic inhibitory and perisomatic inhibitory interneurons add complexity to GABAergic microcircuits in hippocampus.

References

Allen NJ, Attwell D (2002) Modulation of ASIC channels in rat cerebellar Purkinje neurons by ischaemia-related signals. J Physiol 543:521-529.

Alvarez de la Rosa D, Zhang P, Shao D, White F, Canessa C (2002) Functional implications of the localization and activity of acid-sensitive channels in rat peripheral nervous system. Proc Natl Acad Sci U S A 99:2326-2331.

Alvarez de la Rosa D, Krueger S, Kolar A, Shao D, Fitzsimonds R, Canessa C (2003) Distribution, subcellular localization and ontogeny of ASIC1 in the mammalian central nervous system. J Physiol 546:77-87.

Aponte Y, Bischofberger J, Jonas P (2008) Efficient Ca^{2+} buffering in fast-spiking basket cells of rat hippocampus. J Physiol 586:2061-2075.

Aponte Y, Lien CC, Reisinger E, Jonas P (2006) Hyperpolarization-activated cation channels in fast-spiking interneurons of rat hippocampus. J Physiol 574:229-243.

Askwith C, Wemmie J, Price M, Rokhlina T, Welsh M (2004) Acid-sensing ion channel 2 (ASIC2) modulates ASIC1 H^+-activated currents in hippocampal neurons. J Biol Chem 279:18296-18305.

Askwith C, Cheng C, Ikuma M, Benson C, Price M, Welsh M (2000) Neuropeptide FF and FMRFamide potentiate acid-evoked currents from sensory neurons and proton-gated DEG/ENaC channels. Neuron 26:133-141.

Baron A, Waldmann R, Lazdunski M (2002) ASIC-like, proton-activated currents in rat hippocampal neurons. J Physiol 539:485-494.

Baron A, Voilley N, Lazdunski M, Lingueglia E (2008) Acid sensing ion channels in dorsal spinal cord neurons. J Neurosci 28:1498-1508.

Baron A, Schaefer L, Lingueglia E, Champigny G, Lazdunski M (2001) Zn^{2+} and H^+ are coactivators of acid-sensing ion channels. J Biol Chem 276:35361-35367.

Bartos M, Vida I, Frotscher M, Meyer A, Monyer H, Geiger JR, Jonas P (2002) Fast synaptic inhibition promotes synchronized gamma oscillations in hippocampal interneuron networks. Proc Natl Acad Sci U S A 99:13222-13227.

Benson CJ, Xie J, Wemmie JA, Price MP, Henss JM, Welsh MJ, Snyder PM (2002) Heteromultimers of DEG/ENaC subunits form H^+-gated channels in mouse sensory neurons. Proc Natl Acad Sci U S A 99:2338-2343.

Biagini G, Babinski K, Avoli M, Marcinkiewicz M, Séguéla P (2001) Regional and subunit-specific downregulation of acid-sensing ion channels in the pilocarpine model of epilepsy. Neurobiol Dis 8:45-58.

Buzsáki G, Draguhn A (2004) Neuronal oscillations in cortical networks. Science 304:1926-1929.

Carnally S, Dev H, Stewart A, Barrera N, Van Bemmelen M, Schild L, Henderson R, Edwardson J (2008) Direct visualization of the trimeric structure of the ASIC1a channel, using AFM imaging. Biochem Biophys Res Commun 372:752-755.

Chagot B, Escoubas P, Diochot S, Bernard C, Lazdunski M, Darbon H (2005) Solution structure of APETx2, a specific peptide inhibitor of ASIC3 proton-gated channels. Protein Sci 14:2003-2010.

Chen X, Kalbacher H, Gründer S (2005) The tarantula toxin psalmotoxin 1 inhibits acid-sensing ion channel (ASIC) 1a by increasing its apparent H^+ affinity. J Gen Physiol 126:71-79.

Cho JH, Askwith CC (2008) Presynaptic release probability is increased in hippocampal neurons from ASIC1 knockout mice. J Neurophysiol 99:426-441.

Chu X, Wemmie J, Wang W, Zhu X, Saugstad J, Price M, Simon R, Xiong Z (2004) Subunit-dependent high-affinity zinc inhibition of acid-sensing ion channels. J Neurosci 24:8678-8689.
Cobb SR, Buhl EH, Halasy K, Paulsen O, Somogyi P (1995) Synchronization of neuronal activity in hippocampus by individual GABAergic interneurons. Nature 378:75-78.
Cossart R, Dinocourt C, Hirsch JC, Merchan-Perez A, De Felipe J, Ben-Ari Y, Esclapez M, Bernard C (2001) Dendritic but not somatic GABAergic inhibition is decreased in experimental epilepsy. Nat Neurosci 4:52-62.
Davenport CJ, Brown WJ, Babb TL (1990) Sprouting of GABAergic and mossy fiber axons in dentate gyrus following intrahippocampal kainate in the rat. Exp Neurol 109:180-190.
Deval E, Salinas M, Baron A, Lingueglia E, Lazdunski M (2004) ASIC2b-dependent regulation of ASIC3, an essential acid-sensing ion channel subunit in sensory neurons via the partner protein PICK-1. J Biol Chem 279:19531-19539.
Donier E, Rugiero F, Jacob C, Wood J (2008) Regulation of ASIC activity by ASIC4--new insights into ASIC channel function revealed by a yeast two-hybrid assay. Eur J Neurosci 28:74-86.
Duggan A, Garcia-Anoveros J, Corey DP (2002) The PDZ domain protein PICK1 and the sodium channel BNaC1 interact and localize at mechanosensory terminals of dorsal root ganglion neurons and dendrites of central neurons. J Biol Chem 277:5203-5208.
Efron B, Tibshirani R (1998) An introduction to the bootstrap, 1st CRC Press reprint. Edition. Boca Raton, Fla.: Chapman & Hall/CRC.
Engel D, Jonas P (2005) Presynaptic action potential amplification by voltage-gated Na^+ channels in hippocampal mossy fiber boutons. Neuron 45:405-417.
Ettaiche M, Guy N, Hofman P, Lazdunski M, Waldmann R (2004) Acid-sensing ion channel 2 is important for retinal function and protects against light-induced retinal degeneration. J Neurosci 24:1005-1012.
Freund T, Kali S (2008) Interneurons. Scholarpedia 3:4720.
Friese M, Craner M, Etzensperger R, Vergo S, Wemmie J, Welsh M, Vincent A, Fugger L (2007) Acid-sensing ion channel-1 contributes to axonal degeneration in autoimmune inflammation of the central nervous system. Nat Med 13:1483-1489.
Gao J, Wu L, Xu L, Xu T (2004) Properties of the proton-evoked currents and their modulation by Ca^{2+} and Zn^{2+} in the acutely dissociated hippocampus CA1 neurons. Brain Res 1017:197-207.
Gao J, Duan B, Wang D, Deng X, Zhang G, Xu L, Xu T (2005) Coupling between NMDA receptor and acid-sensing ion channel contributes to ischemic neuronal death. Neuron 48:635-646.
García-Añoveros J, Derfler B, Neville-Golden J, Hyman B, Corey D (1997) BNaC1 and BNaC2 constitute a new family of human neuronal sodium channels related to degenerins and epithelial sodium channels. Proc Natl Acad Sci U S A 94:1459-1464.
Gentet LJ, Stuart GJ, Clements JD (2000) Direct measurement of specific membrane capacitance in neurons. Biophys J 79:314-320.
Gibbs JW, 3rd, Shumate MD, Coulter DA (1997) Differential epilepsy-associated alterations in postsynaptic GABA(A) receptor function in dentate granule and CA1 neurons. J Neurophysiol 77:1924-1938.

Hartveit E, Veruki ML (2007) Studying properties of neurotransmitter receptors by non-stationary noise analysis of spontaneous postsynaptic currents and agonist-evoked responses in outside-out patches. Nat Protoc 2:434-448.
Hille B (2001) Ion channels of excitable membranes, 3rd Edition. Sunderland, Mass.: Sinauer.
Hoffman DA, Magee JC, Colbert CM, Johnston D (1997) K^+ channel regulation of signal propagation in dendrites of hippocampal pyramidal neurons. Nature 387:869-875.
Hu H, Martina M, Jonas P (2009) Dendritic mechanisms underlying rapid synaptic activation of fast-spiking hippocampal interneurons. Science 327:52-58.
Ichikawa H, Sugimoto T (2002) The co-expression of ASIC3 with calcitonin gene-related peptide and parvalbumin in the rat trigeminal ganglion. Brain Res 943:287-291.
Immke DC, McCleskey EW (2001) Lactate enhances the acid-sensing Na+ channel on ischemia-sensing neurons. Nat Neurosci 4:869-870.
Immke DC, McCleskey EW (2003) Protons open acid-sensing ion channels by catalyzing relief of Ca^{2+} blockade. Neuron 37:75-84.
Jasti J, Furukawa H, Gonzales E, Gouaux E (2007) Structure of acid-sensing ion channel 1 at 1.9 Å resolution and low pH. Nature 449:316-323.
Jonas P, Bischofberger J, Fricker D, Miles R (2004) Interneuron Diversity series: Fast in, fast out--temporal and spatial signal processing in hippocampal interneurons. Trends Neurosci 27:30-40.
Klausberger T, Somogyi P (2008) Neuronal diversity and temporal dynamics: the unity of hippocampal circuit operations. Science 321:53-57.
Klausberger T, Magill PJ, Marton LF, Roberts JD, Cobden PM, Buzsaki G, Somogyi P (2003) Brain-state- and cell-type-specific firing of hippocampal interneurons in vivo. Nature 421:844-848.
Koh DS, Geiger JR, Jonas P, Sakmann B (1995) Ca^{2+}-permeable AMPA and NMDA receptor channels in basket cells of rat hippocampal dentate gyrus. J Physiol 485 (Pt 2):383-402.
Kraushaar U, Jonas P (2000) Efficacy and stability of quantal GABA release at a hippocampal interneuron-principal neuron synapse. J Neurosci 20:5594-5607.
Lalo U, Pankratov Y, North R, Verkhratsky A (2007) Spontaneous autocrine release of protons activates ASIC-mediated currents in HEK293 cells. J Cell Physiol 212:473-480.
Liao CW, Lien CC (2009) Estimating intracellular Ca^{2+} concentrations and buffering in a dendritic inhibitory hippocampal interneuron. Neuroscience 164:1701-1711.
Lien CC, Jonas P (2003) Kv3 potassium conductance is necessary and kinetically optimized for high-frequency action potential generation in hippocampal interneurons. J Neurosci 23:2058-2068.
Lien CC, Martina M, Schultz JH, Ehmke H, Jonas P (2002) Gating, modulation and subunit composition of voltage-gated K^+ channels in dendritic inhibitory interneurones of rat hippocampus. J Physiol 538:405-419.
Lilley S, Robbins J (2005) The rat retinal ganglion cell in culture: an accessible CNS neurone. J Pharmacol Toxicol Methods 51:209-220.
Liss B (2002) Improved quantitative real-time RT-PCR for expression profiling of individual cells. Nucleic Acids Res 30:e89.

Markram H, Toledo-Rodriguez M, Wang Y, Gupta A, Silberberg G, Wu C (2004) Interneurons of the neocortical inhibitory system. Nat Rev Neurosci 5:793-807.
Martina M, Jonas P (1997) Functional differences in Na^+ channel gating between fast-spiking interneurones and principal neurones of rat hippocampus. J Physiol 505 (Pt 3):593-603.
Martina M, Vida I, Jonas P (2000) Distal initiation and active propagation of action potentials in interneuron dendrites. Science 287:295-300.
Martina M, Schultz JH, Ehmke H, Monyer H, Jonas P (1998) Functional and molecular differences between voltage-gated K^+ channels of fast-spiking interneurons and pyramidal neurons of rat hippocampus. J Neurosci 18:8111-8125.
McBain CJ, Fisahn A (2001) Interneurons unbound. Nat Rev Neurosci 2:11-23.
Meng QY, Wang W, Chen XN, Xu TL, Zhou JN (2009) Distribution of acid-sensing ion channel 3 in the rat hypothalamus. Neuroscience 159:1126-1134.
Metz AE, Jarsky T, Martina M, Spruston N (2005) R-type calcium channels contribute to afterdepolarization and bursting in hippocampal CA1 pyramidal neurons. J Neurosci 25:5763-5773.
Miles R, Tóth K, Gulyás A, Hájos N, Freund T (1996) Differences between somatic and dendritic inhibition in the hippocampus. Neuron 16:815-823.
Molliver DC, Immke DC, Fierro L, Pare M, Rice FL, McCleskey EW (2005) ASIC3, an acid-sensing ion channel, is expressed in metaboreceptive sensory neurons. Mol Pain 1:35.
Morin F, Beaulieu C, Lacaille JC (1998) Selective loss of GABA neurons in area CA1 of the rat hippocampus after intraventricular kainate. Epilepsy Res 32:363-369.
Nusser Z, Hájos N, Somogyi P, Mody I (1998) Increased number of synaptic $GABA_A$ receptors underlies potentiation at hippocampal inhibitory synapses. Nature 395:172-177.
Pignataro G, Simon R, Xiong Z (2007) Prolonged activation of ASIC1a and the time window for neuroprotection in cerebral ischaemia. Brain 130:151-158.
Pouille F, Scanziani M (2004) Routing of spike series by dynamic circuits in the hippocampus. Nature 429:717-723.
Price MP, Snyder PM, Welsh MJ (1996) Cloning and expression of a novel human brain Na^+ channel. J Biol Chem 271:7879-7882.
Ruiz A, Campanac E, Scott RS, Rusakov DA, Kullmann DM (2010) Presynaptic $GABA_A$ receptors enhance transmission and LTP induction at hippocampal mossy fiber synapses. Nat Neurosci 13:431-438.
Samways DS, Harkins AB, Egan TM (2009) Native and recombinant ASIC1a receptors conduct negligible Ca^{2+} entry. Cell Calcium 45:319-325.
Sherwood T, Askwith C (2009) Dynorphin opioid peptides enhance acid-sensing ion channel 1a activity and acidosis-induced neuronal death. J Neurosci 29:14371-14380.
Sík A, Hájos N, Gulácsi A, Mody I, Freund TF (1998) The absence of a major Ca^{2+} signaling pathway in GABAergic neurons of the hippocampus. Proc Natl Acad Sci U S A 95:3245-3250.
Singer W (1999) Neuronal synchrony: a versatile code for the definition of relations? Neuron 24:49-65, 111-125.
Somogyi P, Klausberger T (2005) Defined types of cortical interneurone structure space and spike timing in the hippocampus. J Physiol 562:9-26.

Stuart GJ, Dodt HU, Sakmann B (1993) Patch-clamp recordings from the soma and dendrites of neurons in brain slices using infrared video microscopy. Pflugers Arch 423:511-518.
Sutherland SP, Benson CJ, Adelman JP, McCleskey EW (2001) Acid-sensing ion channel 3 matches the acid-gated current in cardiac ischemia-sensing neurons. Proc Natl Acad Sci U S A 98:711-716.
Taverna S, Tkatch T, Metz AE, Martina M (2005) Differential expression of TASK channels between horizontal interneurons and pyramidal cells of rat hippocampus. J Neurosci 25:9162-9170.
Ugawa S, Ueda T, Yamamura H, Shimada S (2005) In situ hybridization evidence for the coexistence of ASIC and TRPV1 within rat single sensory neurons. Brain Res Mol Brain Res 136:125-133.
Vessey JP, Stratis AK, Daniels BA, Da Silva N, Jonz MG, Lalonde MR, Baldridge WH, Barnes S (2005) Proton-mediated feedback inhibition of presynaptic calcium channels at the cone photoreceptor synapse. J Neurosci 25:4108-4117.
Vida I, Bartos M, Jonas P (2006) Shunting inhibition improves robustness of gamma oscillations in hippocampal interneuron networks by homogenizing firing rates. Neuron 49:107-117.
Waldmann R, Champigny G, Voilley N, Lauritzen I, Lazdunski M (1996) The mammalian degenerin MDEG, an amiloride-sensitive cation channel activated by mutations causing neurodegeneration in Caenorhabditis elegans. J Biol Chem 271:10433-10436.
Waldmann R, Champigny G, Bassilana F, Heurteaux C, Lazdunski M (1997) A proton-gated cation channel involved in acid-sensing. Nature 386:173-177.
Wang W, Duan B, Xu H, Xu L, Xu TL (2006) Calcium-permeable acid-sensing ion channel is a molecular target of the neurotoxic metal ion lead. J Biol Chem 281:2497-2505.
Wemmie J, Price M, Welsh M (2006) Acid-sensing ion channels: advances, questions and therapeutic opportunities. Trends Neurosci 29:578-586.
Wemmie J, Askwith C, Lamani E, Cassell M, Freeman W, MJ (2003) Acid-sensing ion channel 1 is localized in brain regions with high synaptic density and contributes to fear conditioning. J Neurosci 23:5496-5502.
Wemmie J, Chen J, Askwith C, Hruska-Hageman A, Price M, Nolan B, Yoder P, Lamani E, Hoshi T, Freeman W, MJ (2002) The acid-activated ion channel ASIC contributes to synaptic plasticity, learning, and memory. Neuron 34:463-477.
West MJ, Coleman PD, Flood DG, Troncoso JC (1994) Differences in the pattern of hippocampal neuronal loss in normal ageing and Alzheimer's disease. Lancet 344:769-772.
Wittner L, Eross L, Czirják S, Halász P, Freund TF, Maglóczky Z (2005) Surviving CA1 pyramidal cells receive intact perisomatic inhibitory input in the human epileptic hippocampus. Brain 128:138-152.
Wittner L, Maglóczky Z, Borhegyi Z, Halász P, Tóth S, Eross L, Szabó Z, Freund TF (2001) Preservation of perisomatic inhibitory input of granule cells in the epileptic human dentate gyrus. Neuroscience 108:587-600.
Xiong Z, Chu X, Simon R (2006) Ca^{2+} -permeable acid-sensing ion channels and ischemic brain injury. J Membr Biol 209:59-68.
Xiong Z, Pignataro G, Li M, Chang S, Simon R (2008) Acid-sensing ion channels (ASICs) as pharmacological targets for neurodegenerative diseases. Curr Opin Pharmacol 8:25-32.

Xiong Z, Zhu X, Chu X, Minami M, Hey J, Wei W, MacDonald J, Wemmie J, Price M, Welsh M, Simon R (2004) Neuroprotection in ischemia: blocking calcium-permeable acid-sensing ion channels. Cell 118:687-698.

Xu TL, Duan B (2009) Calcium-permeable acid-sensing ion channel in nociceptive plasticity: a new target for pain control. Prog Neurobiol 87:171-180.

Yermolaieva O, Leonard AS, Schnizler MK, Abboud FM, Welsh MJ (2004) Extracellular acidosis increases neuronal cell calcium by activating acid-sensing ion channel 1a. Proc Natl Acad Sci U S A 101:6752-6757.

Zha X, Wemmie J, Green S, Welsh M (2006) Acid-sensing ion channel 1a is a postsynaptic proton receptor that affects the density of dendritic spines. Proc Natl Acad Sci U S A 103:16556-16561.

Zha X, Costa V, Harding A, Reznikov L, Benson C, Welsh M (2009) ASIC2 subunits target acid-sensing ion channels to the synapse via an association with PSD-95. J Neurosci 29:8438-8446.

Zhang M, Gong N, Lu Y, Jia N, Xu T, Chen L (2008) Functional characterization of acid-sensing ion channels in cultured neurons of rat inferior colliculus. Neuroscience 154:461-472.

Zhang P, Canessa C (2002) Single channel properties of rat acid-sensitive ion channel-1alpha, -2a, and -3 expressed in Xenopus oocytes. J Gen Physiol 120:553-566.

Ziemann A, Schnizler M, Albert G, Severson M, Howard W, MJ W, JA (2008) Seizure termination by acidosis depends on ASIC1a. Nat Neurosci 11:816-822.

Ziemann A, Allen J, Dahdaleh N, Drebot I, Coryell M, Wunsch A, Lynch C, Faraci F, Howard W, MJ W, JA (2009) The amygdala is a chemosensor that detects carbon dioxide and acidosis to elicit fear behavior. Cell 139:1012-1021.

Table and Figures

Table. 1 Primers for ScRT-PCR

Gene	Sequence	Size (bp)
ASIC1a	f: 5'-GAACATTCTGGTGCTGGACATT-3'	184
	r: 5'-CCTGTGCTTAATGACCTCGTAG-3'	
ASIC2	f: 5'-CGCACAACTTCTCCTCAGTGTTT-3'	146
	r: 5'-GTACTCATCTTGCTGAATGTCCA-3'	
Calcineurin	f: 5'-CCGAGCCCACGAAGCCCAGG-3'	337
	r: 5'-TGCAGCCGTGGCTCCGTCAA-3'	
Cholecystokinin	f: 5'-GCTGGACAGCAGCCGTTGGA-3'	280
	r: 5'-GGCCAGAGGGAGCTTTGCGG-3'	
GAD65	f: 5'-TGGCATCTCCGGGCTCTGGCT-3'	297
	r: 5'-TGGCAGCAGGTCTGTTGCGTGG-3'	
Neurofilament3	f: 5'-TCGCCGCATATAGGAAACTACTG-3'	95
	r: 5'-GGGCTGTCGGTGTGTGTACA-3'	
Parvalbumin	f: 5'-GGCGATAGGAGCCTTTACTGCTGC-3'	372
	r: 5'-GAAACCCAGGAGGGCCGCGA-3'	
Somatostatin	f: 5'-GGCTGCCACCGGGAAACAGGAAC-3'	119
	r: 5'-CCTGCTCAGCTGCCTGGGGC-3'	

ASIC2a and ASIC2b mRNAs were detected with a pair of common primers.

Fig. 1 Firing Patterns and Morphologies of an O-LMs, a PN and a BC

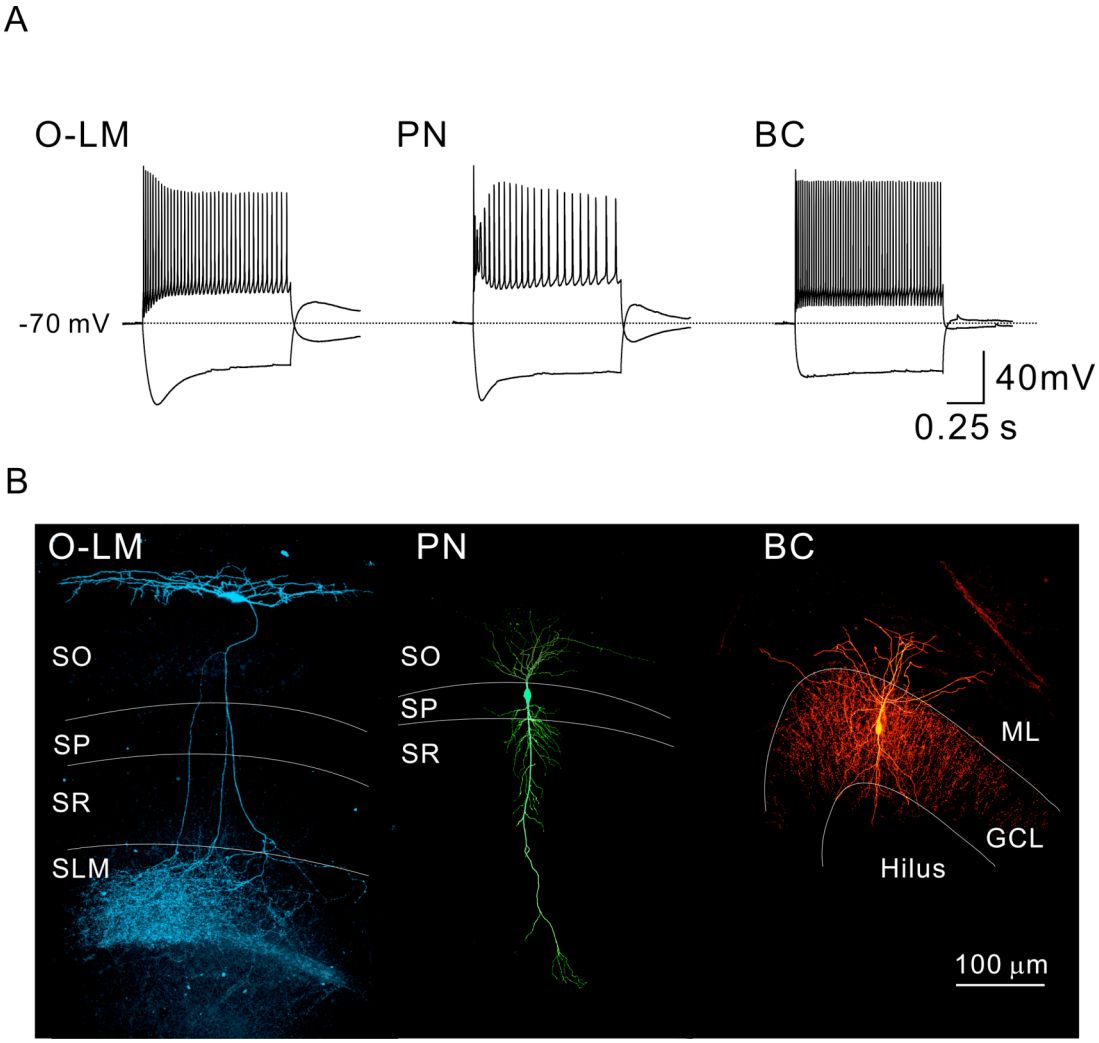

A. Firing patterns induced by 1-s depolarization (600 pA) and hyperpolarization (-300 pA) of an O-LM and a PN in CA1 region and a BC in DG. Whole-cell recordings were current-clamped at -70 mV.

B. Morphological reconstructions of the same three biocytin-loaded cells in (A) by *post hoc* histochemial staining and scanned by two-photon microscopy.

Fig. 2 Different K_V Components among O-LMs, PNs and BCs

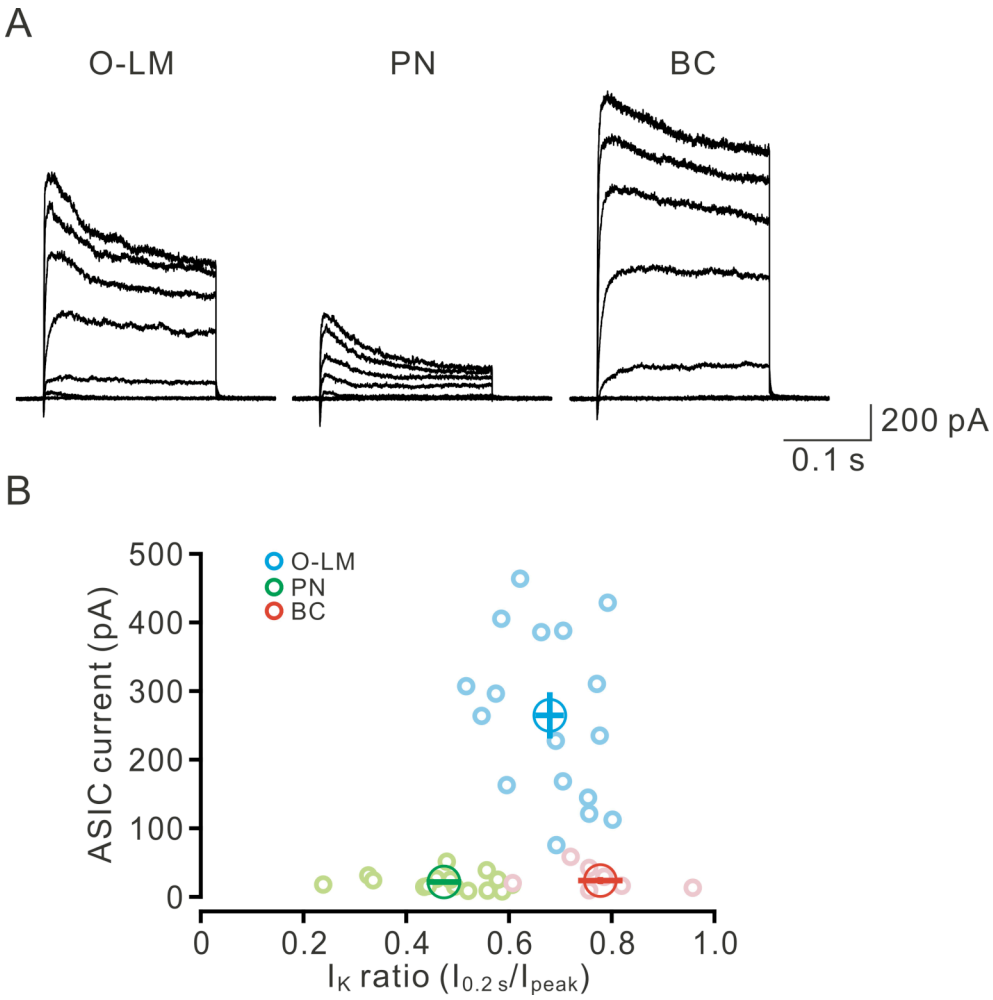

A. K_V current responses of nucleated patches from an O-LM, a PN and a BC under voltage steps from -100 mV to +70 mV for 200 msec.

B. A scatter plot of K_V current ratio (200 ms/peak) against ASIC amplitudes. Blue open circle, O-LMs; green open circle, PNs; red open circles, BCs.

Fig. 3 Cell Type-Specific Markers for O-LMs, PNs and BCs

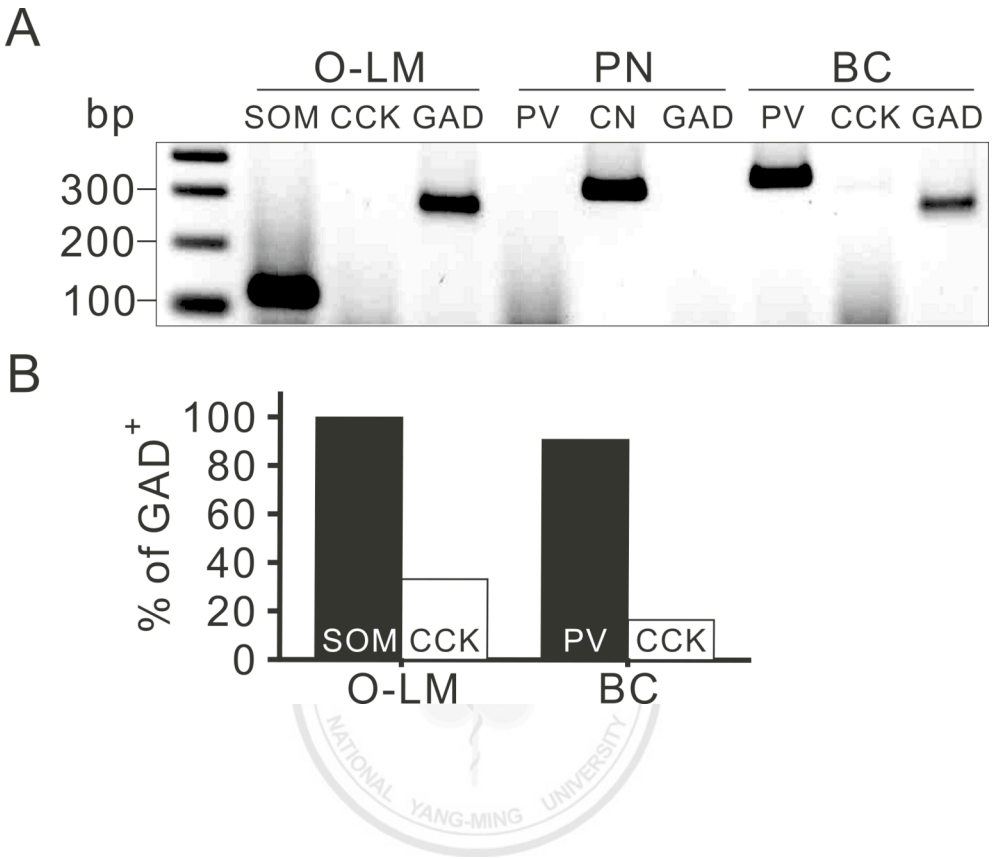

A. An electrophoresis result of scRT-PCR from an O-LM, a PN and a BC. SOM, somatostatin; CCK, cholecystokinin; GAD, glutamate decarboxylase 65; PV, parvalbumin; CN, calcineurin.

B. Statistical results of SOM-, CCK- and PV-positive percentage in all GAD65-positive interneurons.

Fig. 4 Higher Amiloride-Sensitive H^+-Activated Current Density in Nucleated Patches from O-LMs

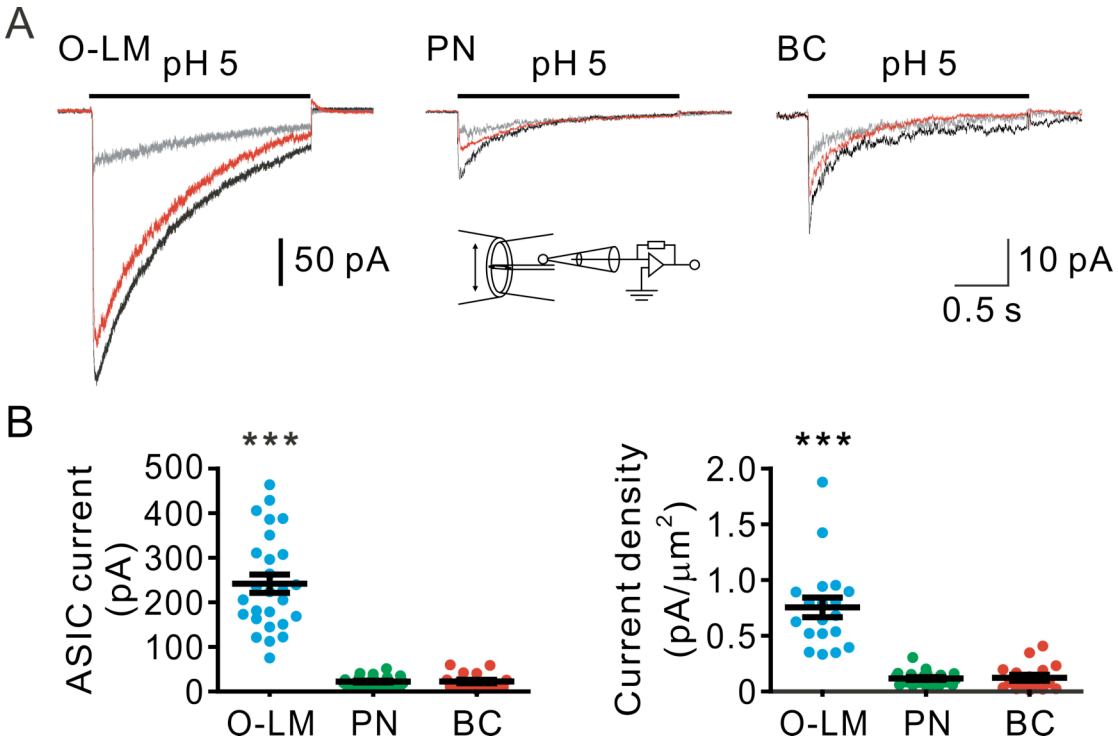

A. H^+-activated currents on nucleated patches from an O-LM, a PN and a BC. Extracellular pH value was switched from 7.4 to 5.0 for 2 seconds at -60 mV. Black, control; gray, 10 μM amiloride; red, washout. Insect, a schematic of a nucleated patch recording in front of the fast application system.

B. Left, ASIC currents on nucleated patches from O-LMs, PNs and BCs. Right, current density of ASIC on nucleated patches. (***$p < 0.0005$, Kruskal-Wallis test).

Fig. 5 Characterizations of ASICs

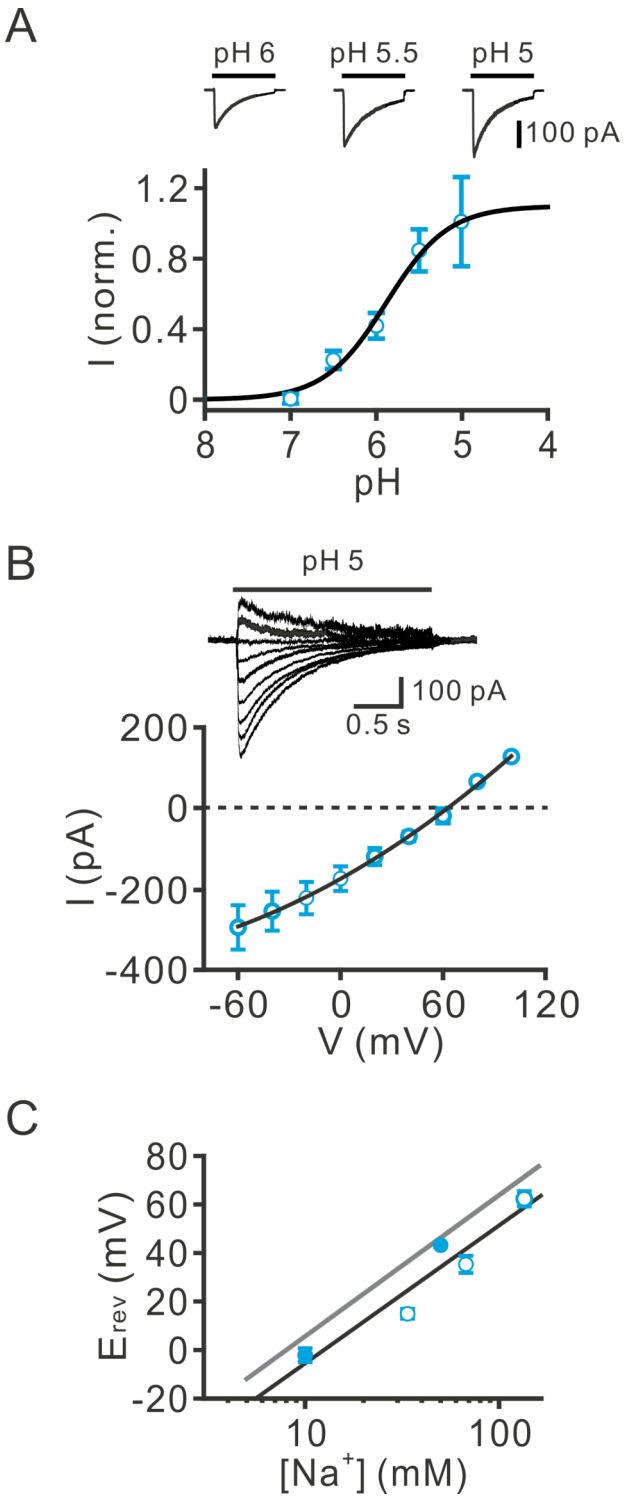

A. The dose responses of ASICs to various extracellular pH values. 2-s acid pulses were given every 20 sec. The $pH_{0.5}$ is 6.0 and Hill coefficient is 1.02.

B. An I-V plot of ASIC currents from a nucleated patch. Voltage steps were given from -60 mV to +100 mV with a increment of 20 mV. 2-s acid pulses were delivered at 0.05 Hz. The average E_{rev} is 62.3 mV.

C. The semi-logarithmic plot of E_{rev} against $[Na^+]_o$. Open circles, E_{rev} was recorded in 135, 62.5 or 33.75 mM of $[Na^+]_o$ and 1.8 mM of $[Ca^{2+}]_o$. Fill circles, $[Ca^{2+}]_o/[Na^+]_o$ are 100/10 and 80/50 mM. Gray line, theoretical E_{rev} change with $[Na^+]_o$ of a pure Na^+ channel. Black line, a linear fit of all experimental results. The slope values are 58.2 mV (gray) and 56.8 mV (black) per 10-fold $[Na^+]_o$ change, respectively.

Fig. 6 Calcium Blockade on ASICs

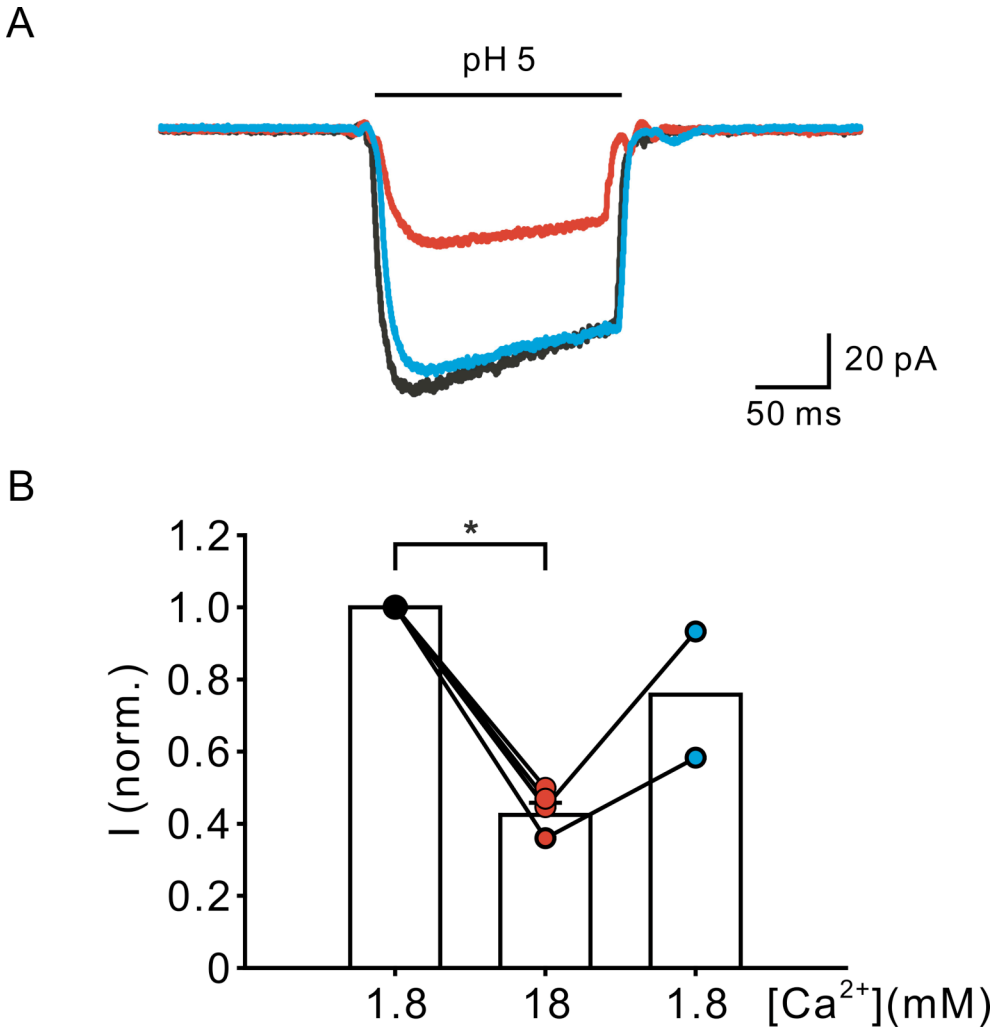

A. ASIC currents of a nucleated patch in 1.8 and 18 mM $[Ca^{2+}]_o$. 200-ms acid pulses were given every 15 sec at -60 mV. Black, 1.8 mM; red, 18 mM; blue, back to 1.8 mM.

B. The bar chart of ASIC currents in 1.8 or 18 mM $[Ca^{2+}]_o$ of 5 nucleated patches. (*p < 0.05, Wilcoxon signed-rank test).

Fig. 7 Non-Stationary Fluctuation Analysis of Single-Channel Properties of ASICs

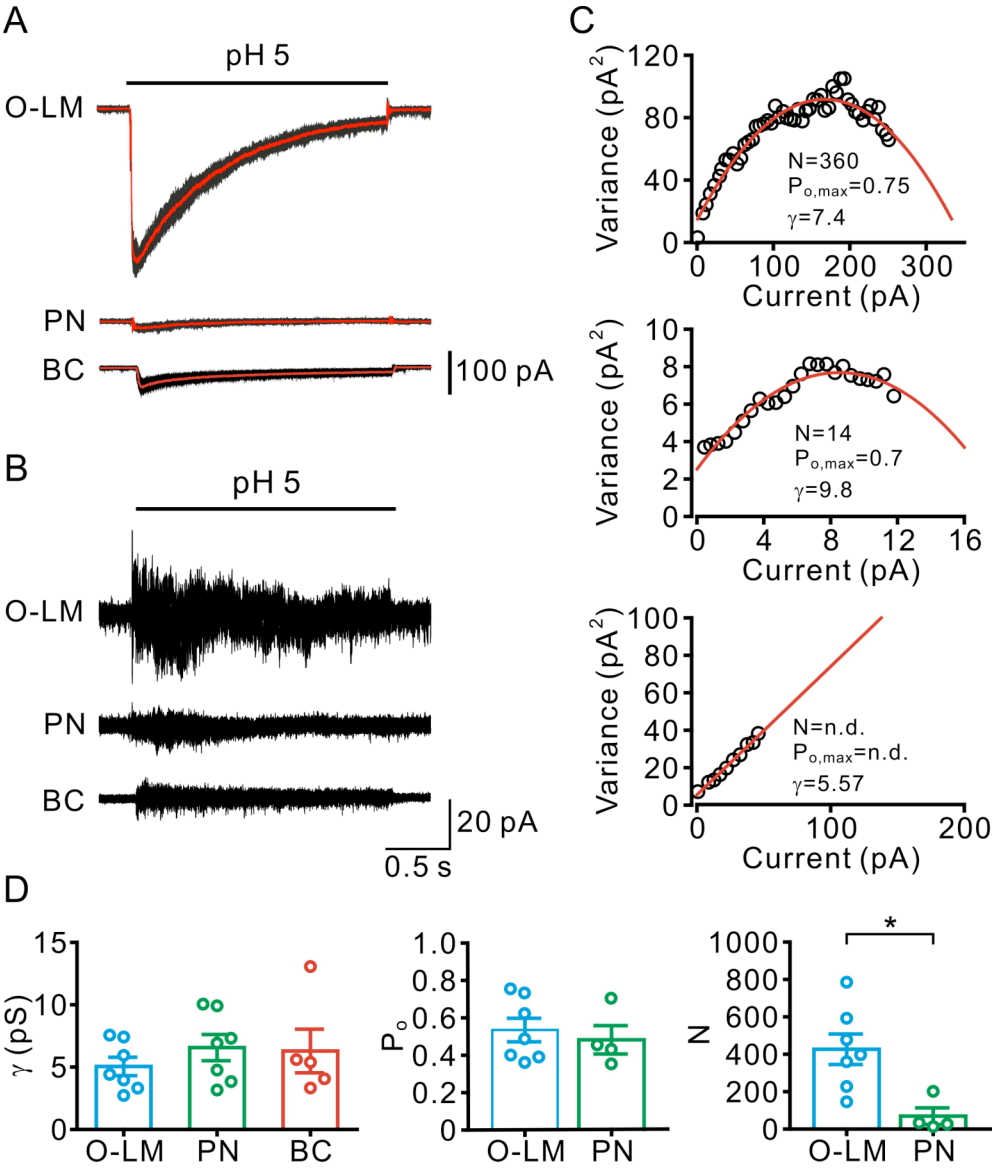

A. A representative ensemble containing 10 ASIC current traces (black) superimposed with the average (red). ASIC currents were recorded from nucleated patches of an O-LM, a PN and a BC. The extracellular pH was switched between 7.4 and 5.0. 2-s acid pulses were given every 15-20 seconds.

B. Deviations of traces obtained from subtracting each single trace with the mean. Traces are from the same patches in (A).

C. Scatter plots of ensemble variances against corresponding ensemble means. The data points are fitted by parabolic or linear functions (red). Same patches as in (A). Top, O-LMs; middle, PNs; bottom, BCs.

D. Bar charts of single-channel conductance (γ), maximum open probability ($P_{O,\,max}$) and channels number (N). (Right, $^{*}p < 0.05$, Wilcoxon rank-sum test; left and middle, no significant difference, $p > 0.05$, Kruskal-Wallis test)

Fig. 8 Distinct ASIC Amplitudes between Fast-Spiking and Non-Fast Spiking Interneurons

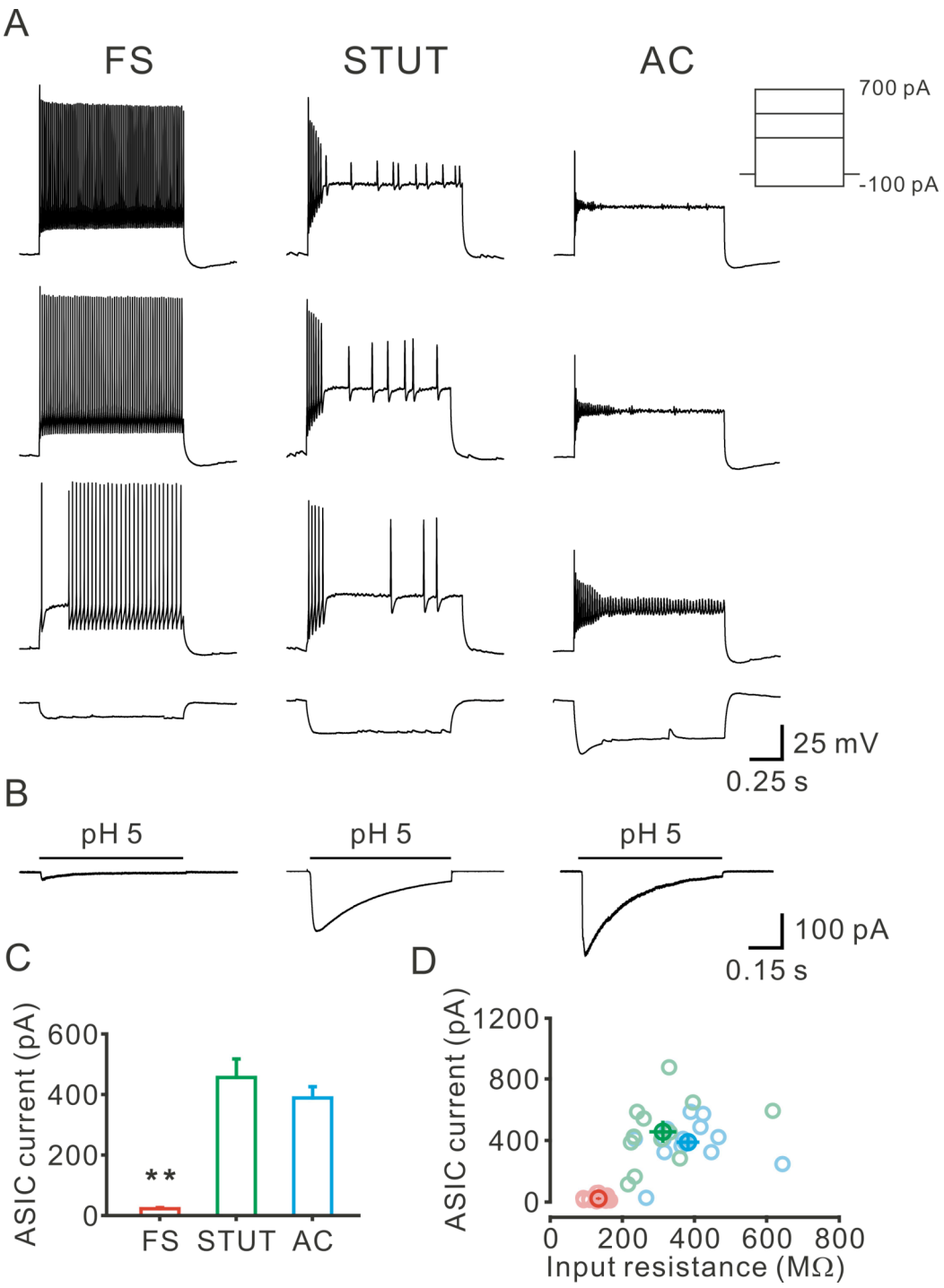

A. Firing patterns of a fast-spiking (FS), a stuttering (STUT) and an accommodating (AC) interneuron. Insect, currents injection of +700, +500, +300 and -100 pA.

B. ASIC currents induced by 2-s acid pulses of nucleated patches at -60 mV.

C. The bar chart of mean ASIC amplitudes of nucleated patches (**p < 0.005, Kruskal-Wallis test).

D. T scatter plot of input resistance against ASIC amplitudes. Red, fast-spiking; green, stuttering; blue, accommodating.

Fig. 9 Functional ASICs on Dendrites of Hippocampal Neurons

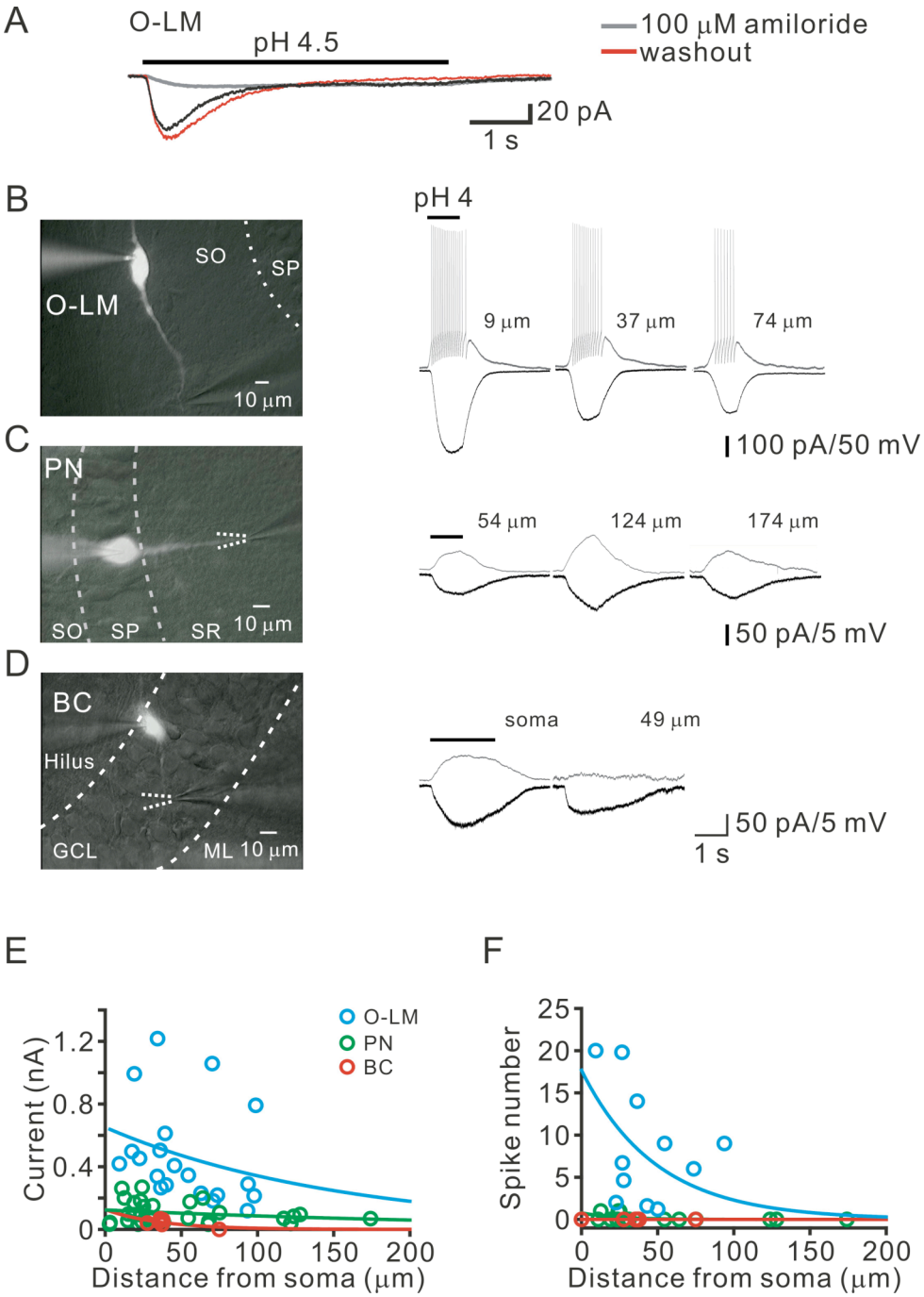

A. Amiloride-sensitive currents activated by focal acid puff on the dendrite of an O-LM.

B. C. D. Left, schematics of whole-cell recordings and focal acid puff merged with epi-fluorescence and IR-DIC images. Neurons of interest were loaded with 10 μM of SR-101. Puff pipettes were placed along the dendrite. Right, voltage (gray) and current (black) responses induced by dendritic acid puff on dendrites of interest. All puff experiments were done with 1-2 mM kynurenic acid and 1 μM SR95531.

E. F. Scatter plots of distance of focal puff from soma against induced spike number and ASIC current amplitudes.

Fig. 10 Different Desensitization and Deactivation Rates among O-LMs, PNs and BCs

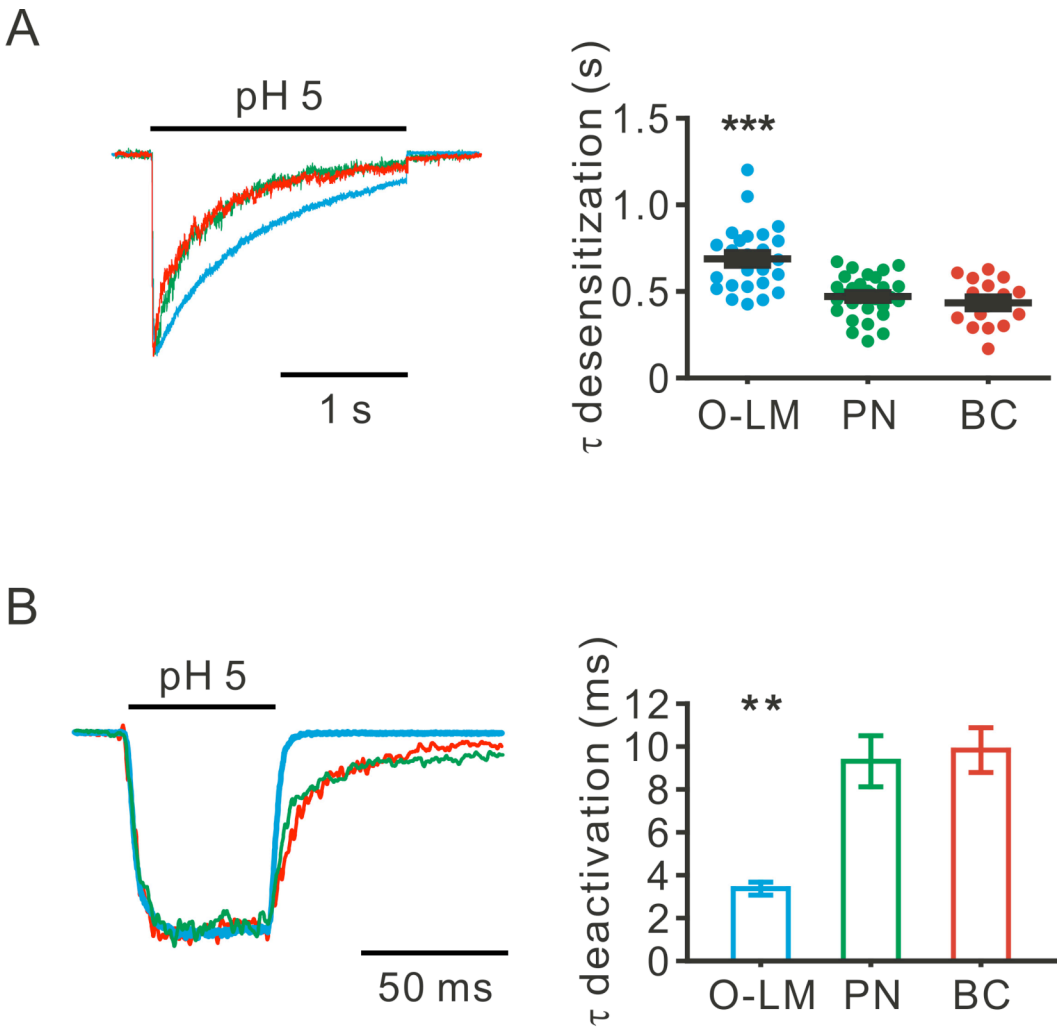

A. The desensitization of ASIC currents. Left, scaled and superimposed ASIC currents induced by 2-s acid pulse on nucleated patches at -60 mV. Blue, O-LM; green, PN; red, BC. Right, statistical results of time constants of desensitization (***$p < 0.0005$, Kruskal-Wallis test).

B. The deactivation of ASIC currents. Left, scaled and superimposed ASIC currents induced by 50-ms acid pulses at -60 mV. Right, statistical results of time constants of deactivation (**$p < 0.005$, Kruskal-Wallis test).

Fig. 11 Different Rates of Recovery from Desensitization and Cumulative Desensitization

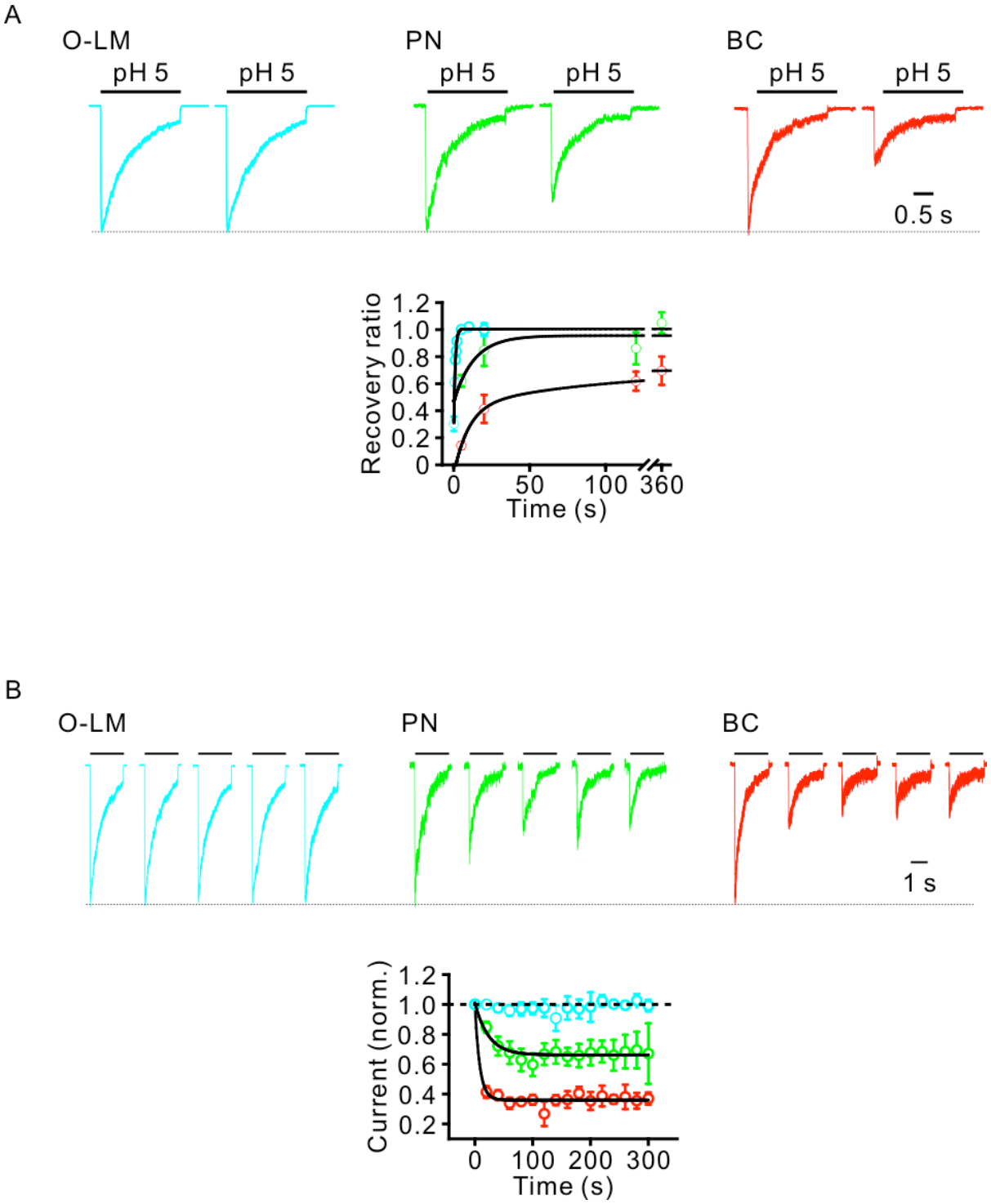

A. The recovery from desensitization of ASIC currents. Left, ASIC currents induced by 2-s acid pulses with a 20-s interval at -60 mV. Right, recovery from desensitization with various intervals. Blue, O-LM; green, PN; red, BC. Black lines are single exponential fitting.

B. The cumulative desensitization of ASIC currents. Left, the first 5 traces induced by repetitive 2-s acid pulse with a 20-s interval at -60 mV. Right, statistical results of cumulative desensitization. Black lines are single exponential fittings.

Fig. 12 Transcripts of ASIC1a and ASIC2 in O-LMs and PNs; ASIC1a in BCs

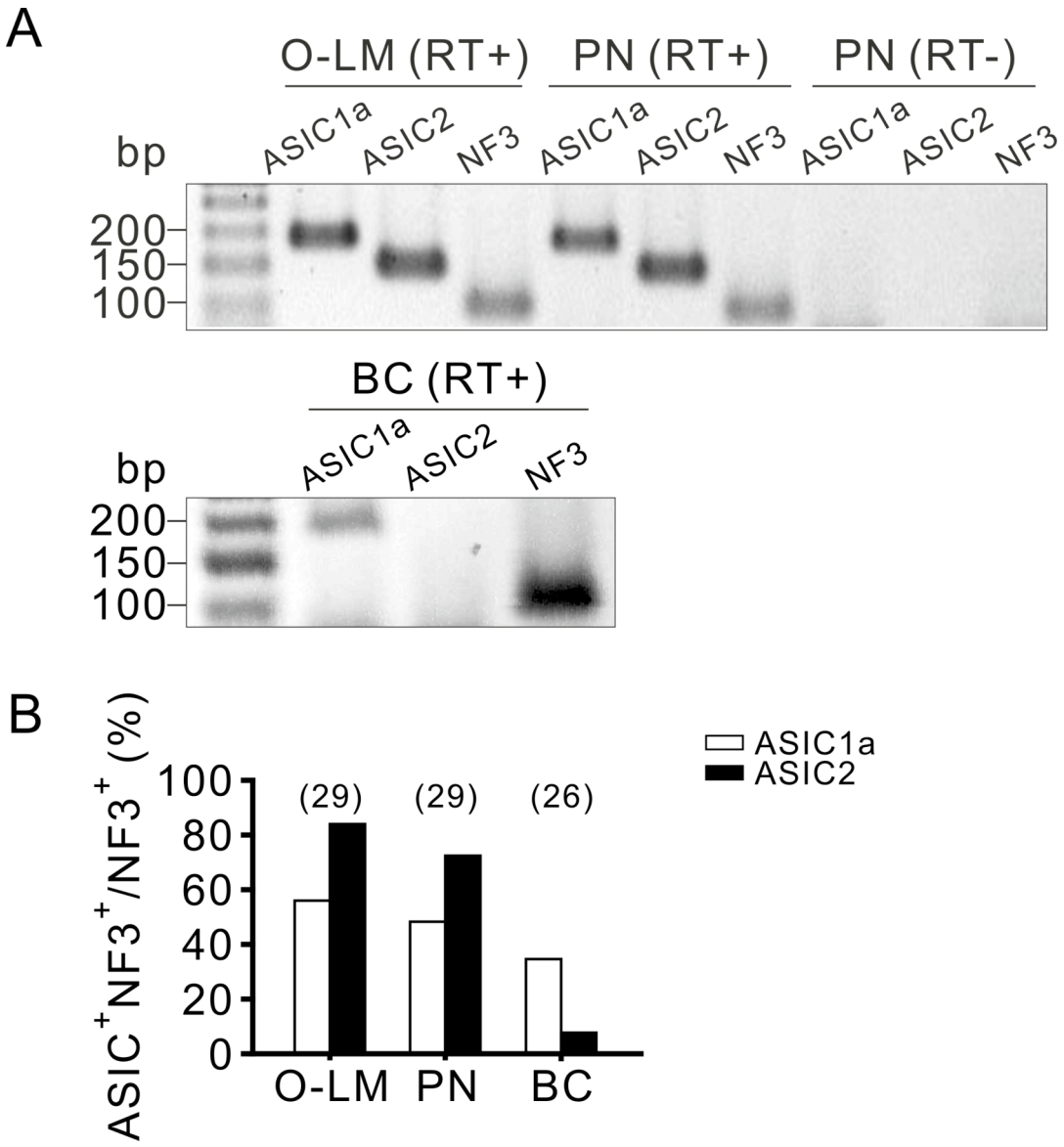

A. Results of gel electrophoresis of scRT-PCR. Upper, ASIC1a and ASIC2 with expected sizes were detected in an O-LM and a PN. Bottom, a BC with ASIC1a only. PN (RT+) and PN (RT-) represent results from the same PN with or without reverse transcriptase.

B. Statistical results of scRT-PCR. *Y*-axis represents the ratio of ASIC- and NF3-positive cells over all NF3-positive cells.

Fig. 13 PcTX1 Blockade on ASIC Currents of BCs

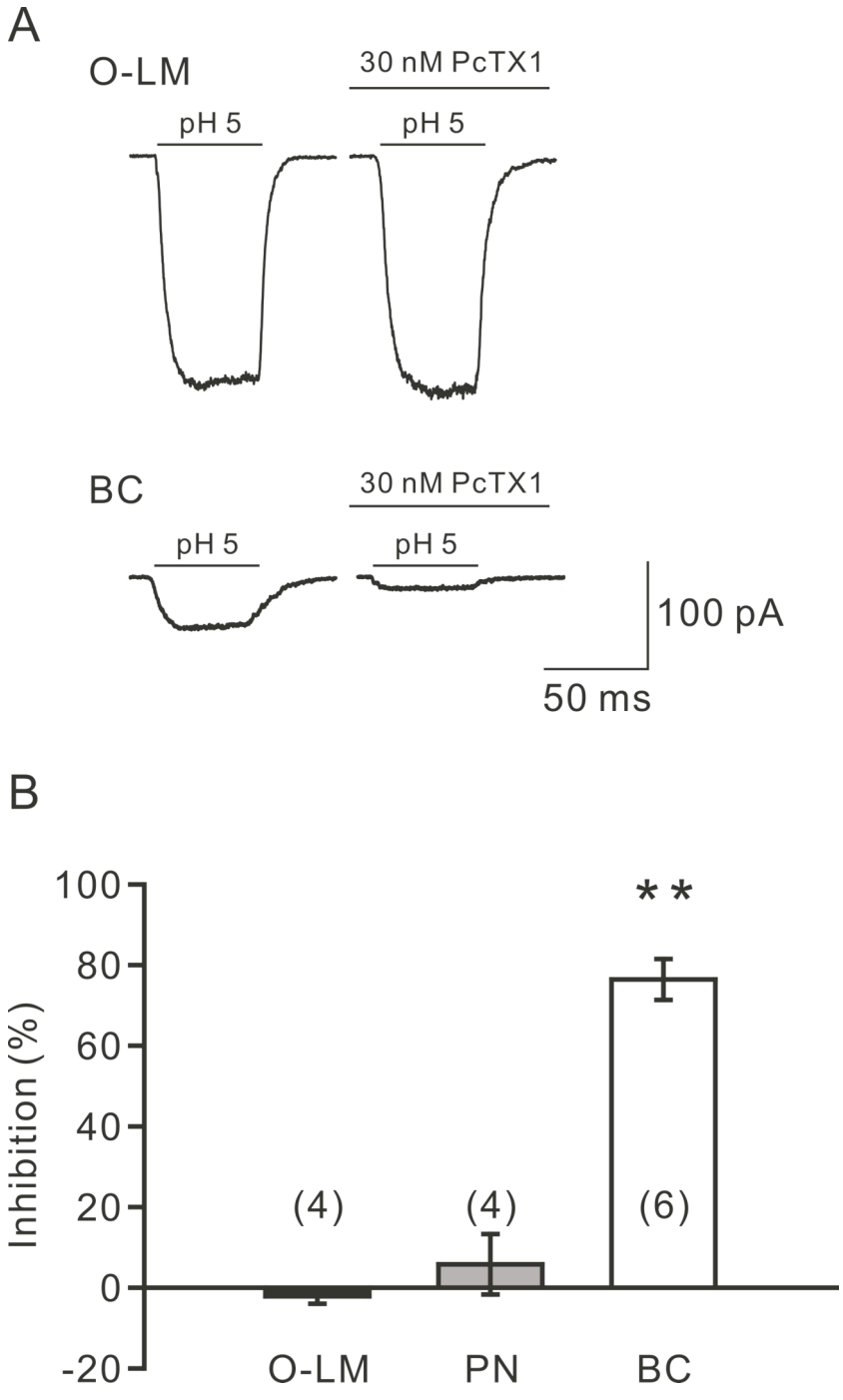

A. Upper, ASIC currents induced by 50-ms acid pulses on a nucleated patch from an O-LM. Bottom, ASIC currents in a BC under the same experimental configuration. Nucleated patches were voltage-clamped at -100 mV.

B. Percentage of inhibition on amplitudes of ASIC currents by 30 nM PcTX1 (**p < 0.005, Kruskal-Wallis test).

Fig. 14 The Comparison in Recovery from Desensitization between Native and Recombinant ASICs

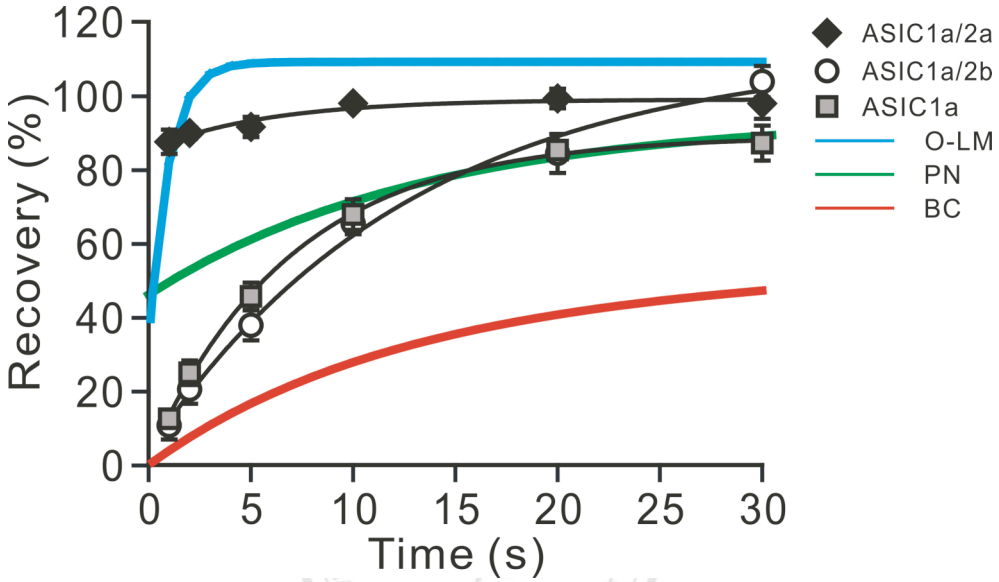

The recovery from desensitization of native and recombinant ASIC subunit compositions. Results of recombinant ASICs overexpressed in CHO cells were copied from Askwith et al., 2004. Blue, O-LMs; green, PNs; red, BCs. Lines are all single exponential fittings.

Fig. 15 No Significant Zn^{2+} Modulation in Our Systems

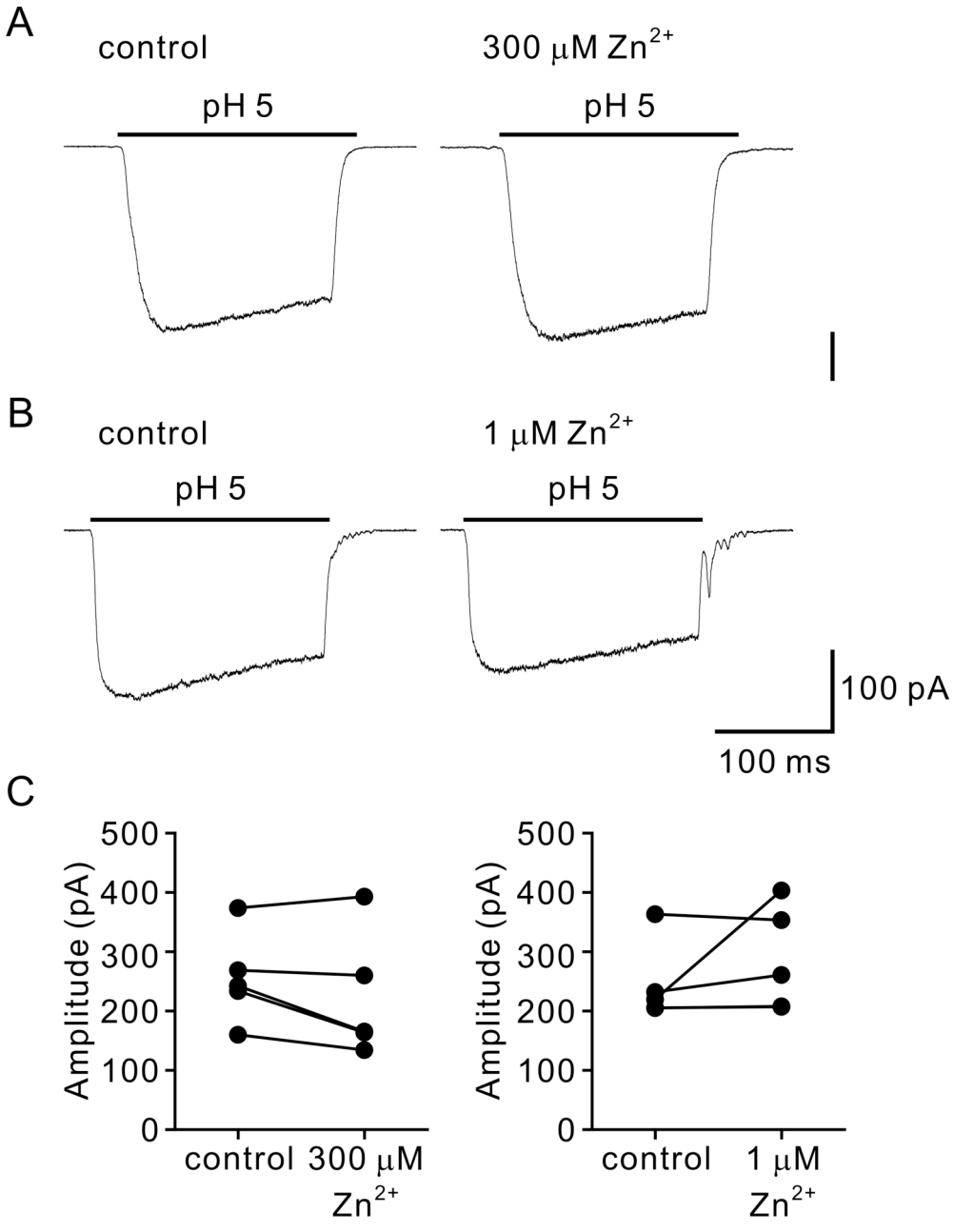

A. ASIC currents of a nucleated patches from an O-LM in the absence (control) or 300 μM of $[Zn^{2+}]_o$. The nucleated patch was voltage-clamped at -60 mV and 200-ms acid pulses were given every 10 sec.

B. ASIC currents of a nucleated patches from an O-LM in the absence (control) or 1 μM of $[Zn^{2+}]_o$ at -60 mV.

C. No significant difference in statistical results of ASIC currents in low or high $[Zn^{2+}]_o$ ($p > 0.05$, Wilcoxon signed-rank test).

Curriculum Vitae

Personal information:

First name: Ju-Yun

Last name: Weng
Gender: male
Date of birth: Mar 08, 1981
Place of birth: Kaohsiung, Taiwan
Nationality: Taiwan
Degree: Ph.D.
E-mail: whindang@gmail.com
Phone: +886-2-2826-7000 ext: 6090
Address: No.155, Sec.2, Linong Street, Taipei, Taiwan
Institution: National Yang-Ming University
Department: Institute of Neuroscience

Education:

Department of Life Science, Chung Shan Medical University, 2000-2004 (Bachelor)
Institute of Neuroscience, National Yang-Ming University, 2004- 2010 (Ph.D.)

Publication:

1. **Weng JY**, Lin YC, Lien CC. Cell type-specific expression of acid-sensing ion channels in hippocampal interneurons. J Neurosci. 2010 May 12;30(19):6548-58
2. Chiang PH, Yeh WC, **Weng JY**, Huang YY, Lee CT, Lien CC. M1-Like Muscarinic Acetylcholine Receptors Regulate Fast-Spiking Interneuron Excitability in Rat Dentate Gyrus. Neuroscience 2010. Neuroscience. 2010 Aug 11;169(1):39-51
3. **Weng JY**, Hsu TT, Sun SH. Functional characterization of P2Y1 versus P2X4 receptors in RBA-2 astrocytes: elucidate the roles of ATP release and protein kinase C. J Cell Biochem. 2008 May 15;104(2):554-67
4. Chou SY, **Weng JY**, Lai HL, Liao F, Sun SH, Tu PH, Dickson DW, Chern Y. Expanded-polyglutamine huntingtin protein suppresses the secretion and

production of a chemokine (CCL5/RANTES) by astrocytes. J Neurosci. 2008 Mar 26;28(13):3277-90.

5. Lin CC, Huang CC, Lin KH, Cheng KH, Yang DM, Tsai YS, **Ong RY**, Huang YN, Kao LS. Visualization of Rab3A dissociation during exocytosis: a study by total internal reflection microscopy. J Cell Physiol. 2007 May;211(2):316-26.

Appendix

Publication: **Weng JY**, Lin YC, Lien CC. Cell type-specific expression of acid-sensing ion channels in hippocampal interneurons. J Neurosci. 2010 May 12;30(19):6548-58

Cellular/Molecular

Cell Type-Specific Expression of Acid-Sensing Ion Channels in Hippocampal Interneurons

Ju-Yun Weng, Yen-Chu Lin, and Cheng-Chang Lien
Institute of Neuroscience and Brain Research Center, National Yang-Ming University, Taipei 112, Taiwan

Acid-sensing ion channels (ASICs), a member of the degenerin/epithelial Na^+ channel superfamily, are widely expressed in the mammalian CNS. Accumulating evidence suggests that ASIC current density is higher in GABAergic interneurons than that in glutamatergic pyramidal neurons (PNs) in the hippocampus. Such differential expression of ASICs in cortical networks is thought to be a key element for seizure termination. However, GABAergic interneurons are highly diverse; it is unclear whether the functional expression of ASICs differs in distinct GABAergic interneuron subtypes. Moreover, the subunit composition of ASICs in individual GABAergic interneurons remains unknown. By combining patch-clamp recording and single-cell reverse transcription (RT)-PCR analysis, we correlated ASIC currents with their gene expression in acute rat hippocampal slices. The results yielded several surprising findings. First, ASIC current density of oriens lacunosum-moleculare (O-LM) cells in the CA1 region, a classical type of dendrite-targeting interneuron, is 6 times greater than that of fast-spiking basket cells (BCs) in the dentate gyrus, a major class of soma-targeting interneuron. Second, the recovery of ASICs from desensitization is slowest in BCs, intermediate in PNs, and fastest in O-LM cells. Third, the tarantula venom psalmotoxin 1, the specific blocker for ASIC1a homomers, inhibits ASIC currents in BCs but not in O-LM cells. Finally, single-cell RT-PCR analysis reveals coexpression of ASIC1a and ASIC2 subunit transcripts in O-LM cells, whereas only ASIC1a subunit transcript is detected in most BCs. Thus, differential expression of ASICs in inhibitory microcircuits likely contributes to the distinct roles of GABAergic interneurons in normal physiology and pathophysiology.

Introduction

Acid-sensing ion channels (ASICs), a member of the degenerin/epithelial Na^+ channel (DEG/ENaC) cation channel superfamily, are widely expressed in the mammalian nervous system (Waldmann et al., 1997; for review, see Wemmie et al., 2006) and have been implicated in pain, ischemic stroke, seizures and many other neurological diseases (Xiong et al., 2004; Mazzuca et al., 2007; Ziemann et al., 2008; Coryell et al., 2009). Many studies showed that GABAergic inhibitory interneurons in the hippocampus have larger ASIC current densities than glutamatergic excitatory pyramidal neurons (PNs) (Bolshakov et al., 2002; Cho and Askwith, 2008; Ziemann et al., 2008). In line with this view, a recent report showed that ASIC1a null mice display delayed seizure termination after seizure induction and suggested that ASIC activation by falls in extracellular pH during seizures increases the cortical inhibition through preferential recruitment of GABAergic inhibitory interneurons (Ziemann et al., 2008).

However, GABAergic inhibitory interneurons consist of a highly heterogeneous population of cells (McBain and Fisahn, 2001; Jonas et al., 2004; Markram et al., 2004; Klausberger and Somogyi, 2008). Different GABAergic interneuron types have specific roles in hippocampal function (Klausberger and Somogyi, 2008). At least two functionally distinct classes of GABAergic interneurons are known to exist in the hippocampus (McBain and Fisahn, 2001; Jonas et al., 2004; Freund and Katona, 2007). Soma-targeting inhibitory interneurons, such as fast-spiking basket cells (BCs), control the spike initiation of principal neurons via axonal innervations onto perisomatic areas of principal neurons (Cobb et al., 1995; Miles et al., 1996; Kraushaar and Jonas, 2000), whereas dendrite-targeting inhibitory interneurons, such as oriens lacunosum-moleculare (O-LM) cells, regulate dendritic Na^+ or Ca^{2+} spikes and synaptic plasticity by innervating dendritic domains of principal neurons (Miles et al., 1996). These two distinct GABAergic interneuron subtypes differ not only in their intrinsic properties, such as neurochemical contents, Ca^{2+}-buffering proteins/homeostasis, ion channels, and transmitter receptors (Koh et al., 1995; Freund and Buzsáki, 1996; Martina et al., 1998; Lien et al., 2002; Pouille and Scanziani, 2004; Aponte et al., 2008; Liao and Lien, 2009), but also in their synaptic and network functions (Klausberger et al., 2003; Pouille and Scanziani, 2004; Klausberger and Somogyi, 2008). Unfortunately, the lack of measurement of ASIC currents from identified GABAergic inhibitory interneurons has left a fundamental question unresolved: is the ASIC expression among hippocampal GABAergic inhibitory interneurons cell type-specific? Moreover, the subunit composition of ASICs in various classes of GABAergic inhibitory interneurons ("perisomatic" versus "dendritic" interneurons) remains to be determined.

Received Jan. 5, 2010; revised Feb. 24, 2010; accepted March 21, 2010.

This work was supported by Yen Tjing Ling Medical Foundation (CI-96-4), Ministry of Education (Aim for The Top University Grant) in Taiwan, National Health Research Institutes (Grants NHRI-EX97-9720NC), and Taiwan National Science Council (Grant 98-2321-B-010-001). We thank Dr. P. Jonas for invaluable comments on initial experiments, Dr. C. C. Askwith for providing ASIC recovery data, Drs. P. Jonas, T. C. Hwang, M. M. Poo, and C. P. Hung for critically reading the manuscript, and Dr. M. Martina for helpful advice.

Correspondence should be addressed to Dr. Cheng-Chang Lien, Institute of Neuroscience and Brain Research Center, National Yang-Ming University 155, Section 2, Li-Nong Street, Taipei 112, Taiwan. E-mail: cclien@ym.edu.tw.

DOI:10.1523/JNEUROSCI.0582-10.2010

 0270-6474/10/306548-11$15.00/0

In this study, we correlated the functional property with gene-expression profile of ASICs in the PNs in the CA1 region and two functionally distinct classes of GABAergic inhibitory interneurons-O-LM cells and fast-spiking BCs in rat hippocampal slices by combining patch-clamp techniques and single-cell reverse transcription (RT)-PCR (Lien et al., 2002; Liss et al., 2004). Using these approaches, we uncovered a previously unknown expression pattern of ASICs in GABAergic inhibitory microcircuits, which likely underlies the selective vulnerability of distinct types of GABAergic inhibitory interneurons under pathological conditions.

Materials and Methods

Patch-clamp techniques in hippocampal slices. Transverse hippocampal slices of 300 μm thickness were cut from the brains of 15- to 23-d-old male Sprague Dawley rats using a vibratome (DSK-1000, Dosaka) as described previously (Lien et al., 2002; Liao and Lien, 2009). Animals were sacrificed by decapitation in agreement with national and institutional guidelines and all procedures were approved by the Animal Care and Use Committee of National Yang-Ming University. Slices were sectioned in the ice-cold cutting saline containing the following (in mM): 87 NaCl, 25 $NaHCO_3$, 1.25 NaH_2PO_4, 2.5 KCl, 10 glucose, 75 sucrose, 0.5 $CaCl_2$ and 7 $MgCl_2$. Following sectioning, slices were incubated in the cutting saline (oxygenated with 95% O_2/5% CO_2) in a holding chamber at 34°C for 30 min, and then at room temperature until used. During experiments, an individual slice was transferred to a submersion recording chamber and was continuously superfused with oxygenated artificial CSF containing the following (in mM): 125 NaCl, 25 $NaHCO_3$, 1.25 NaH_2PO_4, 2.5 KCl, 25 glucose, 2 $CaCl_2$ and 1 $MgCl_2$.

Experiments were performed under visual control using infrared differential interference contrast (IR-DIC) videomicroscopy (Stuart et al., 1993). O-LM cells in the CA1 subfield were selected based on the following criteria (Lien et al., 2002; Liao and Lien, 2009): (1) location of a fusiform soma in the stratum oriens with bipolar dendrites; (2) a pronounced sag response upon 1 s hyperpolarizing current pulse (−300 pA) injection; (3) fast-spiking patterns (50–60 Hz) and pronounced fast afterhyperpolarization during 1 s depolarization. For CA1 pyramidal neuron recording, cells of large somata in the stratum pyramidale with accommodating firing patterns were chosen. Dentate gyrus (DG) BCs were selected in accordance with previous reports (Koh et al., 1995; Martina et al., 1998; Aponte et al., 2008): (1) a relatively large size of cell body near the border between granule cell layer and hilus; (2) high-frequency (≥70 Hz) action potential (AP) phenotype; (3) relatively low input resistance (<170 MΩ); (4) little sag response upon membrane hyperpolarization. The recording temperature was 22–24°C.

Nucleated patch recordings. Nucleated patch recordings were made as described previously (Lien et al., 2002; Lien and Jonas, 2003) using an Axopatch 200B amplifier (Molecular Devices). Pipette capacitance was compensated. Signals were low-pass filtered at 5 kHz (four-pole Bessel), and sampled at 10 kHz using a digitizer Digidata 1322A (Molecular Devices). Pulse sequences were generated by Digidata 1322A via pClamp 9.2 (Molecular Devices). Minor and major axes of nucleated patches were measured. It was assumed that nucleated patches were approximately ellipsoid (Gentet et al., 2000) and the membrane surface area was calculated using the following formula:

$$\text{Surface area} = (\text{major axis} + \text{minor axis})^2(\pi/4) \quad (1)$$

Fast application of H^+. Fast application of H^+ on nucleated patches isolated from identified neurons was performed as described previously (Koh et al., 1995). Fast application experiments were started 1–2 min after the patches were excised. Double-barreled application pipettes were fabricated from theta glass capillaries (2 mm outer diameter, 0.3 mm wall thickness, 0.12 mm septum, Hilgenberg GmbH), and mounted on a piezoelectric-based solution switching system (Burleigh LSS-3000, EXFO). The time necessary for complete exchange of solution was measured with an open patch pipette by switching between Na^+-rich and 20% Na^+-rich solutions. It was 227 ± 50 μs (n = 3) by measuring 20–80% rise time of junction potential change. ASIC currents evoked by 2 s pulses of H^+ were applied every 15–30 s except in some pharmacological experiments (see Fig. 5), short pulses (50 ms) were used.

Focal H^+ puffing to dendrites. To visualize dendrites, we filled neurons with red fluorescent dye sulforhodamine 101 (SR101; 10 μM) via somatic recording. The dendrites were traced under epifluorescence microscope. To evoke ASIC currents along the dendrites, the puffing pipette was placed close to the dendrites (see Fig. 7). Voltage changes or ASIC currents were evoked by focal puffs of H^+ (~6 psi) using PicoSpritzer III (Parker Instrumentation) in whole-cell current or voltage-clamp recording. Acidic pH solution was injected via a patch pipette with an open tip (2 μm). The PicoSpritzer was triggered by an external TTL pulse generated by Digidata 1322A. This approach approximates the ASIC current amplitudes at dendrites and the caveat should be pointed out here. It is clear that the current amplitude did not directly reflect channel density because the surface area exposed to the puff varied.

Morphological analysis. Morphological reconstruction was identical to those reported previously (Liao and Lien, 2009). A separate subset of CA1 pyramidal cells, O-LM cells and BCs were filled with biocytin (0.2%) during recordings. After ~30 min recording, slices were fixed overnight with 4% paraformaldehyde in phosphate-buffered solution (PB; 0.1 M, pH 7.3). Following wash with PB, slices were incubated with fluorescein isothiocyanate (FITC)-conjugated avidin-d (2 μl/ml; Invitrogen) in PB and 0.3% Triton X-100 overnight at 4°C. After wash, slices were embedded in mounting medium Vectashield (Vector Laboratories). Labeled cells were examined by a two-photon microscope using a pulsed titanium/sapphire laser (Chameleon-Ultra II tuned to 800 nm; Coherent) attached to a Leica DM6000 CFS that was equipped with a 20×/0.50 numerical aperture water-immersion objective (HCX APO L; Leica). The two dimensional morphologies of the cells were reconstructed from a stack of 38–455 images (voxel size, 0.378–1.514 μm in the x-y plane; 0.4–0.99 μm along the z-axis) using ImageJ (v. 1.42q).

Solutions and drugs. The HEPES-buffered Na^+-rich external solution used for fast application in the control barrel contained (in mM): 135 NaCl, 5.4 KCl, 1.8 $CaCl_2$, 1 $MgCl_2$, 5 HEPES; pH adjusted to 7.4 with *N*-methyl-D-glucamine (NMDG). To evoke ASIC currents with various pH values, MES-buffered Na^+-rich external solution in the test barrel contained (in mM): 135 NaCl, 5.4 KCl, 1.8 $CaCl_2$, 1 $MgCl_2$, 10 MES, adjusted to the desired values with NMDG. The intracellular solution contained (in mM): 135 K-gluconate, 20 KCl, 0.1 EGTA, 2 $MgCl_2$, 4 Na_2ATP, 10 HEPES; pH adjusted to 7.3 with HCl. For low Na^+ experiments, Na^+ in the buffered Na^+-rich external solution was substituted by NMDG. For low Na^+/high Ca^{2+} experiments, concentrations of NaCl and $CaCl_2$ were varied as indicated (see Fig. 3*C*). Bovine serum albumin (0.1%) was added in external solutions containing the spider toxin Psalmotoxin 1 (PcTX1; Peptides International) to prevent its absorption to tubing and containers. Amiloride from Tocris Bioscience was dissolved in water to give 10 mM stock solution and stored at −20°C. All other chemicals were from Sigma except where noted.

Data analysis and statistics. Data were analyzed and fitted with Clampfit 10.0 (Molecular Devices) and Mathematica 5.2 (Wolfram Research). Apparent input resistance was defined by the ratio of peak voltage change/1 s hyperpolarizing current (−100 pA). Desensitization and deactivation time constants of ASIC currents were obtained by fitting currents with the function:

$$I(t) = \frac{-t}{Ae^{\tau_{\text{decay}}}} + C \quad (2)$$

where A denotes the peak amplitude of current, τ_{decay} represents the desensitization or deactivation time constant, and C denotes the amplitude of steady-state current.

Concentration–response curves were fitted with the function:

$$f(c) = \frac{A}{\left[1 + \left(\frac{\text{EC}_{50}}{c}\right)^n\right]} \quad (3)$$

where A is the constant for the maximal effect, c denotes the concentration, EC_{50} represents the half-maximal effective concentration, and n denotes the Hill coefficient.

For measuring reversal potential, data points of *I–V* relations (see Fig. 3*B*) were fitted with second order polynomials, from which the interpolated potentials were calculated. Theoretical reversal potential of sodium channels (E_{rev}) was plotted against external Na^+ concentration according to the Nernst equation:

$$E_{rev} = \frac{RT}{F} \ln \frac{[Na^+]_O}{[Na^+]_i} \quad (4)$$

where $[Na^+]_o$, $[Na^+]_i$ are outer and inner Na^+ concentrations and *F*, *R*, *T* have standard thermodynamic meanings (Hille, 2001).

The single-channel conductance of ASIC was estimated by nonstationary fluctuation analysis (Hartveit and Veruki, 2007) of ASIC currents from 23 to 50 traces (see Fig. 6*A*). To minimize errors due to rundown, the entire dataset was divided into nonoverlapping subsets of 7–10 traces (Engel and Jonas, 2005). Mean ensemble current and variances were determined for each subset and averaged. Mean variance (σ^2) versus mean current (I), for each sampling point, can then be obtained. To assign similar weights to all phases of the ensemble mean waveform, binning of mean I and corresponding σ^2 were used by dividing the mean current amplitude into a number of bins of equal amplitude (Hartveit and Veruki, 2007). The values of mean I and mean σ^2 within each bin were then further averaged. The averaged mean I was plotted against the averaged mean σ^2 and then fitted with the equation when they look like a parabola:

$$\sigma^2(I) = iI - \frac{I^2}{N} + \sigma_b^2 \quad (5)$$

developed from a binomial model, yielding values for apparent single-channel current i, total number of ion channel N available for activation. σ_b^2 is the variance of the background noise. In all BCs ($n = 5$) and some PNs (3 of 7), the data can be adequately described with a straight line rather than a parabola. The slope of the variance–mean relation was plotted with the equation:

$$\sigma^2(I) = iI + \sigma_b^2 \quad (6)$$

The single-channel chord conductance γ was calculated as follows:

$$\gamma = \frac{i}{(V_m - E_{rev})} \quad (7)$$

The maximum open probability ($P_{o,max}$), corresponding to the fraction of available ion channels open at the time of the peak current (I_{peak}), can then be calculated from the following equation:

$$P_{o,max} + \frac{I_{peak}}{iN} \quad (8)$$

Values indicate mean ± SEM; error bars in figures also represent SEM. Statistical significance among groups was tested using the nonparametric Kruskal–Wallis test. When it was significant, pairwise comparisons by the Wilcoxon rank-sum test were then carried out for each pair of groups. All tests were performed at the significance level (P) indicated using GraphPad Prism 5.0. SEs of reversal potentials were obtained by analyzing data of individual experiments separately. SEs of parameters of dose–response curves were calculated by a parametric bootstrap method (Efron and Tibshirani, 1998). A total of 500 artificial datasets were generated in which the original values were replaced by normally distributed random numbers with means and SEM identical to those of the original data points, and were fitted as the original dataset.

Single-cell RT-PCR. Single-cell gene expression profiles were analyzed using the single-cell RT-PCR approach as previously described (Martina et al., 1998; Lien et al., 2002; Liss and Roeper, 2004; Aponte et al., 2006). RNase-free patch-clamp buffer containing (in mM): 140 KCl, $MgCl_2$, 5 HEPES, 5 EGTA (pH = 7.3) was autoclaved before used. Patch-clamp capillaries were baked overnight at 220°C before use. The cytoplasm of a recorded neuron was harvested into the recording pipette, under visual control, without losing the gigaseal immediately after electrophysiological characterization. The contents of the patch pipette (~2–5 μl) were expelled into a 0.2 ml PCR tube (Axygen Scientific) containing 17 μl of RT mix (SuperScript III platinum Two-Step qPCR Kit with SYBR green I, Invitrogen). The mix contained 5 μl of diethylpyrocarbonate (DEPC)-treated water, 10 μl of 2× RT reaction mix (oligo(dT)$_{20}$, random hexamers, $MgCl_2$ and dNTPs) and 2 μl of RT enzyme mix (SuperScript III reverse transcriptase and recombinant ribonuclease inhibitor). Total volume was ~20 μl. After a series of incubation at different temperatures according to the manufacturer's instructions, the cDNA-containing tube was stored at −70°C until used. The RNA strand in the RNA-DNA hybrid was then removed by adding 1 μl (2 U/μl) of *E. coli* RNase H and incubated at 37°C for 20 min before PCR process.

Table 1. Oligonucleotide primers for RT-PCR

Gene	Forward/Reverse	Product size (bp)
Parvalbumin	5′-GGCGATAGGAGCCTTTACTGCTGC-3′	372
	5′-GAAACCCAGGAGGGCCGCGA-3′	
Somatostatin	5′-GGCTGCCACCGGGAAACAGGAAC-3′	119
	5′-CCTGCTCAGCTGCCTGGGGC-3′	
Calcineurin	5′-CCGAGCCCACGAAGCCCAGG-3′	337
	5′-TGCAGCCGTGGCTCCGTCAA-3′	
GAD65	5′-TGGCATCTCCGGGCTCTGGCT-3′	296
	5′-TGGCAGCAGGTCTGTTGCGTGG-3′	
Neurofilament 3	5′-TCGCCGCATATAGGAAACTACTG-3′	95
	5′-GGGCTGTCGGTGTGTGTACA-3′	
Cholecystokinin	5′-GCTGGACAGCAGCCGTTGGA-3′	280
	5′-GGCCAGAGGGAGCTTTGCGG-3′	
ASIC1a	5′-GAACATTCTGGTGCTGGACATT-3′	184
	5′-CCTGTGCTTAATGACCTCGTAG-3′	
ASIC2[a]	5′-CGCACAACTTCTCCTCAGTGTTT-3′	146
	5′-GTACTCATCTTGCTGAATGTCCA-3′	

[a]ASIC2a and ASIC2b mRNAs were detected with a pair of common primers.

Following cDNA synthesis, the cDNA solution of a single cell was split into 3 aliquots (5 μl) and each of them was used for gene amplification. A PCR approach with Rotor-Gene 3000 (Corbett Research) or StepOnePlus Real-Time PCR system (Applied Biosystems) was performed in a total volume of 25 μl with 1 μl of 10 μM primers (each), 5.5 μl of DEPC-treated water and 12.5 μl of Platinum SYBR Green qPCR SuperMix-UDG (Invitrogen) containing Platinum TaqDNA polymerase, Mg^{2+}, uracil DNA glycosylase, proprietary stabilizers, and dNTPs with dUTP. Primers were designed with Perlprimer v1.1.14 and selected for maximal specificity and intron-overspanning amplicons (Table 1). The molecular weights of the ASIC1a and ASIC2 amplicons and other neuron-specific markers were subsequently examined on ethidium bromide-stained agarose gels; sizes were in close agreement with the expected lengths (see Fig. 4*A*). For ASIC expression profiles, all analyzed neurons expressed neurofilament 3 (NF3), indicating selective harvesting from neurons. To exclude the possibility of contaminations, no template control was performed in parallel to every PCR, and the reverse transcriptase was omitted in a subset of cells. Additional controls to exclude nonspecific harvesting were performed by advancing pipettes into the slice and taking them out without seal formation and suction (Martina et al., 1998; Lien et al., 2002).

Results

Functional ASICs are differentially expressed in hippocampal microcircuits

We made whole-cell patch recordings from neurons in acute rat hippocampal slices under IR-DIC optics (Fig. 1*A*). Neurons in the CA1 area and the DG were selected as previously described (Martina et al., 1998; Lien and Jonas, 2003; Aponte et al., 2008; Liao and Lien, 2009). Under current-clamp configuration at 23 ± 1°C, CA1 PNs generated regular and accommodating AP trains upon injection of 1 s depolarizing current (+600 pA) pulses and exhibited sag responses in response to 1 s hyperpolarizing current (−300 pA) pulses with apparent input resistance of 176 ± 9.1 MΩ ($n = 30$, Fig. 1*A*, middle). Under the same protocol, O-LM

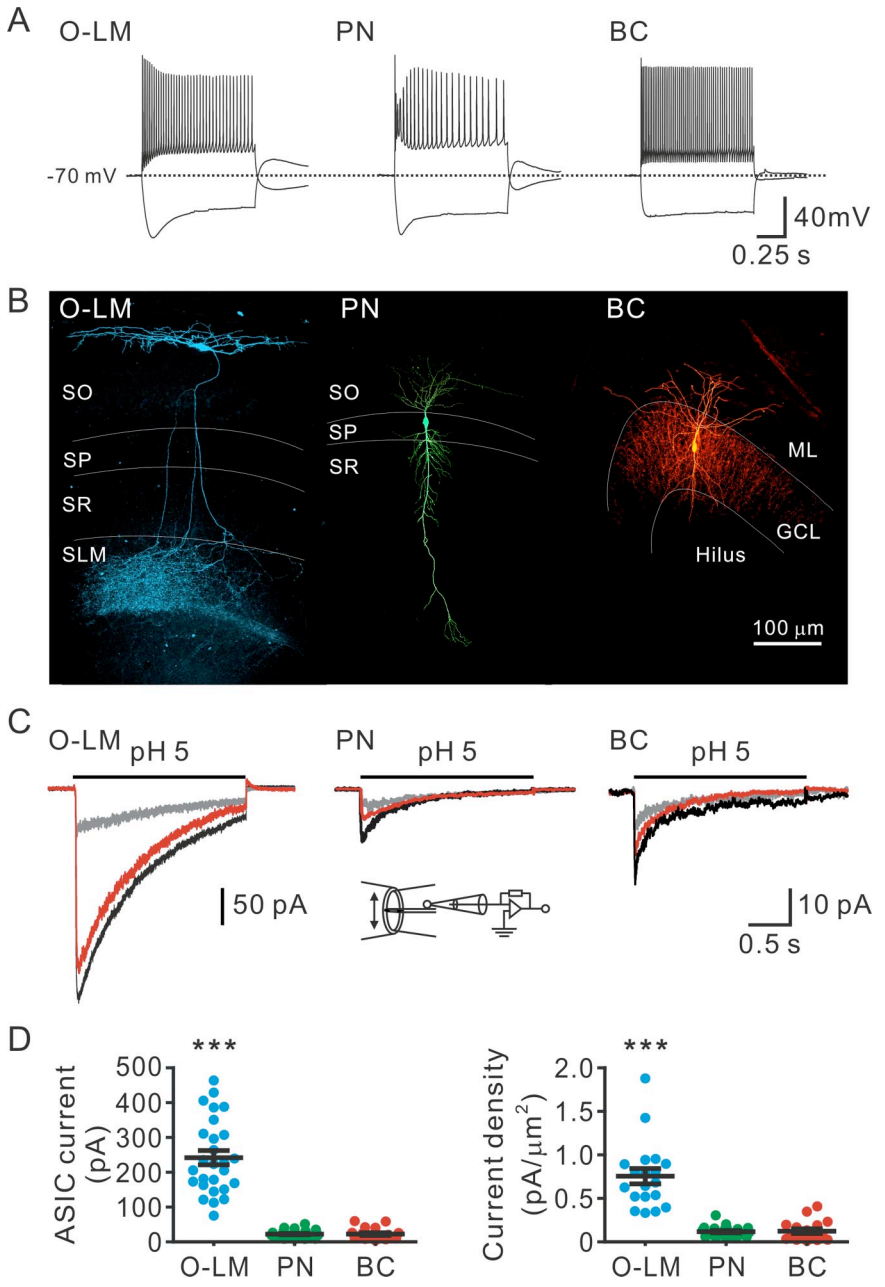

Figure 1. ASIC currents in CA1 PNs and defined interneurons. ***A***, Voltage responses to 1 s depolarizing (+600 pA) or hyperpolarizing (−300 pA) current pulses in the whole-cell current-clamp configuration from an O-LM cell, a PN and a BC, respectively. ***B***, Two-photon *z* stack projection of neurons in ***A*** filled with biocytin and stained with FITC-conjugated avidin. Note that the O-LM cell has its axonal arborization in stratum lacunosum moleculare (SLM), whereas the BC's axon is largely restricted to the granule cell layer (GCL). SR, stratum radiatum; SP, stratum pyramidale; SO, stratum oriens; ML, molecular layer. ***C***, Inward currents recorded at −60 mV after rapid pH changes from pH 7.4 to 5 in nucleated patches from an O-LM cell, a PN and a BC, respectively. Traces are averages of 5–10 sweeps. H^+-evoked currents are reversibly blocked by 10 μM amiloride (control: black; amiloride: gray; washout: red). Inset, Schematic of the experimental configuration. The open tip response was 227 ± 50 μs ($n = 3$) (see Materials and Methods). ***D***, Scatter plots showing that the current amplitude (left) and density (right) of O-LM cells are significantly larger than those of PNs and BCs. ***$p < 0.0005$.

cells generated APs at a frequency ≥50 Hz and showed pronounced sag responses with apparent input resistance of 335.6 ± 25 MΩ ($n = 24$, Fig. 1*A*, left). In contrast to PNs and O-LM cells, BCs in the DG generated high-frequency AP trains (86.7 ± 2.9 Hz, $n = 18$) with negligible sag responses and exhibited relatively low input resistance (133.9 ± 5 MΩ, $n = 18$; Fig. 1*A*, right). In a subset of experiments, the neuron types were further confirmed by *post hoc* morphological reconstruction of the recorded cells (Fig. 1*B*) and cell type-specific markers (supplemental Fig. 1, available at www.jneurosci.org as supplemental material). Consistent with previous reports (Sík et al., 1998; Maccaferri et al., 2000; Klausberger et al., 2003), analyses of single-cell RT-PCR showed that CA1 PNs expressed calcineurin, whereas O-LM cells and BCs expressed somatostatin and parvalbumin, respectively (supplemental Fig. 1, available at www.jneurosci.org as supplemental material). Moreover, nucleated patches subsequently isolated from these three types of neurons after whole-cell recordings exhibited cell type-specific voltage-gated K^+ currents (Du et al., 1996; Martina et al., 1998; Lien et al., 2002). Total outward K^+ currents in nucleated patches from CA1 PNs consisted of a large proportion of A-type currents, whereas patches from O-LM cells or BCs exhibited a predominant sustained component (supplemental Fig. 2, available at www.jneurosci.org as supplemental material).

Extracellular pH reductions evoke ASIC currents in hippocampal PNs (Baron et al., 2002; Bolshakov et al., 2002; Askwith et al., 2004; Ziemann et al., 2008). We next measured ASIC currents in these neurons using nucleated patch configuration, which allowed us to examine channel gating under ideal voltage-clamp conditions. A submillisecond switch of extracellular pH from 7.4 to 5 by fast application induced a transient inward current of 22.3 ± 1.9 pA in CA1 PNs ($n = 27$, Fig. 1*C*, black, middle, Fig. 1*D*, left), corresponding to a current density of 0.11 ± 0.01 pA/μm^2 ($n = 27$; Fig. 1*D*, right). In contrast to CA1 PNs, nucleated patches from O-LM cells upon pH 5 application exhibited a much larger current amplitude (237.9 ± 55.1 pA, $n = 27$; Fig. 1*C* black, left, Fig. 1*D*, left) with a current density of 0.75 ± 0.08 pA/μm^2 ($n = 19$; Fig. 1*D*, right). Surprisingly, the current amplitude (22.4 ± 3.8 pA, $n = 19$; Fig. 1*C*, black, right, Fig. 1*D*, left) and density (0.12 ± 0.02 pA/μm^2, $n = 19$; Fig. 1*D*, right) of nucleated patches from fast-spiking BCs in the DG were at least sixfold smaller than those of O-LM cells ($p < 0.001$, Wilcoxon rank-sum test) but were comparable to those of CA1 PNs ($p = 0.47$, Wilcoxon rank-sum test; Fig. 1*D*). All inward currents of these three cell types were reversibly blocked by the DEG/ENaC channel inhibitor amiloride (10 μM) (Fig. 1*C*, amiloride, gray; washout, red).

Non-fast-spiking interneurons in the DG have relatively large ASIC currents

We next investigated whether the feature of low ASIC current is unique to fast-spiking (FS) cells. In the DG, we classified all re-

corded non-fast-spiking interneurons into two functional groups (stuttering and accommodating) based on their firing patterns (Markram et al., 2004) (Fig. 2*A*). Nucleated patches from both stuttering (STUT) and accommodating (AC) interneurons had significantly larger ASIC currents than FS BCs (Fig. 2*B*,*C*). Overall, the ASIC currents in STUT and AC interneurons were 406 ± 56 pA ($n = 10$) and 399 ± 36 pA ($n = 15$), respectively (Fig. 2*C*). Also, both STUT and AC interneurons had higher input resistance than FS BCs. The scatter plot of the ASIC current against the input resistance revealed that FS BCs are featured by relatively low input resistance and low ASIC currents (Fig. 2*D*).

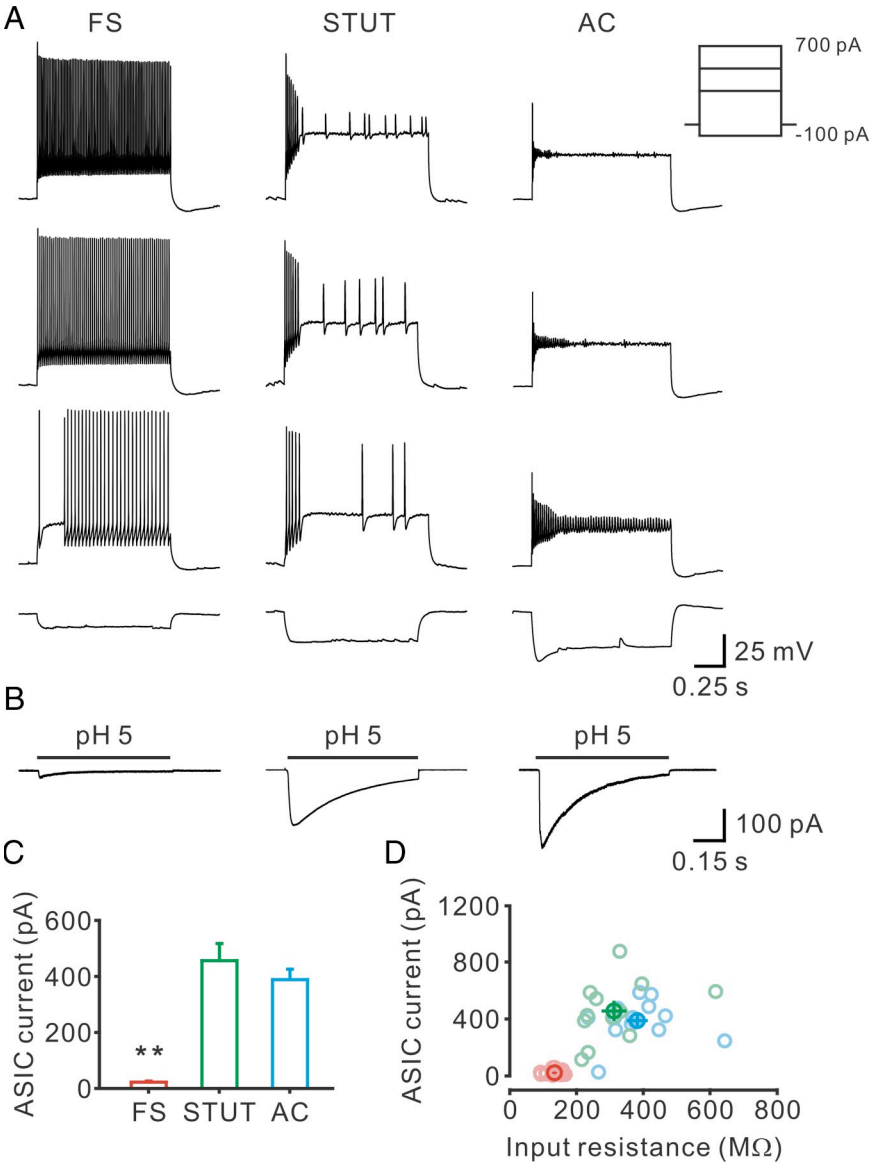

Figure 2. ASIC currents of various interneurons in the DG. ***A***, Voltage responses to 1 s depolarizing (+700, +500 and +300 pA) or hyperpolarizing (−100 pA) current pulses in the whole-cell current-clamp configuration from a FS BC (left) and two non-FS interneurons: middle, STUT firing; right, AC firing. Membrane potentials before the pulses were −70 mV. Inset, stimulation protocol. ***B***, Inward currents recorded at −60 mV after rapid pH changes from pH 7.4 to pH 5 in nucleated patches from a FS BC (left) and non-FS interneurons (middle, STUT; right, AC) in the DG. Traces are average of 11–75 sweeps. ***C***, Bar plot summarizing the amplitude of ASIC currents from FS BCs ($n = 6$), STUT ($n = 10$) and AC ($n = 15$) interneurons. $^{**}p < 0.005$. ***D***, Scatter plot of the input resistance against the ASIC current from all FS and non-FS cells.

ASIC gating is dependent on cell type

Steep pH dependence, Na^+ selectivity, and blockade by amiloride and extracellular Ca^{2+} ions are hallmark properties of ASIC gating (Waldmann et al., 1997; Bolshakov et al., 2002; Immke and McCleskey, 2003; Askwith et al., 2004; Wemmie et al., 2006; Cho and Askwith, 2008; Ziemann et al., 2008). To test pH dependence, we recorded ASIC currents upon different extracellular pH reductions. As represented by Figure 3*A*, the magnitude of ASIC current in an O-LM cell depended on the pH value. The dose–response curve was fitted with the equation (Eq. 3), yielding the pH value of 6.0 ± 0.0 for the half-maximal activation and the Hill coefficient of 1.2 ± 0.0. We further determined the ionic permeability of ASICs by measuring the reversal potentials (E_{rev}) in the presence of varied $[Na^+]_o$. ASIC currents in the normal condition ($[Na^+]_o/[Na^+]_i$ = 135/8 mM) reversed at 62 ± 3 mV ($n = 4$, Fig. 3*B*). The plot of E_{rev} against $[Na^+]_o$ revealed that the values of E_{rev} measured in a variety of $[Ca^{2+}]_o/[Na^+]_o$ solutions were close to the Nernst equilibrium potential for Na^+ (Fig. 3*C*, gray line; also see Eq. 4). These results indicate that Na^+ is the major permeant ion for ASICs. In addition to the sensitivity to amiloride (Fig. 1*C*), extracellular Ca^{2+} was shown to compete with H^+ for the ASIC activation site (Immke and McCleskey, 2003). Consistent with this notion, we found that high $[Ca^{2+}]_o$ (18 mM) inhibited acid (pH 5)-induced currents by 60 ± 2.3% (supplemental Fig. 3, available at www.jneurosci.org as supplemental material).

ASIC1a is a principal subunit for a functional ASIC, whereas ASIC2 subunit plays a modulatory role in the gating of ASIC, such as desensitization and recovery from desensitization (Askwith et al., 2004). We thus explored the potential differences in ASIC subunit composition of these three neuron types by measuring the desensitization time constant (τ_{desen}), deactivation time constant (τ_{deact}) and the recovery from desensitization of ASIC currents. The τ_{desen} values of native ASICs from these three cell types were all <1 s (Fig. 3*D*). On the other hand, τ_{deact} values from three cell types were all <10 ms (Fig. 3*F*). Notably, both τ_{desen} and τ_{deact} of ASICs in O-LM cells were significantly different from those of PNs and BCs. Interestingly, the recovery from desensitization as assessed by the recovery time constant ($\tau_{recovery}$) was fastest ($\tau_{recovery}$ = 0.96 ± 0.00 s) in O-LM cells, intermediate ($\tau_{recovery}$ = 13.2 ± 0.1 s) in CA1 PNs and slowest ($\tau_{recovery}$ = 42.8 ± 1.0 s) in BCs (Fig. 3*F*). Consistent with the recovery time course, cumulative desensitization of ASIC currents evoked by 0.05 Hz repetitive acid (pH 5) pulses was fastest in BCs, intermediate in PNs and slowest in O-LM cells (Fig. 3*G*). Together, these results strongly suggest differences in ASIC subunit composition among these three neuron types.

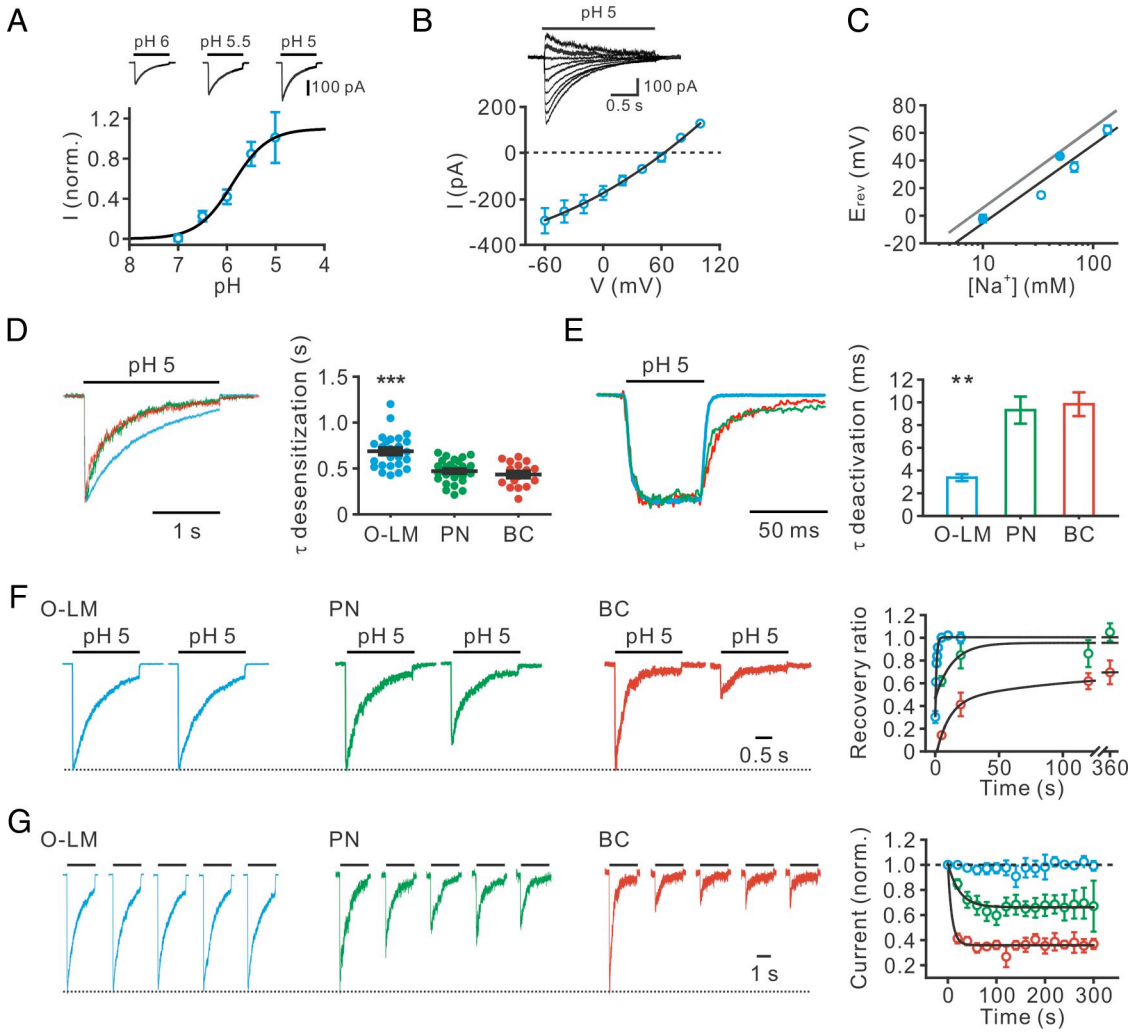

Figure 3. Functional properties of ASIC in different types of neurons. ***A***, Inset, Representative ASIC currents in an O-LM cell induced by pH changes from pH 7.4 to 6, 5.5, and 5. The peak current amplitude, normalized to the mean peak amplitude of pH 5-induced currents, is plotted against the pH value. The continuous curve represents the single Hill equation fitted to the data points. Points represent mean values from 4 to 25 experiments. ***B***, Inset, Representative ASIC currents in a nucleated patch from an O-LM cell were recorded at different membrane potentials (from −60 mV to +100 mV, increments 20 mV). The current–voltage (***I–V***) curve of ASIC currents has the E_{rev} of +62 ± 3 mV. Data points are fitted with a polynomial function. ***C***, Semilogarithmic plot of the E_{rev} against $[Na^+]_o$. Symbols represent the recordings in either 1.8 mM $[Ca^{2+}]_o$ (open symbols) or high $[Ca^{2+}]_o$/low $[Na^+]_o$ (filled symbols: 100/10 and 80/50 mM, respectively). The gray line depicts the Nernst Na^+ equilibrium potential plotted against $[Na^+]_o$; the black line is the linear fit of all data points. The slope values of the relationship between E_{rev} and Log$[Na^+]_o$ correspond to 58.2 mV (gray) and 56.8 mV (black) per tenfold $[Na^+]_o$ change, respectively. ***D***, Left, Representative peak-scaled traces of ASIC currents showing desensitization. Right, Scatter plot of τ_{desen} of ASIC currents of O-LM cells (688 ± 97 ms, $n = 26$), PNs (471 ± 21 ms, $n = 32$) and BCs (434 ± 33 ms, $n = 16$). The τ_{desen} was obtained by fitting the decay phase of the current with a monoexponential function. ***$p < 0.0005$. ***E***, Left, Representative peak-scaled traces of ASIC currents showing deactivation. Right, Bar plot of τ_{deact} of ASIC currents of O-LM cells (3.7 ± 0.3 ms, $n = 10$), PNs (9.3 ± 1.2 ms, $n = 5$) and BCs (9.8 ± 1.0 ms, $n = 5$). The τ_{deact} was obtained by fitting the decay phase of the current with a monoexponential function. **$p < 0.005$. ***F***, Left, Representative traces showing the recovery from desensitization was measured at −60 mV after rapid changes from pH 7.4 to 5 for 2 s and then changed back to pH 7.4 for 20 s, followed by a second pulse to pH 5 for 2 s. The peak current evoked by the second pH 5 pulse divided by the first pH 5 pulse was plotted against the pulse interval. Right, data points obtained from O-LM cells ($n = 6$), PNs ($n = 16$) and BCs ($n = 9$) were fitted with either a mono- or a biexponential function, yielding the weighted recovery time constants of 0.96 s, 13.2 s and 42.8 s, respectively. ***G***, Left, Cumulative desensitization of ASICs (at −60 mV) evoked by repetitive 2 s pulses (from pH 7.4 to 5) at 0.05 Hz in an O-LM, a PN and a BC, respectively. Only the first five traces were shown. Right, Time courses of onset of desensitization in O-LM cells ($n = 6$), PNs ($n = 10$) and BCs ($n = 7$). The peak current amplitude, normalized to the first peak current amplitude, was plotted against the time of each pulse. Curves represent exponential functions fitted to the data points. Time constants for PNs and BCs were 23.6 ± 1.8 and 8.3 ± 0.3 s, respectively.

ASIC2 subunit determines the recovery of native ASICs from desensitization

To further correlate the gating properties with gene-expression profile of individual neurons, we analyzed ASIC1a and ASIC2 subunit mRNAs of each neuron type at the single-cell level (Fig. 4*A*). Single-cell RT-PCR analysis revealed that ASIC1a and ASIC2 mRNAs were coexpressed in CA1 PNs and O-LM cells, whereas only ASIC1a mRNA was detected in most BCs (9 of 11 ASIC-expressing BCs; Fig. 4*B*). These results correlate well with the notion that the rapid recovery of ASIC currents in O-LM cells is mediated by ASIC1a/2a heteromers, while the prolonged recovery of ASICs from desensitization in BCs is largely attributed to the expression of ASIC1a homomers (Askwith et al., 2004). To make this point clear, we illustrated the recovery time courses of ASICs from O-LM cells (blue line) and BCs (red line) together with those of various recombinant ASICs (Fig. 4*C*; change to curves obtained by fitting data from Askwith et al., 2004).

PcTX1 preferentially inhibits ASIC currents in basket cells

Homomeric ASIC1a channel is potently inhibited by the PcTX1 (Baron et al., 2002; Chen et al., 2005; Xiong et al., 2008). We, therefore, examined the effects of PcTX1 on functionally distinct

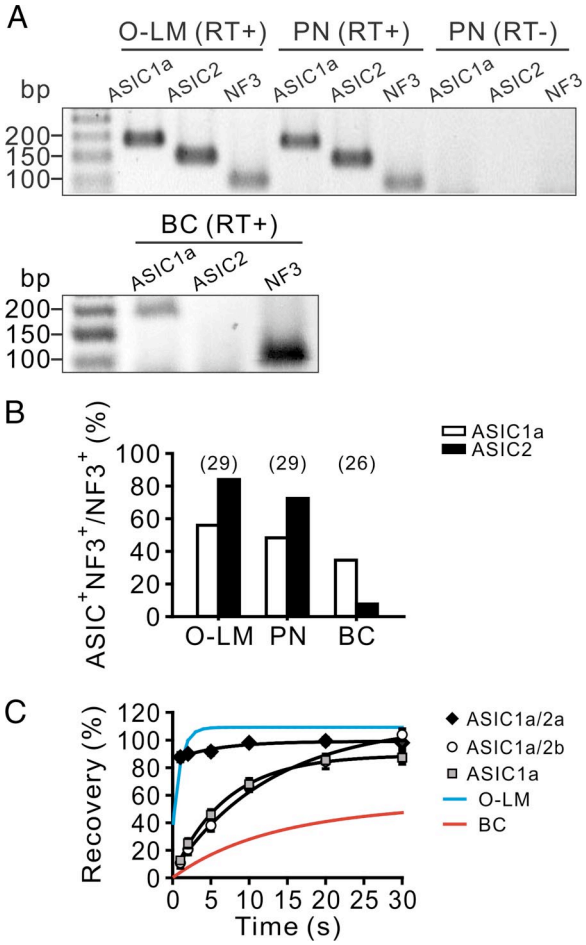

Figure 4. Expression of ASIC subunit transcripts in single hippocampal neurons. ***A***, Ethidium bromide-stained gels of the PCR products amplified with primers specific for ASIC1a, ASIC2 and NF3 transcripts. Molecular weight markers were shown in the left upper and lower lanes, together with the corresponding number of base pairs. Plus and minus signs indicate samples with or without RT. All analyzed neurons expressed NF3. ***B***, Bar graph showing the percentage of NF3-positive neurons expressing ASIC1a and ASIC2 transcripts. Number in parentheses indicates the number of the NF3-positive cells. ***C***, Time courses of recovery from desensitization of ASICs from O-LM cells (blue line) and BCs (red line) were plotted together with data from heterologously expressed mouse ASICs in CHO (change to curves obtained by fitting data from Askwith et al., 2004). Lines represent exponential functions fit to the data points.

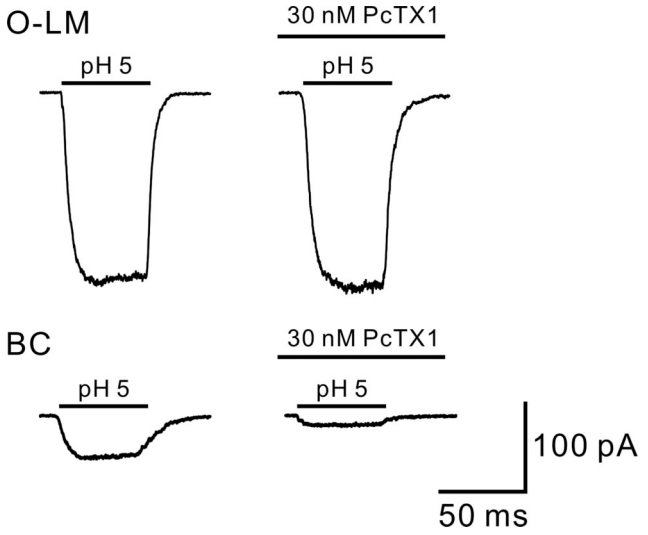

Figure 5. PcTX1 preferentially inhibited ASIC currents of BCs. Top, Traces showing ASIC currents (evoked by pH 5 at −100 mV) in a nucleated patch from an O-LM cell in the control and in the presence of 30 nM PcTX1. Bottom, PcTX1 (30 nM) inhibited 74% of ASIC currents in a nucleated patch from a BC. Traces were average of 5–7 sweeps.

ASIC currents in nucleated patches from either O-LM cells or BCs. Because of the very slow recovery time course ($\tau_{recovery}$ = 42.8 s) of ASICs in BCs, we thus obtained stable ASIC current amplitudes by applying short (50 ms) acid pulses to nucleated patches (Fig. 5). In control conditions, ASIC currents of O-LM cells and BCs showed little desensitization and were stable over time (Fig. 5, left traces). PcTX1 (30 nM) had only minimal effects on ASIC currents in nucleated patches from O-LM cells (Fig. 5, top, right). The peak current in the presence of PcTX1 was 102 ± 1% of the control ($n = 4$, $p > 0.05$; Fig. 5, top, right). In contrast, PcTX1 (30 nM) significantly blocked 76 ± 5% of the ASIC currents in nucleated patches from BCs ($n = 6$, $p < 0.005$; Wilcoxon signed-rank test; Fig. 5, bottom, right).

ASIC channel number accounts for differences in current density

Finally, we determined whether the remarkable differences in current densities among the neuron types were derived from differences in channel number (N), maximum open probability ($P_{o,\,max}$) or single-channel conductance (γ). We retrieved N, $P_{o,\,max}$ and γ from the ensembles of macroscopic currents (Fig. 6*A*) using nonstationary fluctuation analysis. The ensemble variance was calculated from the fluctuation of ASIC currents around the mean (Fig. 6*B*), plotted against the ensemble mean, and fitted with a parabolic function (Fig. 6*C*). Analysis from patches of O-LM cells yielded the γ of 5.05 ± 0.74 pS ($n = 7$; Fig. 6*D*) and the channel number N of 427 ± 82 ($n = 7$). For CA1 PNs, though the γ (6.57 ± 1.05 pS, $n = 7$) was comparable to that of O-LM cells, the estimated N was 69 ± 45 ($n = 4$; 3 of 7 cells were fitted with a linear function; see below), significantly less than that of O-LM cells ($p < 0.05$, Wilcoxon rank-sum test). Notably, the variance–mean relation of ASIC currents from all BCs ($n = 5$) displayed a straight line rather than a parabola, indicating low open-channel probability (Alvarez et al., 2002). In this case, we can determine the γ, but not the N and $P_{o,\,max}$ in the membrane (Alvarez et al., 2002). By fitting the data points with a linear function, we obtained the γ of 6.29 ± 1.75 pS ($n = 5$; Fig. 6*D*) from the slope. Collectively, the γ values were not significantly different among the three groups ($p = 0.72$, Kruskal–Wallis test). Similarly, the $P_{o,\,max}$ values at pH 5 were not significantly different between O-LM cells and CA1 PNs (O-LM cells, 0.54 ± 0.06, $n = 7$ versus PNs, 0.48 ± 0.08, $n = 4$; $p = 0.65$, Wilcoxon rank-sum test). In sum, ASIC channel number greatly contributes to the cell type-specific difference in current density.

Dendritic ASIC currents in O-LM cells are higher than those of PNs and BCs

ASICs are distributed at somatodendrites of neurons (Wemmie et al., 2002; Alvarez de la Rosa et al., 2003; Zha et al., 2006, 2009). After filling neurons with red fluorescent dye SR101 (10 μM) via somatic recording, dendrites were traced under epifluorescent microscope. Similar to somatic ASIC currents, dendritic ASIC currents of O-LM cells (V-clamp at −70 mV) evoked by local acid puffing were transient and reversibly inhibited by amiloride (100 μM) (Fig. 7*A*). Then we determined whether dendritic ASIC currents differed among three distinct types of neurons by local acid puffing along the apical dendrites of CA1 PNs (Fig. 7*B*), bitufted dendrites of O-LM cells (Fig. 7*C*) and apical dendrites of

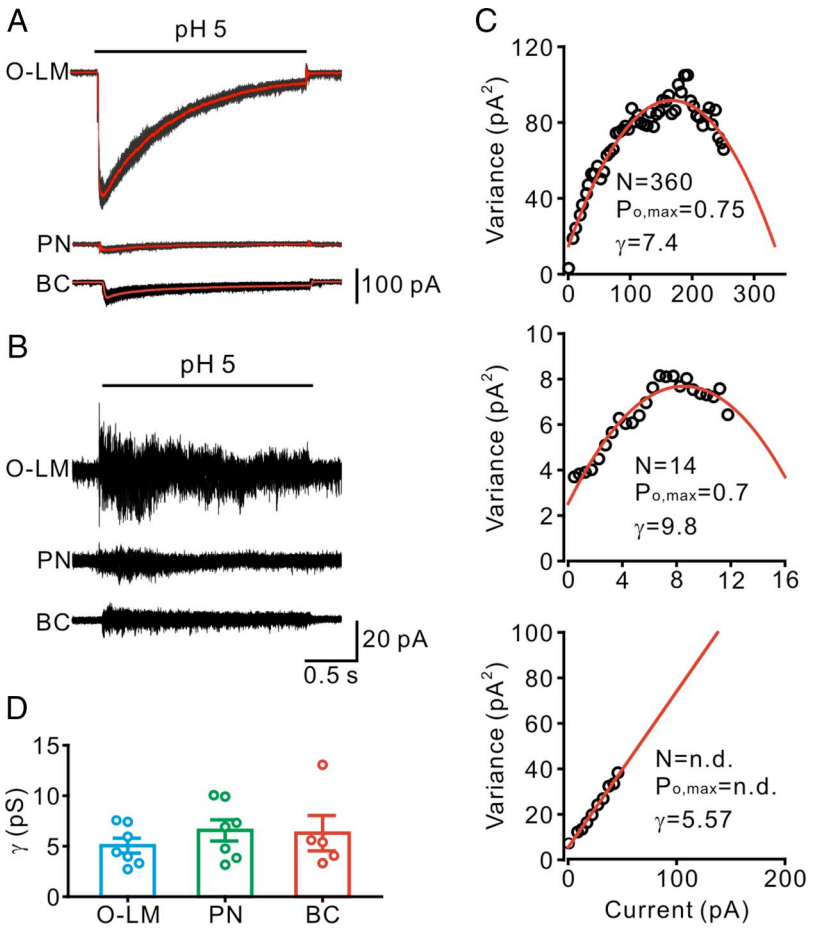

Figure 6. Nonstationary fluctuation analysis of single-channel properties of ASICs. ***A***, Representative ensemble of 10 consecutive ASIC current traces (black) superimposed with the averaged current traces (red) recorded in nucleated patches from an O-LM cell, a PN and a BC. ***B***, Traces illustrating deviation of three representative individual traces from the mean. Traces from the same cells in ***A***. ***C***, The ensemble variance was calculated from the fluctuations of ASIC currents around the mean, plotted against the ensemble mean, and fitted with a parabolic function. Each plotted point is the average of 10 sampling points. Same patches as shown in ***A***. Red curves are parabolic or linear functions fitted to the data points. ***D***, A bar plot summarizing γ values for O-LM cells, PNs and BCs.

BCs (Fig. 7*D*). ASIC currents in dendrites with the puffing site at distances of 30–100 μm from the soma (280 ± 65 pA, $n = 8$) of O-LM cells are much larger than those of CA1 PNs (132 ± 28 pA, $n = 9$) and BCs (52 ± 8 pA, $n = 6$) (Fig. 7*E*). Consistently, ASIC currents effectively generated AP trains in O-LM cells when neurons were recorded in the current-clamp configuration but only caused subthreshold membrane depolarization in PNs and BCs under the same conditions (Fig. 7*F*).

Discussion

Earlier studies reported that GABAergic inhibitory interneurons possess larger ASIC current density than pyramidal cells in the hippocampus (Bolshakov et al., 2002; Cho and Askwith, 2008; Ziemann et al., 2008). In contrast to them, our study shows that fast-spiking, parvalbumin-expressing BCs have comparable ASIC current density to CA1 PNs. Moreover, ASIC current densities and gating greatly differ between two functionally distinct GABAergic (perisomatic versus dendritic) inhibitory interneurons. Furthermore, single-cell RT-PCR analysis reveals coexpression of ASIC1a and ASIC2 subunits in O-LM cells, whereas only ASIC1a is detected in most BCs. The lack of the ASIC2 subunit likely accounts for the prolonged recovery of native ASICs from desensitization in BCs.

Comparisons between native and recombinant ASICs

Heterologously expressed mouse ASIC1a homomers and ASIC1a/2 heteromers in CHO cells desensitize rapidly ($\tau_{decay} < 1$ s) (Askwith et al., 2004). In comparison with them, the values of τ_{desen} of native ASICs from all three cell types are <1 s (Fig. 3*D*), suggesting that either ASIC1a homomers or heteromeric channels assembled by ASIC1a/2a or ASIC1a/2b combination likely mediate the majority of native channels. Further analyses of ASIC gating implicate differential expression of ASIC subunits in different cell types. Most obviously, the recovery from desensitization of ASICs is fastest in O-LM cells, intermediate in CA1 PNs and slowest in BCs (Fig. 3*F*). These suggest that ASIC1a/2a heteromers likely mediate ASICs of O-LM cells because the recovery from desensitization of heterologously expressed mouse ASIC1a/2a heteromers as estimated by the $\tau_{recovery}$ is <1 s, whereas the values of $\tau_{recovery}$ of either recombinant ASIC1a homomers or ASIC1a/2b heteromers are relatively slow (Fig. 4*C*). Conversely, the very slow recovery of ASICs from desensitization in BCs strongly suggests that the majority of ASICs in BCs is assembled as ASIC1a homomers. This notion is strongly supported by the results of single-cell RT-PCR and pharmacological sensitivity to PcTX1.

However, differences between native and recombinant ASICs still exist, despite that the recovery time course of native ASICs qualitatively recapitulates those of heterologously expressed ASICs in CHO cells. First, there are quantitative differences in the recovery time course of ASICs, particularly between the native ASICs in BCs ($\tau_{recovery}$ ~42.8 s) and the recombinant ASIC1a homomers ($\tau_{recovery}$ ~7 s) (Fig. 4*C*). Second, recombinant mouse ASIC1a/2a heteromers generate currents that desensitize faster than ASIC1a homomers (Askwith et al., 2004). In contrast, ASICs in O-LM cells (putative "ASIC1a/2a" heteromers) significantly desensitize slower than those (putative "ASIC1a" homomers) in BCs (Fig. 3*D*). These could be attributed to the differences in expression systems.

The estimated values of γ are not significantly different among the three groups. Notably, single-channel conductances of native ASICs compare well with those measured directly from unitary currents (from 4.2 pS under 10 mM $[Ca^{2+}]_o$ to 11.2 pS under 1 mM $[Ca^{2+}]_o$) (Immke and McCleskey, 2003). Also, the values of $P_{o,\,max}$ at pH 5 are not significantly different between O-LM cells and CA1 PNs. As for BCs, analysis of cumulative desensitization reveals that desensitization of ASICs in nucleated patches of BCs develops more rapidly than those of PNs and O-LM cells during repetitive application of acid pulses (Fig. 3*G*). This is in agreement with the suggestion that the open probability of ASICs in BCs is relatively low by the nonstationary fluctuation analysis.

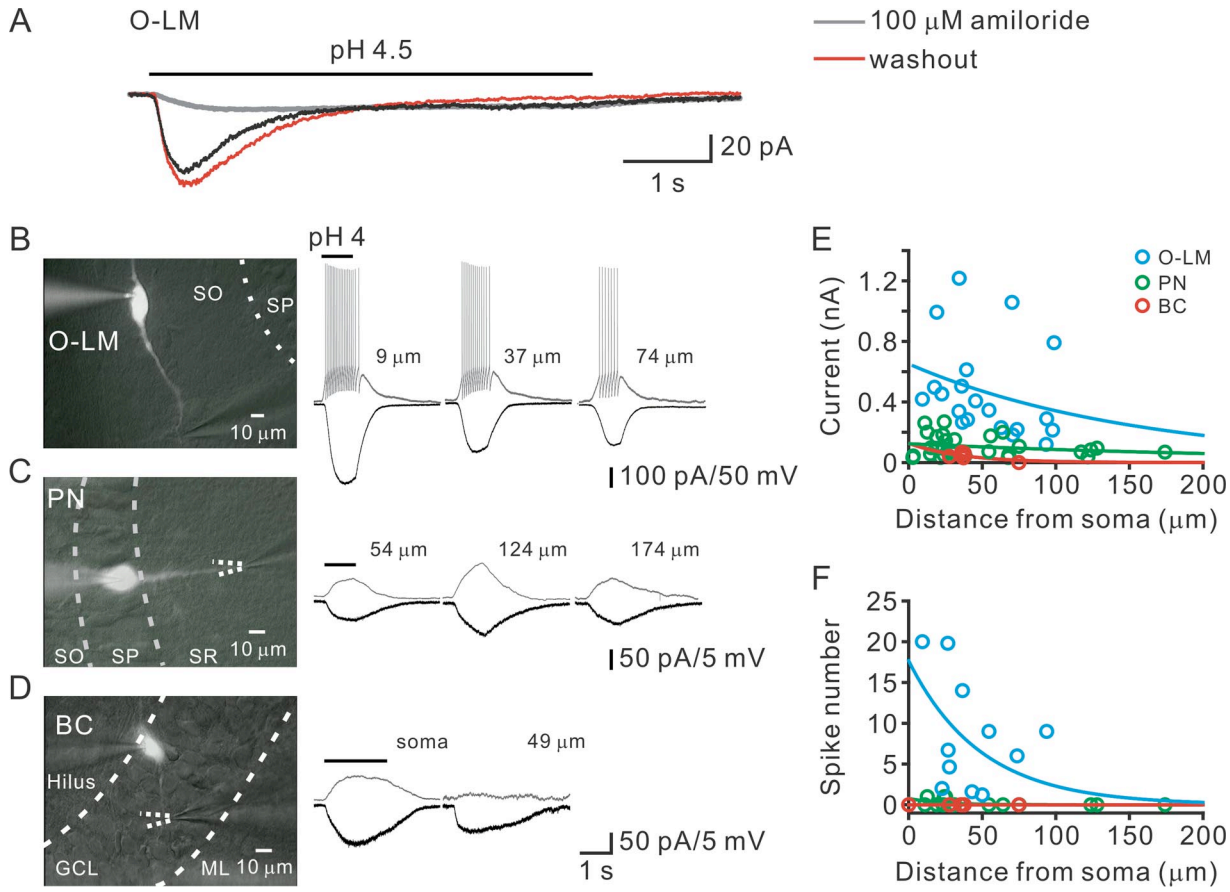

Figure 7. Dendritic ASIC currents in distinct types of neurons. ***A***, Focal acid puffs (5 s, pH 4.5) to the O-LM cell dendrite (at the distance of 23 μm from the soma) evoked a desensitizing inward current, which was reversibly blocked by amiloride (100 μM). Black, Control; gray, amiloride; red, washout. ***B***, Left, An O-LM cell filled with SR101 via somatic recording; the puff pipette was placed near the dendrite. Right, Brief acid puffs (1 s, pH 4) at different distances along the O-LM dendrite evoked large inward currents at the voltage-clamp potential (V-clamp) of −70 mV and spike trains in the current-clamp recording (holding potential −70 mV), respectively. ***C***, Left, A PN filled with SR101 and the puff pipette was placed near the apical dendrite. Right, Brief acid puffs (1 s, pH 4) at different distances along the PN dendrite evoked relatively smaller inward currents (V-clamp = −70 mV) and subthreshold membrane depolarization in the current-clamp recording (holding potential −70 mV), respectively. ***D***, Left, A BC filled with SR101 and the puff pipette was placed near the apical dendrite. Right, Local acid puffs (2 s, pH 4) evoked relatively smaller ASIC currents (V-clamp = −70 mV) and subthreshold membrane depolarization in the current-clamp recording (holding potential −70 mV), respectively. ***E***, ASIC currents as a function of distance from the soma. Lines represent exponential functions fit to the data points. Data are from 8 O-LM cells, 9 PNs and 6 BCs. ***F***, Summary plot of spike number plotted against distance from the soma. Lines represent exponential functions fit to data points. Data are from 8 O-LM cells, 9 PNs and 6 BCs. All experiments were performed in the presence of 1 mM kynurenic acid and 1 μM SR95531.

Possible functions of ASICs in perisomatic and dendritic inhibitory interneurons

Although our understanding of interneuron heterogeneity is still far from being complete, a major dichotomy in the inhibitory control of pyramidal cells has already been established (Freund and Katona, 2007). Dendritic inhibitory interneurons (for instance, O-LM cells) are responsible for the control of the efficacy and plasticity of glutamatergic inputs from specific sources that terminate in the same dendritic domain (Miles et al., 1996). On the other hand, perisomatic inhibitory interneurons (for instance, BCs) control the output of pyramidal cells (Miles et al., 1996). In addition, several intrinsic properties (see Introduction of this study) of these two major types of interneurons are found to be very different. In this study, we uncover the expression of ASICs as a novel cell type-specific property which might underlie their differences in synaptic transmission and relative susceptibility to brain injury.

Several lines of evidence suggest that ASICs play crucial roles in synaptic transmission. First, long-term potentiation, a form of synaptic plasticity underlying learning and memory, is abrogated at Schaffer collateral-CA1 pyramidal cell synapses in ASIC1a knock-out mice (Wemmie et al., 2002). Second, presynaptic release probability is increased in hippocampal neurons from ASIC1a knock-out mice (Cho and Askwith, 2008). Finally, ASICs interact with several postsynaptic scaffolding proteins such as PSD-95, PICK1 and CaMKII (for review, see Wemmie et al., 2006). More recently, ASIC2 subunits, but not ASIC1a subunits, were shown to target ASICs to the synapse via an association with PSD-95 and loss of ASIC2 subunits decreases the percentage of spines responding to acid (Zha et al., 2009). Interestingly, our results demonstrate that ASIC2 subunit mRNAs were not detected in most BCs and relatively small ASIC currents were detected in BC dendrites. Thus, subunit composition of ASICs in different types of GABAergic inhibitory interneurons might also contribute to cell type-specific long-term plasticity at glutamatergic synapses onto hippocampal interneurons (Nissen et al., 2010).

Deletion of ASIC1a gene was shown to increase the presynaptic release probability and led to paired-pulse depression at the hippocampal glutamatergic synapses (Cho and Askwith, 2008). Conversely, overexpression of ASIC1a subunits in ASIC1a knock-out neurons increases paired-pulse ratio. Thus, relative abundance of ASICs might underlie the heterogeneity of GABAergic inhibitory outputs (Maccaferri et al., 2000). Intrigu-

ingly, consistent with this notion, we found a similar correlation between the functional ASIC current and the release probability of interneurons. In this study, BCs with relatively low ASIC expression have high release probability and exhibit paired-pulse depression at short interspike intervals (Kraushaar and Jonas, 2000; Maccaferri et al., 2000). On the contrary, O-LM cells with relatively high ASIC expression have low release probability and show no paired-pulse modulation. (Maccaferri et al., 2000).

Functional implications

Interneurons exhibit differential susceptibility to injury by epileptic insults that are accomplished by transient acidification (Morin et al., 1998; Cossart et al., 2001; Wittner et al., 2001, 2005). In experimental epilepsy, dendrite-targeting interneurons, such as O-LM cells, selectively degenerate, leading to "disinhibition" in dendritic compartments of PNs. In contrast, soma-targeting interneurons, mainly BCs, are relatively spared, resulting in enhanced somatic inhibition (Cossart et al., 2001; Wittner et al., 2005). Increasing studies showed that neurons lacking ASICs are resistant to ischemic/acid injury (Xiong et al., 2004; Gao et al., 2005; Wemmie et al., 2006). Our data show that BCs, in contrast to O-LM cells and other non-fast-spiking interneurons, have strikingly low-density and rapidly desensitizing ASICs. Furthermore, BCs have relatively low input resistance ($\sim$134 MΩ, see Results) compared with O-LM cells ($\sim$336 MΩ). Consequently, relatively large ASIC currents in O-LM cells during transient acidification together with the high input resistance will lead to membrane depolarization and firing of O-LM cells (Fig. 7). Thus, acidification can preferentially induce firing of O-LM cells accompanied by massive Ca^{2+} influx via voltage-gated Ca^{2+} channels and thereby might have a greater impact on O-LM cells than BCs. Interestingly, in addition to the unique ASIC expression feature, fast-spiking BCs have very efficient Ca^{2+} buffer capacity (Aponte et al., 2008). Quantitatively, the magnitude of Ca^{2+} binding ratio (κ_s) of BCs ($\kappa_s \sim 200$; Aponte et al., 2008) is tenfold larger than that of O-LM cells ($\kappa_s \sim 20$; Liao and Lien, 2009). Together, all these factors likely contribute to selective degeneration of O-LM cells and disinhibition of pyramidal cell dendrites induced by experimental epilepsy.

Perspectives

Our results point to the cell type-specific expression of ASICs in hippocampal GABAergic inhibitory microcircuits and the findings demonstrate how the distribution and proportions of ASIC subunits vary in different cells under physiological conditions. Our work provides a better understanding of how acidosis in the hippocampus could influence the network and how hippocampal acidosis might suppress seizure activity. A challenge of future studies will be to delete ASIC gene in a cell type-restricted manner to address the meaning of differential expression of ASICs in the brain.

References

Alvarez de la Rosa D, Krueger SR, Kolar A, Shao D, Fitzsimonds RM, Canessa CM (2003) Distribution, subcellular localization and ontogeny of ASIC1 in the mammalian central nervous system. J Physiol 546:77–87.

Alvarez O, Gonzalez C, Latorre R (2002) Counting channels: a tutorial guide on channel fluctuation analysis. Adv Physiol Educ 26:327–341.

Aponte Y, Lien CC, Reisinger E, Jonas P (2006) Hyperpolarization-activated cation channels in fast-spiking interneurons of rat hippocampus. J Physiol 574:229–243.

Aponte Y, Bischofberger J, Jonas P (2008) Efficient Ca^{2+} buffering in fast-spiking basket cells of rat hippocampus. J Physiol 586:2061–2075.

Askwith CC, Wemmie JA, Price MP, Rokhlina T, Welsh MJ (2004) Acid-sensing ion channel 2 (ASIC2) modulates ASIC1 H^+-activated currents in hippocampal neurons. J Biol Chem 279:18296–18305.

Baron A, Waldmann R, Lazdunski M (2002) ASIC-like, proton-activated currents in rat hippocampal neurons. J Physiol 539:485–494.

Bolshakov KV, Essin KV, Buldakova SL, Dorofeeva NA, Skatchkov SN, Eaton MJ, Tikhonov DB, Magazanik LG (2002) Characterization of acid-sensitive ion channels in freshly isolated rat brain neurons. Neuroscience 110:723–730.

Chen X, Kalbacher H, Gründer S (2005) The Tarantula toxin psalmotoxin 1 inhibits acid-sensing ion channel (ASIC) 1a by increasing its apparent H^+ affinity. J Gen Physiol 126:71–79.

Cho JH, Askwith CC (2008) Presynaptic release probability is increased in hippocampal neurons from ASIC1 knockout mice. J Neurophysiol 99:426–441.

Cobb SR, Buhl EH, Halasy K, Paulsen O, Somogyi P (1995) Synchronization of neuronal activity in hippocampus by individual GABAergic interneurons. Nature 378:75–78.

Coryell MW, Wunsch AM, Haenfler JM, Allen JE, Schnizler M, Ziemann AE, Cook MN, Dunning JP, Price MP, Rainier JD, Liu Z, Light AR, Langbehn DR, Wemmie JA (2009) Acid-sensing ion channel-1a in the amygdala, a novel therapeutic target in depression-related behavior. J Neurosci 29:5381–5388.

Cossart R, Dinocourt C, Hirsch JC, Merchan-Perez A, De Felipe J, Ben-Ari Y, Esclapez M, Bernard C (2001) Dendritic but not somatic GABAergic inhibition is decreased in experimental epilepsy. Nat Neurosci 4:52–62.

Du J, Zhang L, Weiser M, Rudy B, McBain CJ (1996) Developmental expression and functional characterization of the potassium-channel subunit Kv3.1b in parvalbumin-containing interneurons of the rat hippocampus. J Neurosci 16:506–518.

Efron B, Tibshirani RJ (1998) An introduction to the bootstrap. London: Chapman and Hall/CRC.

Engel D, Jonas P (2005) Presynaptic action potential amplification by voltage-gated Na^+ channels in hippocampal mossy fiber boutons. Neuron 45:405–417.

Freund TF, Buzsáki G (1996) Interneurons of the hippocampus. Hippocampus 6:347–470.

Freund TF, Katona I (2007) Perisomatic inhibition. Neuron 56:33–42.

Gao J, Duan B, Wang DG, Deng XH, Zhang GY, Xu L, Xu TL (2005) Coupling between NMDA receptor and acid-sensing ion channel contributes to ischemic neuronal death. Neuron 48:635–646.

Gentet LJ, Stuart GJ, Clements JD (2000) Direct measurement of specific membrane capacitance in neurons. Biophys J 79:314–320.

Hartveit E, Veruki ML (2007) Studying properties of neurotransmitter receptors by nonstationary noise analysis of spontaneous postsynaptic currents and agonist-evoked responses in outside-out patches. Nat Protoc 2:434–448.

Hille B (2001) Ion channels of excitable membranes, Ed 3. Sunderland, MA: Sinauer.

Immke DC, McCleskey EW (2003) Protons open acid-sensing ion channels by catalyzing relief of Ca^{2+} blockade. Neuron 37:75–84.

Jonas P, Bischofberger J, Fricker D, Miles R (2004) Interneuron diversity series: fast in, fast out—temporal and spatial signal processing in hippocampal interneurons. Trends Neurosci 27:30–40.

Klausberger T, Somogyi P (2008) Neuronal diversity and temporal dynamics: the unity of hippocampal circuit operations. Science 321:53–57.

Klausberger T, Magill PJ, Márton LF, Roberts JD, Cobden PM, Buzsáki G, Somogyi P (2003) Brain-state- and cell-type-specific firing of hippocampal interneurons in vivo. Nature 421:844–848.

Koh DS, Geiger JR, Jonas P, Sakmann B (1995) Ca^{2+}-permeable AMPA and NMDA receptor channels in basket cells of rat hippocampal dentate gyrus. J Physiol 485:383–402.

Kraushaar U, Jonas P (2000) Efficacy and stability of quantal GABA release at a hippocampal interneuron-principal neuron synapse. J Neurosci 20:5594–5607.

Liao CW, Lien CC (2009) Estimating intracellular Ca^{2+} concentrations and buffering in a dendritic inhibitory hippocampal interneuron. Neuroscience 164:1701–1711.

Lien CC, Jonas P (2003) Kv3 potassium conductance is necessary and kinetically optimized for high-frequency action potential generation in hippocampal interneurons. J Neurosci 23:2058–2068.

Lien CC, Martina M, Schultz JH, Ehmke H, Jonas P (2002) Gating, modu-

lation and subunit composition of voltage-gated K^+ channels in dendritic inhibitory interneurones of rat hippocampus. J Physiol 538:405–419.
Liss B, Roeper J (2004) Correlating function and gene expression of individual basal ganglia neurons. Trends Neurosci 27:475–481.
Maccaferri G, Roberts JD, Szucs P, Cottingham CA, Somogyi P (2000) Cell surface domain specific postsynaptic currents evoked by identified GABAergic neurones in rat hippocampus in vitro. J Physiol 524:91–116.
Markram H, Toledo-Rodriguez M, Wang Y, Gupta A, Silberberg G, Wu C (2004) Interneurons of the neocortical inhibitory system. Nat Rev Neurosci 5:793–807.
Martina M, Schultz JH, Ehmke H, Monyer H, Jonas P (1998) Functional and molecular differences between voltage-gated K^+ channels of fast-spiking interneurons and pyramidal neurons of rat hippocampus. J Neurosci 18:8111–8125.
Mazzuca M, Heurteaux C, Alloui A, Diochot S, Baron A, Voilley N, Blondeau N, Escoubas P, Gélot A, Cupo A, Zimmer A, Zimmer AM, Eschalier A, Lazdunski M (2007) A tarantula peptide against pain via ASIC1a channels and opioid mechanisms. Nat Neurosci 10:943–945.
McBain CJ, Fisahn A (2001) Interneurons unbound. Nat Rev Neurosci 2:11–23.
Miles R, Tóth K, Gulyás AI, Hájos N, Freund TF (1996) Differences between somatic and dendritic inhibition in the hippocampus. Neuron 16:815–823.
Morin F, Beaulieu C, Lacaille JC (1998) Selective loss of GABA neurons in area CA1 of the rat hippocampus after intraventricular kainate. Epilepsy Res 32:363–369.
Nissen W, Szabo A, Somogyi J, Somogyi P, Lamsa KP (2010) Cell type-specific long-term plasticity at glutamatergic synapses onto hippocampal interneurons expressing either parvalbumin or CB1 cannabinoid receptor. J Neurosci 30:1337–1347.
Pouille F, Scanziani M (2004) Routing of spike series by dynamic circuits in the hippocampus. Nature 429:717–723.
Sík A, Hájos N, Gulácsi A, Mody I, Freund TF (1998) The absence of a major Ca^{2+} signaling pathway in GABAergic neurons of the hippocampus. Proc Natl Acad Sci U S A 95:3245–3250.
Stuart GJ, Dodt HU, Sakmann B (1993) Patch-clamp recordings from the soma and dendrites of neurons in brain slices using infrared video microscopy. Pflugers Arch 423:511–518.
Waldmann R, Champigny G, Bassilana F, Heurteaux C, Lazdunski M (1997) A proton-gated cation channel involved in acid-sensing. Nature 386:173–177.
Wemmie JA, Chen J, Askwith CC, Hruska-Hageman AM, Price MP, Nolan BC, Yoder PG, Lamani E, Hoshi T, Freeman JH Jr, Welsh MJ (2002) The acid-activated ion channel ASIC contributes to synaptic plasticity, learning and memory. Neuron 34:463–477.
Wemmie JA, Price MP, Welsh MJ (2006) Acid-sensing ion channels: advances, questions and therapeutic opportunities. Trends Neurosci 29:578–586.
Wittner L, Maglóczky Z, Borhegyi Z, Halász P, Tóth S, Eross L, Szabó Z, Freund TF (2001) Preservation of perisomatic inhibitory input of granule cells in the epileptic human dentate gyrus. Neuroscience 108:587–600.
Wittner L, Eross L, Czirják S, Halász P, Freund TF, Maglóczky Z (2005) Surviving CA1 pyramidal cells receive intact perisomatic inhibitory input in the human epileptic hippocampus. Brain 128:138–152.
Xiong ZG, Zhu XM, Chu XP, Minami M, Hey J, Wei WL, MacDonald JF, Wemmie JA, Price MP, Welsh MJ, Simon RP (2004) Neuroprotection in ischemia: blocking calcium-permeable acid-sensing ion channels. Cell 118:687–698.
Xiong ZG, Pignataro G, Li M, Chang SY, Simon RP (2008) Acid-sensing ion channels (ASICs) as pharmacological targets for neurodegenerative diseases. Curr Opin Pharmacol 8:25–32.
Zha XM, Wemmie JA, Green SH, Welsh MJ (2006) Acid-sensing ion channel 1a is a postsynaptic proton receptor that affects the density of dendritic spines. Proc Natl Acad Sci U S A 103:16556–16561.
Zha XM, Costa V, Harding AM, Reznikov L, Benson CJ, Welsh MJ (2009) ASIC2 subunits target acid-sensing ion channels to the synapse via an association with PSD-95. J Neurosci 29:8438–8446.
Ziemann AE, Schnizler MK, Albert GW, Severson MA, Howard MA 3rd, Welsh MJ, Wemmie JA (2008) Seizure termination by acidosis depends on ASIC1a. Nat Neurosci 11:816–822.